pH-DEPENDENT PROCESSES IN PROTEINS

Authors: **James B. Matthew**
Department of Protein Engineering
Genex Corporation
Gaithersburg, Maryland

Frank R. N. Gurd
Bertrand Garcia-Moreno E.
Department of Chemistry
Indiana University
Bloomington, Indiana

Margaret A. Flanagan
Laboratory of Chemical Biology, NIADDK
National Institutes of Health
Bethesda, Maryland

Keith L. March
Department of Medical Sciences
Indiana University School of Medicine
Indianapolis, Indiana

Steven J. Shire
Department of Protein Biochemistry
Genentech, Incorporated
San Francisco, California

Referees: Sir David Phillips
Laboratory of Molecular Biophysics
Oxford University
Oxford, England

Neil K. Rogers
Laboratory of Molecular Biophysics
Oxford University
Oxford, England

I. GENERAL CONSIDERATIONS

A. Historical Perspective

The purification, stability, and function of proteins were early shown to be sensitive to electrolytes, acids, bases, and sometimes specific salts. Their charged nature was demonstrated directly by electrophoresis[1] and the pH dependence of biological function and states of aggregation were recognized.[2,3] However, the stoichiometric basis for the bound charges was not clear for some time.

The idea that the pH-dependent processes in proteins could be interpretable in terms of the laws of physical chemistry applied systematically to their constituent functional groups was explored in detail by Cohn[4] and his colleagues. Coming shortly after the work of Bjerrum[5] and of Debye and Hückel[6] on the properties of electrolyte solutions, the sustained work of Cohn, Edsall, Scatchard, Oncley, and their co-workers established the continuity of proteins,

peptides, amino acids, and simple model compounds with respect to their electrolyte interactions.[7] This approach demonstrated the dipolar nature of amino acids, the possibility of group-by-group analysis of titration curves, the observation of neighboring effects between dissociating groups, and the patterns of effects of ionic strength and solvent mixtures on pK values, solubility, and other properties.

From measurements on individual amino acids and some of their chemical relatives, it was possible to establish ranges for the characteristic pK values of the side-chain and terminal groups to be encountered in proteins. Ascribing such pK values to the corresponding groups in a protein according to its amino acid composition became a provisionally accepted procedure.[8,9] In certain cases some members of a particular class of proton binding groups, for example, sulfhydryl groups or imidazole of histidine residues, were found not to titrate except after disruption of the protein and were taken to be masked from the solvent in the native structure.[9,10]

During titration of a protein positive or negative charges on dissociable groups are formed or neutralized. Hence, the electrostatic field bearing on any given dissociable group will vary causing its apparent pK to be continuously altered. Linderstrøm-Lang[11] introduced a formalism to account for the variation in overall charge by adapting the Debye-Hückel treatment to a large protein ion bearing the appropriate net charge smeared over its surface. This simple interactive formalism was useful in describing overall protein titration behavior, and responded to the qualitative effects of electrostatic shielding by counterions and added salts.[7,8,12] It was also helpful for analysis of binding of ions other than hydrogen ion[13] as well as for describing conformational transitions.[8,9,14] Since the Linderstrøm-Lang formalism deals with a smeared net charge it makes no predictions of individual site behavior and predicts only destabilizing electrostatic interactions in a protein molecule. As discussed later, the interplay of individual oppositely charged loci will often provide strong stabilization.

Electrostatic shielding by low concentrations of ions was also observed to influence the solubility of many proteins,[15] particularly in mixtures of macromolecules of opposite net charge.[16,17] The electrostatic nature of the solubility effects was confirmed by numerous experiments in which the dielectric constant of the medium (a measure of shielding defined later) was manipulated. For example, solvent shielding could be reduced by adding ethanol and increased by adding glycine, the former with potentiation of the salt effects and the latter with their diminution.[7]

The first systematic studies of polypeptide conformation in solution were based on relatively simple polyamino acids.[18-20] In a homopolymer the side-chain dissociation can be clearly specified and any change in backbone conformation can be followed unambiguously by measurements of viscosity, optical rotation, or circular dichroism. Coulombic repulsion between the fixed charges under given conditions produces two effects. The first is the progressive displacement of the apparent pK value so as to diminish the charge-bearing fraction of the residues, and the second is the separation of the charged groups in a swollen, mobile configuration of the polymer containing both solvent and counterions within its boundary volume. Lessening the repulsive potentials by titration or by adding salts produces a contraction of the volume swept out by the polymer and may accommodate an ordered, condensed conformation of the backbone such as a helix or β-structure.[21] Note that in this type of system the hydrogen ion dissociation is linked cooperatively to a conformational transition mediated by coulombic interactions. The transition involves free energy changes associated not only with the electrostatic interactions, but also with respect to configurational order, solvation, hydrogen bonding, and other factors.

The availability of X-ray crystallographic analysis of protein structures now offers detailed information about molecular architecture, including the geometrical relationships of dissociable groups of both charge types. To illustrate the concept of solvent exclusion during protein folding and the redistribution of solvent counterions a hypothetical expanded section through myoglobin is shown in Figure 1A compared with the corresponding crystal structure

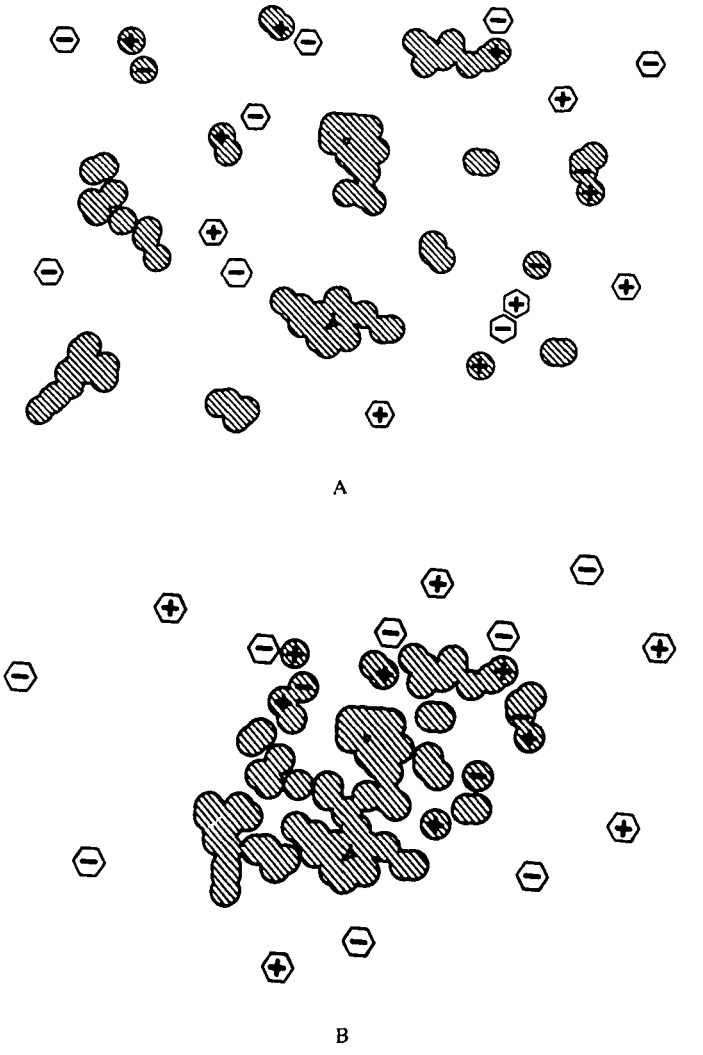

FIGURE 1. Diagrams portraying the substance of sperm whale myoglobin at the level of a slice through the molecule with the fixed protein charges shown on the cross-hatched protein material. Mobile counterions and salt ions are shown as hexagons. (A) The material of the slice is shown arbitrarily dispersed to portray penetration of solvent and ions between the elements of the protein matrix. (B) The protein matrix is condensed to the form determined in the native crystal structure. Relative to (A), this entails the displacement of the intervening solvent molecules and mobile ions as the continuous interface is formed.

section in Figure 1B.[22] The individual "fixed" charges on the protein are indicated within circles representing the N or O atoms in question. All other parts of the protein in the section, polar and nonpolar, are shown without identification.

In Figure 1A solvent and dissolved ions are interspersed between the structural elements of the protein and make an extensive interface with them. Since the fixed charges number six positive and three negative, the mobile ions (hexagons) include three more negative than positive offsetting counterions, as well as an arbitrary number of matched positive and negative salt ions. The mobile ions and the polar water molecules, respectively, tend to distribute themselves and to orient their partial charge dipoles so as to shield the fixed protein charges from each other.

In Figure 1B the protein matrix is close packed and the solvent has been expelled or excluded from much of the intervening volume represented in Figure 1A. The reduced

counterion screening and closer approach of protein sites favor strong interactions between the fixed charges, especially when contact becomes direct as the solvent and dissolved salts are displaced and ion pairs form. Compared with the dissociable groups in the homopolymers cited previously, those in the protein (Figure 1B) are far more site-specific as to solvent interface, variety of immediate contacts with neighboring structures, and range of categories of dissociable amino acids represented.

The effect of the pH-dependent electrostatic interactions in the condensed protein structure is, first, to influence the apparent pK of each group under the accumulated electrostatic potential at its location; second, to contribute to the overall electrostatic stabilization or destabilization of the conformation; third, to impose electrostatic field gradients on polar or polarizable structures in the molecule; and fourth, to provide binding or docking potentials for other ionic species including simple ions and ionic cofactors, substrates or products, proteins, and nucleic acids.

In addition to the interactions between formal unit charges, a closely related effect to be considered involves the fields from the partial charge distributions responsible for side-chain and peptide bond dipole moments. The properties of a hydrogen bond network such as an α-helix can be described as a set of interacting peptide unit dipoles resulting from the electron distribution on the individual atoms.[23,24] The unit formal charges that we have been considering interact with such dipoles both within the protein and in the solvent water molecules.

Under conditions that apply to biological systems, the energy of interaction between two isolated ions in vacuo varies with $1/r$, where r is the distance of separation. That between an ion and a dipole varies with $1/r^2$, with an additional factor dependent on the orientation of the dipole relative to a line joining the ion to the center of the dipole. That between two dipoles varies with $1/r^3$, again with a factor reflecting their relative orientation. The absolute magnitudes of the interaction energies in each case decrease sharply in the order given. The interionic interactions have the largest range and strength in the absence of other influences.[25]

In this review we shall deal principally with the interactions among the formal charge array, both intra- and intermolecular, because of their intrinsic importance and the abundance of experimental data. What we learn about the nature of the interactions between titratable charge sites will bear in turn on partial charge-dipole interactions. The effects which lead to a net reduction of formal charge interaction are quantified under the term "effective dielectric" for later dissection into contributions from water, mobile ions, and the protein matrix.

B. Experimental Approaches

The primary experimental requirement is to discover the distribution of hydrogen ions among the potential binding sites or groups in the protein as a function of pH and ionic strength. The classical titration curve relates the overall number of equivalents of hydrogen ions bound or released to changes in pH, and so defines the sum of the individual changes in site occupancy as a function of pH. The titration results are tested against the expected number of titratable groups from amino acid composition. Any discrepancies may indicate masking of a group in which the effective pK is so strongly linked to the conformational state of the protein that its titration is not observed in the native structure.[9,26]

Titration of individual groups is most generally observed in small proteins by ^1H or ^{13}C NMR measurements to determine pK_{obs} values.[27-29] The NMR resonance positions are often sensitive enough to environmental factors in the protein that individual groups are distinguishable. The chemical shift of one or more observable nucleus in a dissociable residue is affected by the protonation state so that its resonance position is found to titrate according to the proportions of protonated and unprotonated forms. Under most conditions, the method is less effective for observing the relatively immobilized masked or buried residues. Identification of resonances according to chemical class, e.g., histidine or carboxylic acid, is

usually straightforward. Specific assignments of resonances to given residues depend most often on reference to the crystal structure for prediction of chemical shift values, chemical modification procedures, or comparison of natural or semisynthetic variants.[27,30] Absorbance measurements may describe the dissociation of residues such as tyrosine or certain prosthetic groups.[26,31]

The crystalline structure provided by X-ray or neutron diffraction scattering is assumed to be a good approximation of the structure in solution which is needed to interpret the titration measurements. This underlying assumption has been tested in some cases by chemical modification,[32] catalytic activity,[33] or spectroscopic techniques.[34] To make the most of the analogy between crystal and solution structure as broad a range as possible of graded crystallization conditions should be studied to parallel the titrations in solution.[35] The composition of the crystal with respect to pH, ionic, and cosolvent components should be defined, for example, by NMR methods.[36] Nevertheless, the range of solution conditions desirable for study often extends well beyond those that can be observed in the crystalline state. When pH-dependent conformational changes occur in solution, the changes detectable by NMR will characteristically reflect both titrating and nontitrating residues.[29]

Any interpretation of the pH-dependent properties of a protein must take into account binding of charged species other than hydrogen ions. The stoichiometry and affinity of binding can be estimated by such standard methods as ion-specific electrode potentials, dialysis or gel equilibrium measurements, or differential titration procedures.[37,38] In some cases, direct NMR or absorbance measurements, including circular dichroism or fluorescence quenching, can be useful. Crystallographic evidence of binding is especially useful in the cases of inhibitors, substrates or their analogs, or allosteric effectors. However, the occupancy of a given binding site may be appreciably changed relative to the solution state because of intercalation between molecules or constrictions in the crystal lattice. Correspondingly, the relaxation of the electrostatic and other constraints on the crystal lattice when the protein is dissolved may allow transitions to different local structures with altered binding characteristics.[27,39] The ion binding process reflects both the intensity of electrostatic fields around the surface of the protein, the energetics of substitution of the given ion by another in the solvent and the opportunity for multiple stabilizing contacts (chelation) in the binding site.

The distribution of hydrogen ions among the potential binding sites depends on the intrinsic acidity of each residue modulated by the electrostatic fields of other ions and of partial-charge dipoles. Either field source can be found in the solvent or in the protein proper. The reference state for the intrinsic pK of a particular dissociable group is usually taken as that of a small monomeric molecule or nonassociating peptide fragment.[8,40-42] The variations that may be encountered with different nonionizing peptide sequences containing a given ionizing amino acid residue have received little attention. Amino- and carboxyl-terminal residues in a sequence are distinctive and call for reference pK values specific to the amino acid residue in question.

The expanded protein conformation schematized in Figure 1A shows the titratable groups in segments fully exposed to solvent, corresponding most nearly to the conditions in the small reference molecules on which the intrinsic pK values are based. The conversion to the native conformation (Figure 1B) both excludes ions and solvent water molecules and brings the individual components of the protein into more intimate and usually more specific contact with each other. The exclusion as such affects mainly shielding between ions, while the details of the folded state determine their distances of separation from each other and their interactions with other polar components. Between each class of dissociating group represented by a given amino acid type, and within each such class, a gradation of the effects just described may be encountered producing individual effective pK values under given conditions. Correspondingly, each protonation event may be linked with localized or widespread conformational changes.

C. Theoretical Approaches

In a vacuum the energy required to bring two charges i and j from infinity to a separation distance r_{ij} is

$$W_{ij} = \frac{Z_i Z_j}{r_{ij}} \quad (1)$$

where Z_i and Z_j are the appropriate electronic charges. If the charges are brought together in the presence of polar and polarizable molecules such as water, the interaction energy is

$$W_{ij} = Z_i Z_j / r_{ij} D_{ij} \quad (2)$$

where D_{ij} is referred to as the dielectric constant. This value refers to the screening effect the surrounding medium has on the apparent interaction energy of charge sites i and j when compared to the vacuum interaction. The macroscopic dielectric constant value of pure water at 25°C is 78.5 and varies inversely with temperature due to the tendency of thermal motion to overcome the orientational effects of the charge sites on the water dipoles. Thus, the interaction energy for a protein charge array can be described as:

$$\Delta G_{el} = \sum W_{ij} = \frac{1}{2} \sum_{i=1}^{n} \sum_{j \neq 1}^{n} \frac{Z_i Z_j}{r_{ij} D_{ij}^{eff}} \quad (3)$$

where Z_i and Z_j are the electronic charges, r_{ij} is the separation distance, and D_{ij}^{eff} is the effective dielectric constant. High-resolution crystallographic structures of globular proteins provide the r_{ij} charge site separation distances assuming that they represent the time average distances in solution.

The complex nature of the protein-solvent interface makes difficult the estimation of the coulombic screening term, D_{ij}^{eff}, for each charge pair on the protein. The essential distinctions between different electrostatic calculations that have been applied to proteins lie in their definitions of the coulombic screening by the medium. Two approaches have been taken: first, a macroscopic model which assigns continuous values to certain portions or all of the surrounding space (e.g., the protein volume of dielectric constant, $D_{protein}$, surrounded by the solvent dielectric constant, $D_{solvent}$); second, a microscopic model in which the details of the molecular structure are explicitly taken into account, e.g., the atomic positions and polarizabilities. These two approaches are not mutually exclusive. The principles and formalisms developed for a macroscopic dielectric approach are amenable to a microscopic application (see Section II.E).

In microscopic dielectric formalisms the calculated "dielectric effect" is based on the electrostatic fields due to the dipoles induced by polarizing the protein atoms and the dipoles induced by orienting the surrounding water molecules.[43] The electrostatic energy of a group of charges inside a region of protein is composed of (1) charge-charge interactions and (2) the inductive interactions between the charges of the protein and the polarizable electrons of the protein. The dielectric due to interactions with water around the protein is treated differently. The electric field from the charges and induced dipoles of the protein causes the orientation of the permanent water dipole moments. As a first step, the protein is surrounded by a cluster of solvent molecules. Each solvent molecule is represented by a point dipole. The interaction between solvent molecules is represented by dipole-dipole and van der Waals potential functions, and the interaction between solvent and protein atoms is represented by the dipole-charge relationship. The electric fields from the atomic partial

charges of the protein interact with the point dipoles of water causing them to become partially aligned. The microscopic approach could potentially provide a more complete and satisfying solution. However, simplifying assumptions are required to make the current computations manageable; among the more promising means for expressing the solvent effects may be brute force computer simulations, molecular dynamics computations, or Monte Carlo-type calculations.

In a recent article, Warshel et al.[43a] conclude that the polar nature of the protein surface and surface crevices (i.e., the permanent and induced dipoles, and the intimate proximity of the solvent interface) results in a large effective dielectric constant for protein charge-charge interactions in general. This model has not been systematically applied to a number of different proteins; therefore, its value as a predictive tool is unknown. It does have the attractive feature of giving a plausible microscopic explanation for the observation that many side-chain pK_{eff} values seem to be unaffected by their fractional exposure to bulk solvent. However, until the authors recognize the necessity of incorporating the effects of the mobile ion distribution, ion binding, and pH-dependent ionizations, the method cannot account for the observed pH- and ionic strength-dependent effects observed in all protein systems.

The macroscopic dielectric approach to coulombic screening is currently amenable to various computational methods and, as we shall see, in the cases where dielectric boundary conditions are assigned to an approximate protein-solvent interface, the agreement with experiment is good. Models based on this approach recognize the protein-solvent interface and mobile counterions in the solvent. Structural studies of globular proteins have shown that charged atoms, rarely, if ever, occur in the largely hydrophobic interior. Therefore, the modeling of a protein-solvent interface includes a region of low dielectric, representing the less polar organic nature of the protein interior, surrounded by a region of high dielectric constant, representing a polar solvent such as H_2O. The ionizable charge sites are taken to be at or near the dielectric boundary. Additional screening due to diffusible counterions in the high dielectric region can be included by describing the expected equilibrium distribution of counterions around the charge sites.

Any polyion with a net charge will have an equal number of associated small ions, even in the absence of added salt, to conserve electroneutrality. It is expected that when the charge array of the protein is sufficiently asymmetric, either by composition, geometry, or both, the electrostatic potential distribution in the absence of steric hindrance will dictate a specific counterion distribution. However, as shown in Figure 1B, proteins are dense, compact structures which are relatively impenetrable to electrolyte and hence capable of limiting the extent of clustering of counterions. Given that the time average counterion distribution does not significantly violate the protein boundary, the effective counterion concentration around the protein charge sites will depend both on the electrostatic potential and on the topographical consideration of steric hindrance to the effective clustering of counterions.

The simplest macroscopic approach is to neglect the dielectric boundary and diffusible ions and simply treat the charge interactions in a continuous uniform medium. Calculations of this type have been used to estimate peptide unit dipole interactions within the protein (dielectric constants of 1 or 4).[44-46] Similarly, Margoliash and co-workers have used a uniform dielectric of 80 to estimate the electrostatic field around cytochrome c and various modified derivatives.[47] In several molecular dynamics and energy minimization potential functions the effective dielectric value has been set equal to the separation distance ($D_{ij}^{eff} = r_{ij}$, with an interaction cutoff distance of 8 Å).[48] The interaction energies with close approach of oppositely charged sites in proteins could then approximate the values in a vacuum. However, a polar medium need not intervene between the interacting charge sites in order to reduce their interaction substantially.[49]

The most neglected aspect of the macroscopic problem is the inclusion of the mobile ion distribution and its effect on propagation of electrostatic fields. When small diffusible ions such as NaCl are included in a solvent such as water, the dielectric constant (i.e., the coulombic screening) of the solution increases. For instance, Hill[50] described the coulombic screening effect by small ions in terms of an effective dielectric constant estimated as:

$$D_{ij}^{eff} = D_{H_2O}\, e^{\kappa r_{ij}} \tag{4}$$

where κ is the usual Debye-Hückel[6] parameter proportional to the square root of the ionic strength.

1. Tanford-Kirkwood Formalism

Tanford and Kirkwood[51] calculated the electrostatic free energy for a set of discrete point charges on a spherical surface of radius b and ion exclusion radius, a, illustrated in Figure 2A. The pairwise treatment of charges is illustrated in Figures 2B and 2C. Each particular pair of charges is considered to be placed at the surface of the sphere which is assumed to form a continuous medium of low dielectric (region I) surrounded by solvent with an external dielectric constant, D, and mobile counterions whose coulombic screening is proportional to square root ionic strength (region III). LaPlace's equation was applied in the low dielectric region and in the ion exclusion region which consists of solvent dielectric without mobile ions (region II). The Poisson-Boltzmann equation was applied in the high dielectric mobile ion region (region III) with the same assumptions that are inherent in the Debye-Hückel treatment.[6]

The solutions to these equations, with the usual boundary conditions that the potential be continuous and dielectric displacements normal to the spherical dielectric boundary be equal, were first obtained by Kirkwood[52] and later converted to a form amenable to calculation.[51] The consequences of the Debye-Hückel approximation are apparent.[53] The theory rigorously applies only when the electrostatic potential energy $\epsilon\psi$ is less than kT, while the electrostatic potential energy of a small ion in the vicinity of a highly charged polymer is often several kT. The well-known phenomenon of specific ion "site binding" is not directly accounted for by the Debye-Hückel approximation used in the Tanford-Kirkwood treatment. However, sites of specific ion binding can be explicitly included in the discrete charge array.

Numerical solutions to the nonlinearized Poisson-Boltzmann equation were obtained by Nagasawa and Holtzer in the analysis of protein potentiometric data.[54] They suggested that observed deviations from the behavior predicted by the Linderstrøm-Lang smeared charge model[11] or Tanford-Kirkwood[51] theories need not be the result of specific ion binding as an independent process separate from electrostatic binding. Rather, they concluded that the combination of the discrete charge model and the use of the nonlinearized Poisson-Boltzmann equation can also account for deviations, which led them to support a general electrostatic interpretation of ion binding.

2. Charge Site Interactive Energy

In both the Tanford-Kirkwood discrete charge model and the static accessibility version of it, the Debye-Hückel theory is used in calculating the electrostatic free energy of interaction for a set of discrete point charges on a sphere of radius *b*, and ion exclusion radius *a*, where *a-b* is the distance of closest approach of counterion to the protein molecule (Figure 2). The charges are conventionally treated at the surface of the equivalent sphere which is assumed to form a continuous medium with low internal dielectric constant, D_{int}, surrounded by solvent water with external dielectric constant D_{ext}.

Figure 3 illustrates the direct application of the Tanford-Kirkwood formalism to two cases represented by spheres of radii 27 Å and 18 Å. The plot shows the variation of W_{ij} with

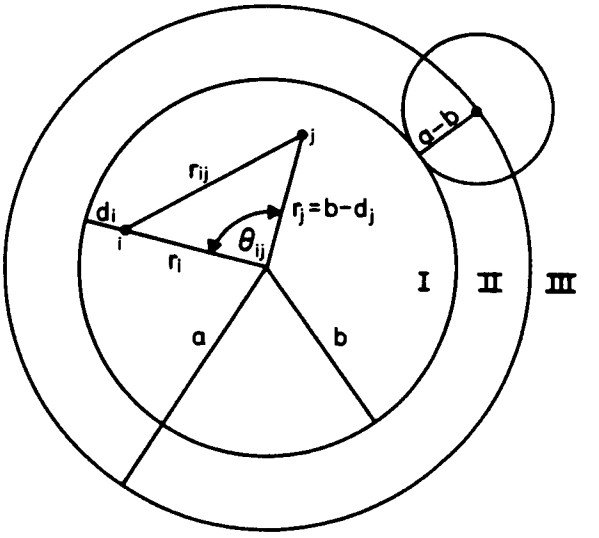

A

FIGURE 2. Diagrammatic representation of the Tanford-Kirkwood discrete-charge model for the protein-solvent interface. The inner spherical region, I, of radius b consists of a continuous low dielectric with point charges on or within its surface. The next spherical shell, II, defines the exclusion distance in the external solvent of counterions at the distance a from the center. The external region, III, is composed, with II, of a continuous high dielectric medium but also contains mobile ions. (A) Scheme showing locations of charge sites i and j with radii of r_i and r_j, respectively, with separation distance r_{ij} subtended by the angle θ_{ij}. The closest approach of a counterion of radius a-b is shown at the boundary between regions I and II. (From Shire, S. J., Determination and Interpretation of Hydrogen Ion Equilibria in Ferrimyoglobin, Ph.D. thesis, Indiana University, Bloomington, 1974.) (B) Cross section of myoglobin as in Figure 1A positioned within equivalent circle to bring a pair of positive charge sites to the dielectric boundary between regions I and II. (C) As in (B), for a pair of sites, one positive and one negative.

separation distance r_{ij}. As Figure 3 shows, interaction energy is only slightly reduced on decreasing the size of the sphere (curves 1 and 2) but is substantially lowered upon raising the ionic strength from 0 to 0.1 (curves 3 and 4). It is a very sensitive function of r_{ij}.

Figure 4 illustrates in another way the direct application of this calculation to a sphere of radius 18 Å. The variation of W_{ij} with separation distance r_{ij} is cast in terms of the reciprocal of effective dielectric using the Bjerrum formalism $1/D_{eff} = W_{ij}r_{ij}/e^2$, at 0.0, 0.01, 0.10, and 0.50 ionic strengths. The reduction in interactive free energy at finite ionic strength, i.e., the increase in apparent effective dielectric, as discussed before, is based on the linearized Poisson-Boltzmann approximation. For comparison the effective dielectric values at the same ionic strengths were calculated for Debye-Hückel screening for small ions in solution as a function of separation calculated according to the formalism in Equation 3.

3. Solvent Accessibility Modified Tanford-Kirkwood Theory

A solvent static accessibility parameter[55] for each protein charge site was incorporated by Shire et al.[56] into the Tanford-Kirkwood discrete charge electrostatic theory. This modification was introduced to overcome the uncertainty of an adjustable charge burial parameter beneath the dielectric interface required in the original treatment to fit protein titration curves[57-59] and to allow for the irregular protein solvent interface.[59]

Lee and Richards introduced the concept of static solvent accessible surface[55] by defining the "accessible surface area" as the area around an atom over which the center of the solvent (i.e., water) molecule can be placed, enabling it to maintain van der Waals contact without

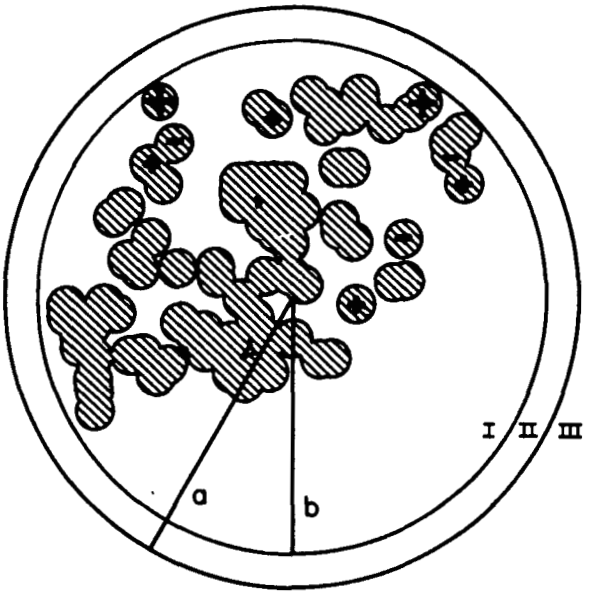

FIGURE 2B

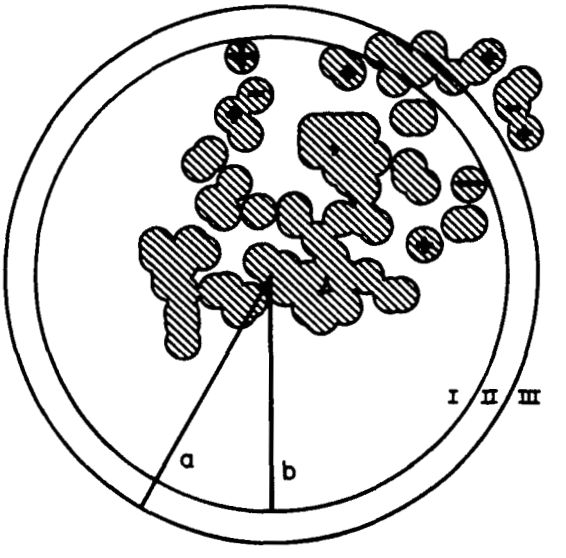

FIGURE 2C

penetrating any other atom in the protein (Figure 5). The accessibility of a protein charge site is then defined as its accessible surface area in Å². A clearer appraisal of the influence of protein structure on the solvent accessibility to individual charge sites is obtained by normalization to that in a model tripeptide where accessibilities are assumed to attain their maximum value indicative of the fully hydrated site.

Fractional static solvent accessibilities (SA) have been calculated for proton binding sites in several globular proteins.[29,55,60-63] These values vary from 0.01, indicating virtually no van der Waals contact with water in the static structure, to 1.0, inferring no structural

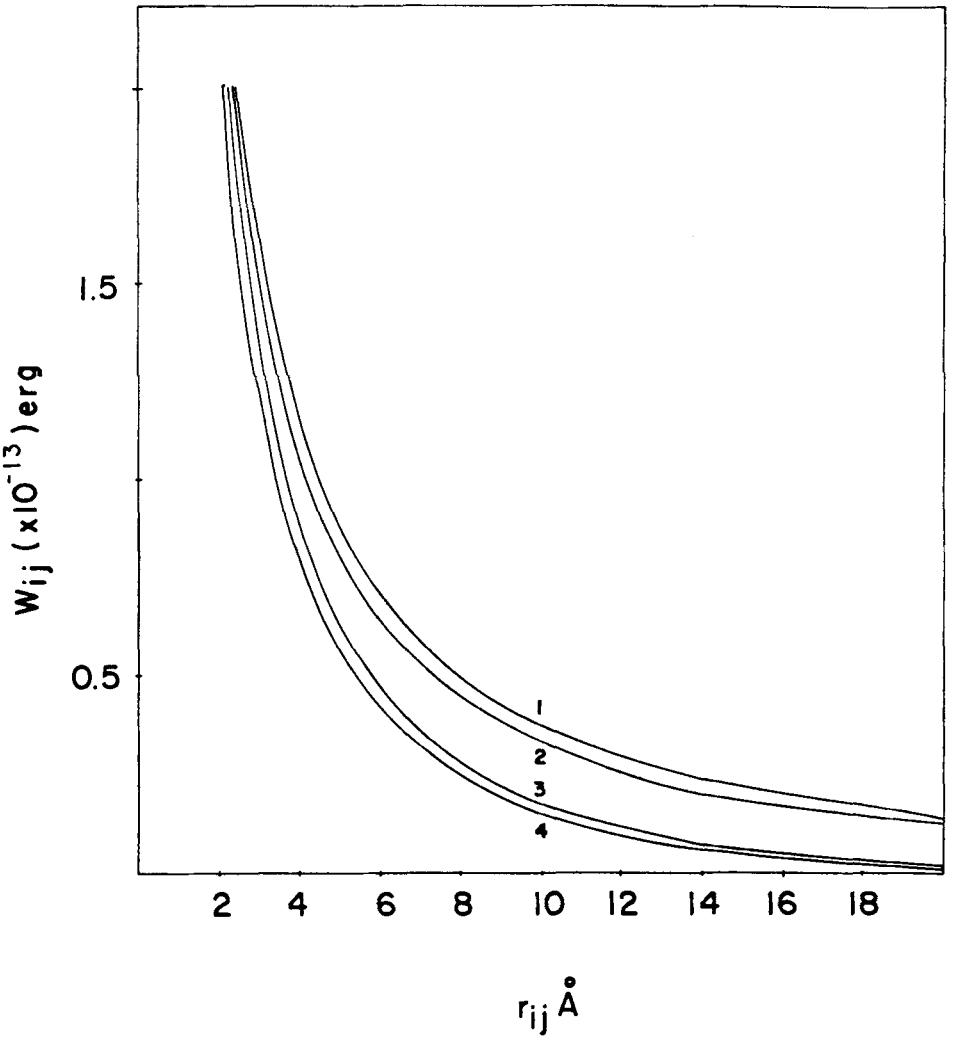

FIGURE 3. Plots of computed electrostatic free energy, W_{ij}, in units of 10^{-13} erg, for two charges i and j placed on a sphere at a separation distance r_{ij}. T = 25°C; dielectric constant D_{ext} = 78.5, D_{int} = 4.0. Four curves are shown: (1) I = 0.0 *M*, b = 27.0 Å, a = 29.0 Å; (2) I = 0.0 *M*, b = 18.0 Å, a = 20.0 Å; (3) I = 0.10 *M*, b = 27.0 Å, a = 29.0 Å; (4) I = 0.10 *M*, b = 18.0 Å, a = 20.0 Å; where *b* is the radius of the sphere, and *a* is the closest approach of counterions. The 27.0 Å sphere corresponds to the hemoglobin tetramer equivalent sphere, while an 18.0 Å radius would correspond to a monomer equivalent sphere. (From Matthew, J. B., Hanania, G. I. H., and Gurd, F. R. N., *Biochemistry*, 18, 1919, 1979. With permission.)

restraints on solvation. In the cases studied each protein charge site known to be titratable in the native structure has some solvent contact; thus they are all indeed at the protein-solvent interface.

Examination of known protein structures substantiates the assertion that protein ionizable charge sites are generally localized at the protein solvent interface. Rashin and Honig[63a] have recently reported the solvent accessibilities for the ionizable groups of 36 globular proteins. It was reported that less than 5% of all the ionizable groups of these proteins are not solvent accessible as determined by the Lee and Richards algorithm.[55] Of these buried "ionizable" groups, many are "buried" in salt bridges at or near the protein solvent

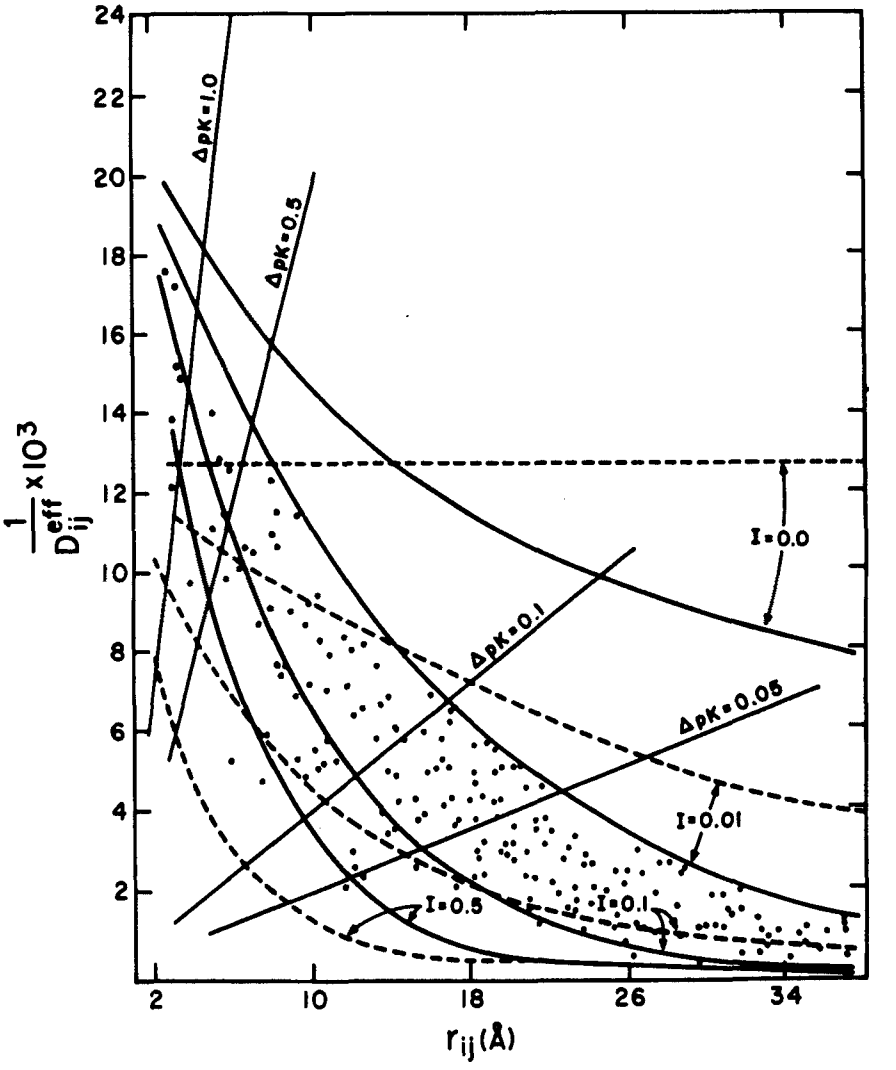

FIGURE 4. Energy of interaction for pairs of unit charges placed on a sphere with b = 18 Å, and a = 20 Å, T = 25°C, D_{ext} = 78.5, D_{int} = 4.0. The charges are separated by a distance r_{ij}. The energy is presented as the reciprocal of the effective dielectric constant D_{ij}^{eff}, for the particular charge pair. This parameter was calculated from the Tanford-Kirkwood procedure, Equation 1, for ionic strengths 0.0, 0.01, 0.10, and 0.50, shown as solid lines and from the Debye-Hückel screening relationship, Equation 3, at the same ionic strengths, broken lines. A sample of the parameters used in the calculations for RNase-S at ionic strength 0.01 is shown as solid circles. These values were derived from the Tanford-Kirkwood relations as modified by the incorporation of the mean static accessibility factor as indicated in Equation 7. The values of $(D_{ij}^{eff})^{-1}$ and r_{ij} which lead to four particular changes in ionization behavior are shown by the contours of constant ΔpK. (From Matthew, J. B. and Richards, F. M., *Biochemistry*, 21, 4989, 1982. With permission.)

boundary. Interestingly, six of the "completely buried" salt bridges are found in active site crevices of their respective enzymes.

4. Incorporation of Solvent Accessibility Parameter

In the modification of the Tanford-Kirkwood treatment, (SA), specific for each group, was incorporated into the calculation of W_{ij}.[56] The practical limits for SA of 0.98 to 0.02

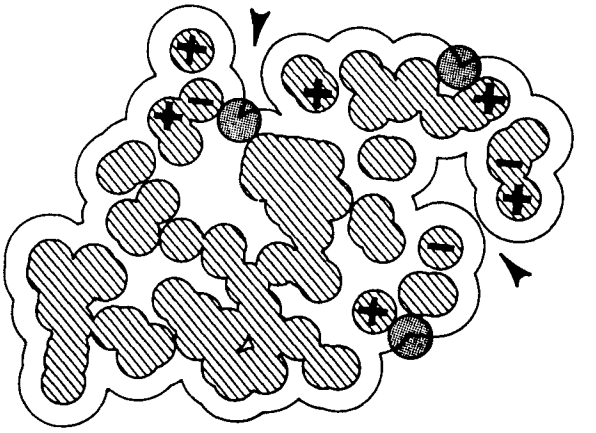

FIGURE 5. Diagram according to the approach of Lee and Richards[55] showing the cross section of Figure 1B. Three spheres of radius 1.4 Å are shown stippled to represent solvent water molecules rolling over the surface of the same myoglobin protein section tracing out the connecting curve of arcs defining the accessibility of each atom to the solvent.

corresponded to substantially complete solvation on the one and to virtually desolvated charge at the dielectric interface on the other. A formalism was adopted which linearly reduced the Tanford-Kirkwood interactive energy at a dielectric interface by the degree of solvent exposure

$$W'_{ij} = W_{ij}\,(1 - SA_j) \tag{5}$$

Equation 5 implies a reduction of electrostatic free energy for each group and leads to an apparent thermodynamic inconsistency:

$$W'_{ij} = W_{ij}\,(1 - SA_j) \neq W_{ij}\,(1 - SA_i) = W'_{ji} \tag{6}$$

Fortunately the iterative procedure used there and in subsequent work results in an effective averaging. An alternative formalism,[64]

$$W'_{ij} = W_{ij}\,(1 - \overline{SA}_{ij}) \tag{7}$$

where $\overline{SA}_{ij}$ is the average accessibility of sites i and j, eliminates the apparent inconsistency, results in a more rapid convergence of the iterative procedure, and yields individual site pK values and overall titration curves whose agreement with experiment is nearly indistinguishable from previous calculations.

The electrostatic interactive energies W'_{ij} for the pairwise interactions of all sites i and j on ribonuclease are plotted as points in Figure 4. It is shown that these values calculated for the Tanford-Kirkwood formalism at I = 0.01, when adjusted by $1 - SA_{ij}$, are distributed between an ionic strength of 0.01 as their upper energy limit and a coulombic screening curve equivalent to I = 0.50. Likewise, the interactive energies, W'_{ij}, for ribonuclease at I = 0.10 fall between the coulombic screening curves of I = 0.10 and 0.50. It is clear that the Tanford-Kirkwood formalism differs from the Debye-Hückel treatment in the critical 2 to 10 Å region of separation. However, once the choice of the appropriate effective dielectric

constant in Equation 3 is derived from the Tanford-Kirkwood model, the simple exponential can replace the full treatment for certain purposes.

Because of the role that the calculated accessibility plays in these computations, the variability due to the quality of the crystallographic data must be considered. Even in a refined high-resolution crystal structure, side-chain placement of surface charge residues is often completely arbitrary. To address this issue the accessibility results for two sets of sperm whale ferrimyoglobin coordinates have been compared.[60]

On the whole, the results were similar but the magnitudes were significantly different for many surface residues. Changes in atomic coordinates which altered the number of neighboring atoms within 6.40 Å of the principal atom gave accessibility differences which were traced to the repositioning of the principal atom or of its neighboring atoms. A comparison of all charged residue accessibilities between the two data sets indicates that about half of the accessibility values differ by 20% from the previously published data, and in some cases the difference exceeds 50%. It is clear that computations of surface areas and accessibilities for protein atoms need to be interpreted in the context of the refinement procedure and possible poetic license exercised.

5. Physical Interpretation of the Formalism

Different accessibilities of the various groups reflect the ability of the protein to restrict both solvent interactions and the effective sequestering of counterions. When SA_{ij} exceeds 0.95, the interaction energy between the two charge sites is negligible and neither one perturbs the pK value of the other. For lower values of SA_{ij} the protein prevents access (Figure 1B) of solvent and mobile counterions to the high local field of the charge sites: $\epsilon\psi > kT$. At an average accessibility of 0.05 or less, the protein is assumed to restrict the counterions to the ionic exclusion radius where the linearized Poisson-Boltzmann ionic strength approximation is valid, i.e., $\epsilon\psi < kT$. Hence, the charge sites at low accessibility are allowed to interact as calculated by the Tanford-Kirkwood formalism. The linear relation between W'_{ij} and SA_{ij} approximates the r^{-1} dependence of the local field around a point charge. The use of the SA_{ij} factor in reducing the electrostatic free energy estimate accounts for a higher effective coulombic shielding for solvent-exposed sites. This shielding, due to higher local ionic strength, can be interpreted as a higher effective local dielectric constant.[64]

The effects on charge-site interaction mediated by steric constraints on counterion approach are shown in Figure 6. Figure 6A shows the field calculated for two univalent ions immersed in a uniform dielectric with no mobile ions. In panels B through D, an anion is allowed to approach the cationic pair with various geometrical restrictions that control the field distributions.

6. Extension to Ion Site Binding

As discussed above the use of the solvent-accessibility factor in reducing charge site interactions introduces a higher effective local ionic strength for a solvent exposed site than predicted for a Poisson-Boltzmann distribution. Even with this higher local ionic strength specific sites can be located on the protein surface where the electrostatic potential exceeds 2 kT, an energy sufficient to localize a spherically symmetric ion with translational kinetic energy 3/2 kT. Drawing on the protein charge array and the known protein topography, Matthew and Richards have developed a procedure for locating the areas of high electrostatic potential at the protein solvent interface.[62] At a given pH and ionic strength the potential defines the site affinity. The site occupancy is given from the calculated site potential and ion concentration. In a case where proton site occupancies are affected the proton and ion site occupancies are calculated in an iterative fashion to reach the most stable configuration.

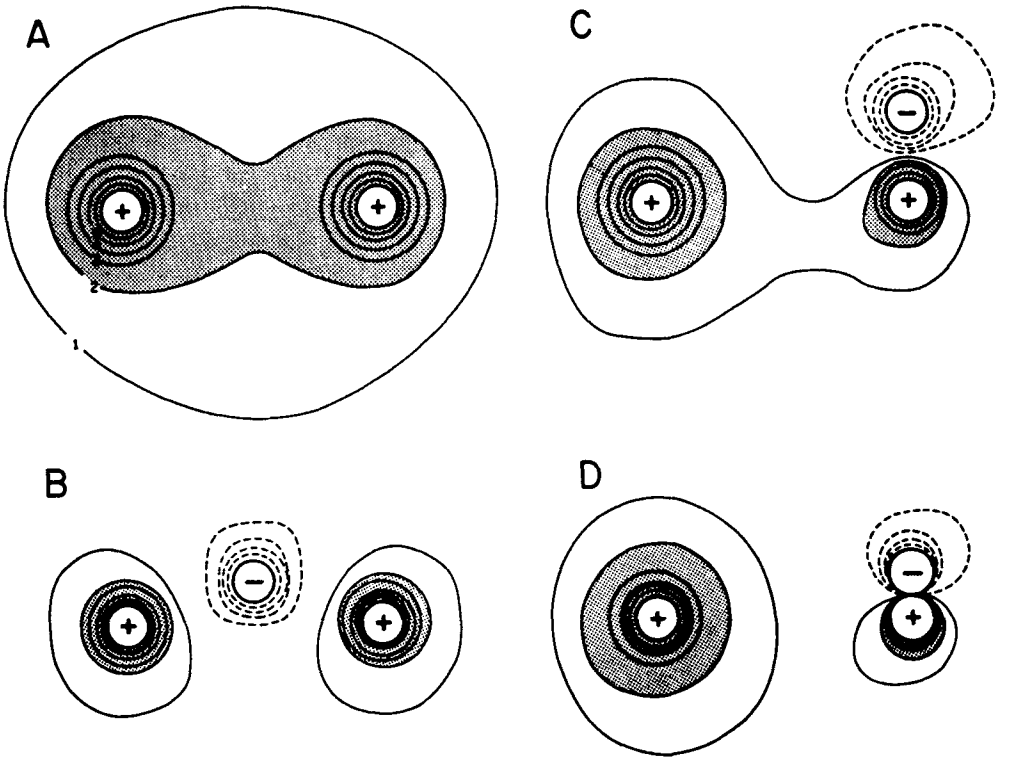

FIGURE 6. Potential fields calculated for two cationic unit charges, immersed in a uniform medium with a bulk dielectric constant of 70. The field contour values are in units of kT. The positive field values are shown as solid lines. The points were calculated on a 1-Å square grid. In each panel the cationic point charges are 18 Å apart. In panels B through D, a negative counterion is inserted in different positions. In (B) it is approaching the midpoint between the two cationic sites. In (C) it is assumed to be sterically excluded from intercalation but allowed to approach one charge asymmetrically to a distance of 7 Å. In (D) the counterion is close enough to form an ion pair with a separation of 3 Å. All positive contours of 2 kT and above are shaded. (From Matthew, J. B. and Richards, F. M., *Biochemistry*, 21, 4989, 1982. With permission.)

7. pH-Independent Partial Charges

The interiors of most proteins of known structure are composed of closely packed helixes and beta sheet structures whose underlying structural element is the peptide-peptide hydrogen bond. The uneven distribution of electrons in the carbon-oxygen bond and the nitrogen-hydrogen bond of each peptide unit gives rise to a net electric dipole moment. It has been accepted for some time that the alignment of these peptide dipoles parallel to a helix axis may give rise to a macrodipole.[23] Partial charges which lead to a peptide dipole value of 3.5 Debye (the value supported by in vacuo experimental evidence)[23] have been reported as: oxygen, −0.42; carbon, +0.42; nitrogen, −0.20; hydrogen, +0.20.[44] Given the numerous unique hydrogen bonding geometries in any single protein and their various distance relationships to the protein-solvent interface and/or ionized side chains, it is incorrect to uniformly assign the same set of partial charges to peptide dipoles throughout the structure; however, it is computationally convenient.

In calculations where these peptide dipoles are included, the charges are usually positioned at the N, C, O, and H atoms of each peptide group in the protein.

A number of in vacuo helix dipole calculations have been reported where the vacuum dielectric dramatically overestimates the magnitude and the extent of the electrostatic field attributable to the peptide dipole.[44,64a] Sheridan and Allen[45] and Allen[64b] addressed the relative

importance of the helix dipole to that of ionized residues in determining the electrostatic field around proteins. Their calculations led to the conclusion that a single charged side chain will dominate the helix dipole potential. Hydration, the presence of counterions and solvent dielectric will reduce the influence of the charged residue; however, these factors will no doubt influence the helix dipole field as well. A numerical method using the finite difference technique has been introduced[64c] as an alternative treatment of irregular dielectric boundary at the protein solvent interface. The protein geometry is inscribed on a Cartesian grid and the protein volume is assigned a low dielectric value, in a uniform high dielectric solvent. The calculation has been used to show that the protein geometry around the active site cleft can enhance the electrostatic attraction between the enzyme helix dipole moment and the charged substrate. Rogers and Sternberg[24] have recently reported a variation of the finite difference procedure which was used to study the dipole electrostatic packing energies between helixes in proteins. They found that the calculated electrostatic interaction energy between two helixes is strongly dependent on the proximity of the helix termini to the high dielectric region. For helixes with exposed termini the interhelix electrostatic packing energy was an order of magnitude lower than the 5 kcal interaction energy obtained using a uniform low dielectric model.[44,46,64a] This method, when extended to include the protein charges other than helix dipole and diffusible counterion distributions, may prove to be a valuable tool in understanding the propagation of electric fields across irregular boundaries.

D. Major Questions

Over 30 years ago Scatchard[65] listed four questions pertaining to ion binding by proteins: "How many? How tightly? Where? Why?" To these he later added "What of it?"[13] The list was subsequently extended by the questions "How distorted? How fast? How coupled? How cooperative?"[66] The following list of more specific questions is partly implied by those quoted above and may prove appropriate for a variety of proteins. They foreshadow the range of topics to be touched on below.

1. How should intrinsic equilibrium constants (or pK values) be arrived at?
2. How valid is it to treat binding sites of a given chemical nature according to a common intrinsic equilibrium constant which is modulated in each case by the summed effect of the impinging electrostatic fields of the other charged sites?
3. How is the binding of other ions interrelated with proton binding, and how is their binding behavior best incorporated in an overall treatment of electrostatic interactions?
4. What differences may result from the use of a formalism postulating fixed point charges in the array when motility of the protein structure or some degree of delocalization of charge within a chemical group would be anticipated?
5. In what ways connected with electrostatic effects do posttranslational modifications or effector binding control the function of a protein?
6. Are asymmetric charge distributions in proteins associated with the preferential binding of ions at given sites and with special ion exchange effects?
7. Will asymmetry of charge distributions affect functions such as pH-buffering, catalytic action, and docking of substrates or interacting proteins?
8. What is the role of electrostatic interactions in conferring relative stability on a given protein structure or in facilitating conformational transition?
9. In what ways connected with electrostatic effects do uncharged polar or polarizable structures influence the properties of a protein?

II. METHODS AND FORMALISMS

In this section we introduce the formalisms for modeling, interpreting, and predicting pH-dependent behavior of proteins. In each case the calculated or predicted values which can

be compared to experimental determinations depend on several model-independent parameters such as intrinsic pK values of charge sites and charge array geometry. Following are formalisms for calculation of: (1) effective pK values of charge sites, (2) the electrostatic contribution to stability, and (3) the identification of sites of bound ions and their occupancies. We shall also show how these electrostatic formalisms can be extended to the consideration of protein subunit assembly or protein-protein docking. Finally, we examine the pH-rate profile for the exchange of buried amide protons with solvent, thereby introducing the relation to protein dynamics and the role that electrostatic interactions can play in modulating structural fluctuations or reaction rates in proteins. In all cases we shall use the macroscopic effective dielectric model which we refer to as the solvent accessibility Tanford-Kirkwood algorithm.

As will be seen in the application section to follow, this dielectric model is extremely successful in predicting the pH and ionic strength dependence of diverse properties without evoking the use of adjustable parameters. When and if a more appealing dielectric model becomes available, a new pattern of formalism need not be developed. Rather, a new library of charge site interaction energies, W_{ij}, would be calculated (see Equation 2) and become incorporated into the existing formalisms outlined below.

A. Calculation of pK_i

The influence of the summed electrostatic fields at a given site controlling its effective pK_i is derived by an iterative scheme[59,61] and is expressed as:

$$pK_i = (pK_{int})_i - \frac{1}{2.303\ RT} \sum_{i \neq j}^{n} W'_{ij} Z_j = (pK_{int})_i + \sum_{i \neq j}^{n} \Delta pK_{ij} Z_j \qquad (8)$$

where $(pK_{int})_i$ is an intrinsic equilibrium constant in the absence of effects from other charged sites on the protein, W'_{ij} is the work factor based on the mean SA treatment for the interaction of unit charges at the two sites i and j, and Z_j is the fractional occupancy of the jth site. For a given pH the initial set of Z_j values is calculated from the pK_{int} values with the Henderson-Hasselbalch relationship. A set of effective pK values (pK_i) are now calculated (Equation 8), giving rise to new Z_j values which are used to calculate a new set of pK_i values. The iterative scheme is considered converged when two consecutive iterations yield a set of Z_j values whose sums differ by less than 0.01.

At a given pH, the charge distribution on the protein confers a unique effective pK_i value on each titratable site i. As expressed above, the coulombic influence on site i exerted by each of the other sites j is proportional to Z_j and inversely proportional to the average solvent accessibility SA_{ij} and the intercharge distance r_{ij}. Figure 7 shows the final iterative calculation of pK_i at five pH values for two sites in deoxyhemoglobin tetramer, Val-1α (A) and His-117β (B), respectively. In Figure 7, the individual $\Delta pK_{ij}Z_j$ contributions (Equation 8) are summed cumulatively from left to right along the abscissa following the j site residue number in the respective chain.[61]

The pK_i of almost every group is found to vary with pH. It is convenient to define the parameter $pK_{1/2}$ as the pH at which a particular group is half-titrated. In the absence of electrostatic interactions, $\sum_{i \neq j} \Delta pK_{ij}$ goes to zero, pK_{int} equals $pK_{1/2}$, and the variation of pK_i with pH goes to zero also. Curves corresponding to ΔpK_{ij} values of 0.50, 0.10, and 0.05 for unit charge were given in Figure 4.

B. Intrinsic pK Values

Intrinsic proton dissociation constants for acidic and basic groups of proteins are based on measured apparent pK values for model compounds. An ideal model compound contains

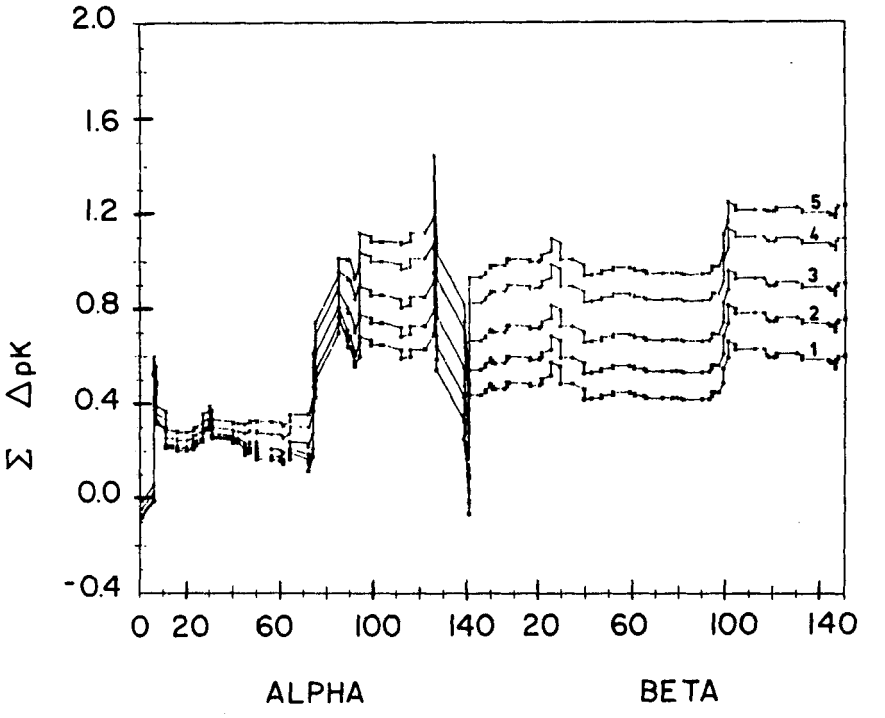

FIGURE 7A. Summation plots of intramolecular electrostatic contributions, ΔpK_i, defined in Equation 8, to the value of pK_i of the amino acid residue Val-1α in deoxy Hb tetramer, computed at I = 0.01 *M* and at pH 5.0, 6.0, 7.0, 8.0, and 9.0 (curves 1 through 5, respectively). The sums are cumulative, showing the residue sequence numbers of the groups in their α and β chains. A contribution attributed to a particular site represents the summed effect of that site from each dimer. In the case of Val-1α, being very near the hemoglobin tetramer symmetry axis, the effects are nearly equal between dimers. The net values at the extreme right represent the electrostatic potential acting on the deoxy Hb Val-1α site at the given pH.

one ionizable group but not other charge sites. Even small molecules are subject to secondary intramolecular interactions which affect their conformations and the pK of constituent groups.

Two categories of proton binding sites are distinguished.[61,64,67,68] The first comprises all groups with normal pK_{int}: terminal carboxyl, 3.60; Asp, 4.00; Glu, 4.50; His N^{π}, 6.00; His N^{τ}, 6.60; terminal amino, 8.00; Cys, 9.00; Tyr, 10.00; Lys, 10.40; and Arg, 12.00. All of these values are consistent with expected values based on model compounds such as isoasparagine and isoglutamine for the aspartyl and glutamyl groups.[69] ^{13}C-NMR studies on the titration behavior of Gly-Gly-X-Gly-Gly pentapeptides further substantiate the use of these values: X = Asp or Glu;[40] X = His or Tyr;[70] X = Arg or Lys.[41] The terminal amino and carboxyl values depend on the particular amino acid residues involved. In the pentapeptides described these values group around 8.2 and 3.2, respectively. Since it is difficult to define precisely the influence of a neighboring hydrogen-bonding group on the pK of a dissociable group, the arbitrary practice is often followed by adjusting the pK_{int} by ±0.50 to allow provisionally for the stabilizing effect of the interaction at a particular site.[29,56,61] Where the structural indications are negative or tenuous, these adjustments are best omitted.[14,62,63] The converse (i.e., the effect of a nonpolar environment) is represented at the extreme by the second class referred to as "masked" nontitratable groups. These residues are generally potential charge sites which are buried in their neutral form well within the low dielectric of the protein.[9,71] This class is most clearly demonstrated in the hysteresis observed in the titration of myoglobin or hemoglobin involving the histidine titration before and after the

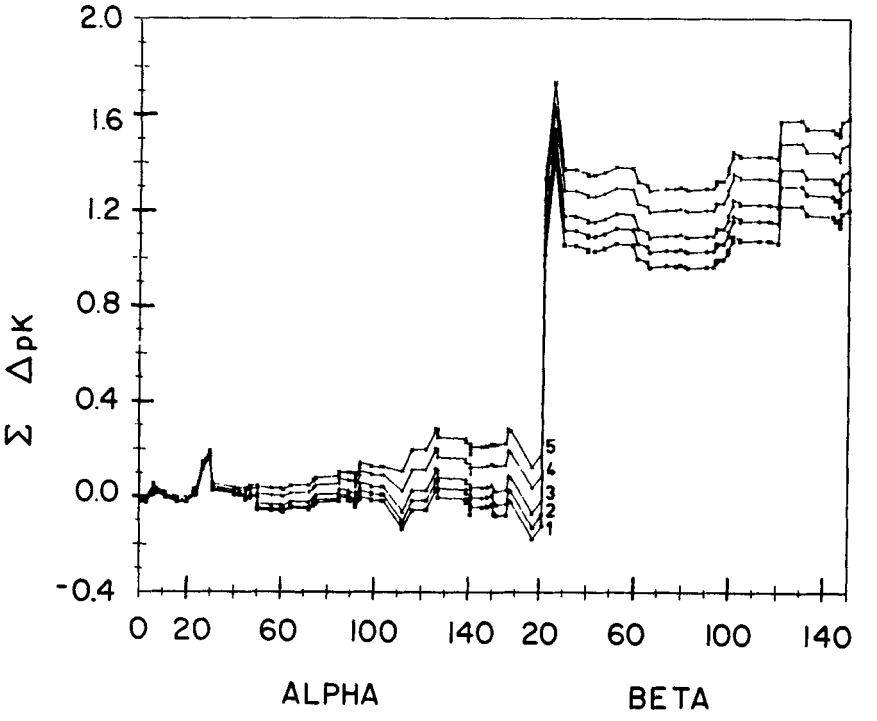

FIGURE 7B. Summation plots, corresponding to those in (A) and under the same conditions, showing electrostatic contributions to the value of pK_i of the amino acid residue His-117β. The sharp rises at Glu-22β and Glu-26β illustrate the dominating effect of close interaction with these two negative sites, yielding the extremely high pK_i value of 8.2 for His-117β at pH 9.0. In contrast to Val-1α, the His-117β site is off the dyad axis and the effects are primarily the result of one dimer site, the second being generally at a greater r_{ij}. (From Matthew, J. B., Hanania, G. I. H., and Gurd, F. R. N., *Biochemistry*, 18, 1919, 1979. With permission.)

exposure to acidic pH.[9,38,71] This masking with shift of pK value probably reflects the energetics of solvent stripping required to bury the residue and is an example of strong linkage between conformational and titration states.

The intermediate case where the pK_{int} is considered to be altered in a less polar environment but still titratable is not treated. The variance of apparent pK values for model compounds in mixed solvents of lower dielectric value is well established, anionic acids being more sensitive than cationic acids because of an enhanced charge pair interaction in the lower dielectric medium.[7,72,73] In either case, the equilibrium is expected to shift to favor the neutral species in the lower dielectric. For a protein residue this expectation is complicated by the partitioning of the proton between the bulk-solvent dielectric and the protein-solvent dielectric interface; however, this effect is usually discussed in terms of the "self-energy" associated with an ion at lower values of dielectric constant. Because the charge-site interactions at the protein surface are consistent with effective dielectric values greater than 50 (see Figure 4), a formulation has not been introduced which would create a continuum of pK_{int} values between that in water and that corresponding to the uncharged (masked) state in the low dielectric interior.

C. Electrostatic Stabilization

The electrostatic free energy of placing a pair of unit charges i and j on the protein is W'_{ij} where W'_{ij} is 2.303 $RT\Delta pK_{ij}$ kcal/mol. By summing W'_{ij} terms for all pairwise inter-

actions, the total electrostatic free energy with respect to a completely solvated noninteracting charge configuration is obtained:

$$\left(\Delta G_{el} = \frac{1}{2}\sum_{i}^{n}\sum_{j\neq i}^{n} W'_{ij}\, Z_i Z_j\right) = \left(\frac{2.303\ RT}{2}\sum_{i}^{n}\sum_{j\neq i}^{n} \Delta pK_{ij}\, Z_i Z_j\right) \quad (9)$$

in which Z_i and Z_j represent the final charge occupancy for each site calculated from the iterative procedure represented in Equation 8 at any given pH or ionic strength.[29,71,74,75]

D. Specific Ion Sites

1. Location

In earlier work we relied on chemical or crystallographic data for specific ion site location.[64,68,74] The coordinates chosen for many current studies are determined by locating the regions of significant electrostatic potential at the protein-solvent interface. The electrostatic potentials external to the protein were calculated as a sum of simple coulombic terms from all charge sites to each point of influence, interacting through a medium of dielectric constant 50. Because the potential at a given site varies with pH and ionic strength, the identification and selection of the high potential sites was facilitated by carrying out the calculations over a range of ionic strengths to find those sites that persist as the fields collapse toward the protein surface. For example, a site whose potential is calculated to be 5 kT at 0 ionic strength, 3 kT at 0.01, and 2 kT at 0.10 *M* would express monovalent anion affinities of 150, 20, and 7 M^{-1}, respectively, indicating significant occupancy in each case. Unless other information about conformational effects is available, no side-chain rearrangement has been allowed for in response to binding. Thus, arbitrary structural rearrangements are never included and the calculated magnitudes of interaction may be underestimated. Nonelectrostatic contributions to binding are neglected in these calculations.

The calculated electrostatic potential contours, expressed in units of kT, in the active site of ribonuclease S are shown in parts A and B of Figure 8 for pH values of 8 and 6, respectively.[62] The pH-dependent development of the anion binding site is evident. At pH 8, where the two active-site histidines are essentially unprotonated, with $pK_{1/2}$ values of ~6.3, the active-site potential is 2 to 3 kT compared with 5 to 6 kT at pH 6. Figure 8C illustrates the long-range effect of binding a divalent anion in this site at pH 6.0. The effect of including two negative charges is offset in part by an increase in protonation of the active-site histidines.

Nucleotides such at 2′-CMP or 3′-CMP binding to the active site of RNase S present the additional complexity of substantial nonelectrostatic components to the binding energy. In these cases the anionic portion of the ligand may have to compromise the charge placement that would maximize electrostatic interaction in order to accommodate the steric restraints conferred by hydrogen bonding or nonpolar interactions. In these cases the possible variation in the pH-dependent component of binding is evaluated by testing the sensitivity of charge placement within the binding site.[62]

2. Treatment of Specific Ion Sites

The presence of bound anions, such as chloride and inorganic or organic phosphates, requires special consideration in a more general sense. These ions contribute to coulombic influences and may themselves represent titratable proton sites. They also have the ability to diffuse, relieve, or enhance interactions rather than to respond only by shifting protonation state. Ambiguities concerning the thermodynamics of ion binding with regard to the pH-dependent binding equilibrium are treated by one or another of the following approaches.[68]

The pH dependence of an ion binding constant is calculated by comparing the pH-

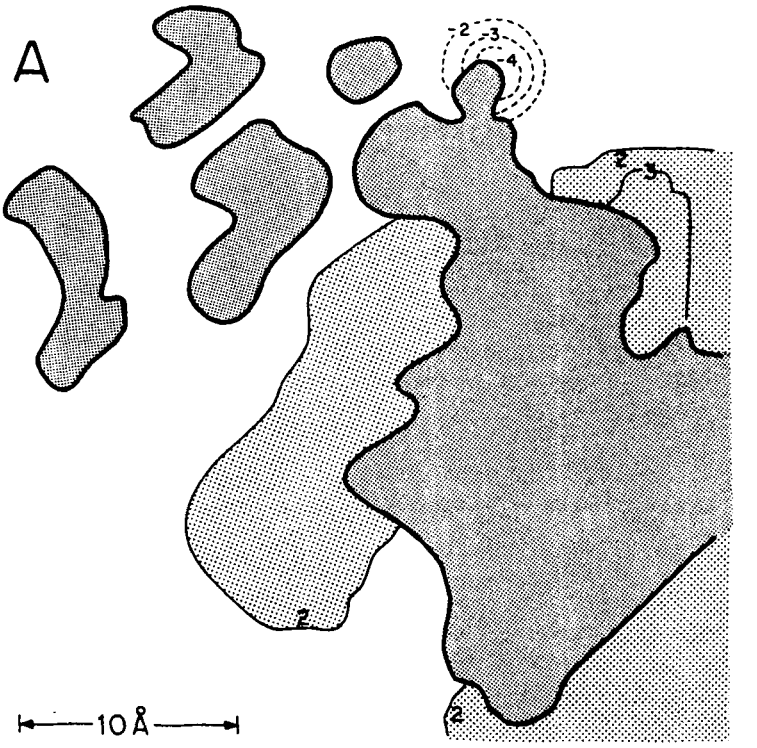

FIGURE 8. Calculated electrostatic field for a cross section through the active site of ribonuclease S perpendicular to the y axis at position y = −6. The calculations were made on a square grid 1 Å on a side. The heavily shaded areas are inside the van der Waals envelope of the protein. The contour interval is 1 kT. Positive values are given by the solid contour and negative values by dashed contours. Positive field contours of 2 kT and above are lightly shaded. (Panel A) pH 8.0, anion site(s) unoccupied; (panel B) pH 6.0, anion site(s) unoccupied; (panel C) pH 6.0, phosphate in anion site A2. These contours were drawn for an effective ionic strength of zero. (From Matthew, J. B. and Richards, F. M., *Biochemistry*, 21, 4989, 1982. With permission.)

dependent protein charge array stabilities, ΔG_{el}, in the presence and absence of full ligand occupancy. The difference in ΔG_{el} in the presence and absence of charged ligand is assumed to represent the pH-dependent component of the ligand binding constant. Univalent anions such as chloride are included as nontitrating negative point charges. If the ligand is itself titratable, its proton affinity is allowed to vary in the iterative procedure in the same manner as a protein charge site. Intrinsic pK values for the free anion, such as inorganic phosphate, are assigned to approximate its proton affinities in solution.[68]

These computations which rely on the energy difference between an all-or-none ligand occupancy can be rigorously applied to cases like the 2,3-diphosphoglycerate-hemoglobin interaction where a single site with large binding constant confers full occupancy under all simulated conditions.[64] However, in a case such as ribonuclease S, the number of significant anionic binding sites is two or more over a wide range of pH. Therefore, the possibility of cross interactions, either direct or indirect (i.e., through perturbation of proton site occupancies), requires that ion site occupancy be treated overtly in the iterative procedure.[62]

As discussed above, the coordinates of all recognized high potential sites (positive or negative) are identified for the pH range of interest. This involves the examination of the field potentials drawn from the converged proton site occupancies at each pH. For example,

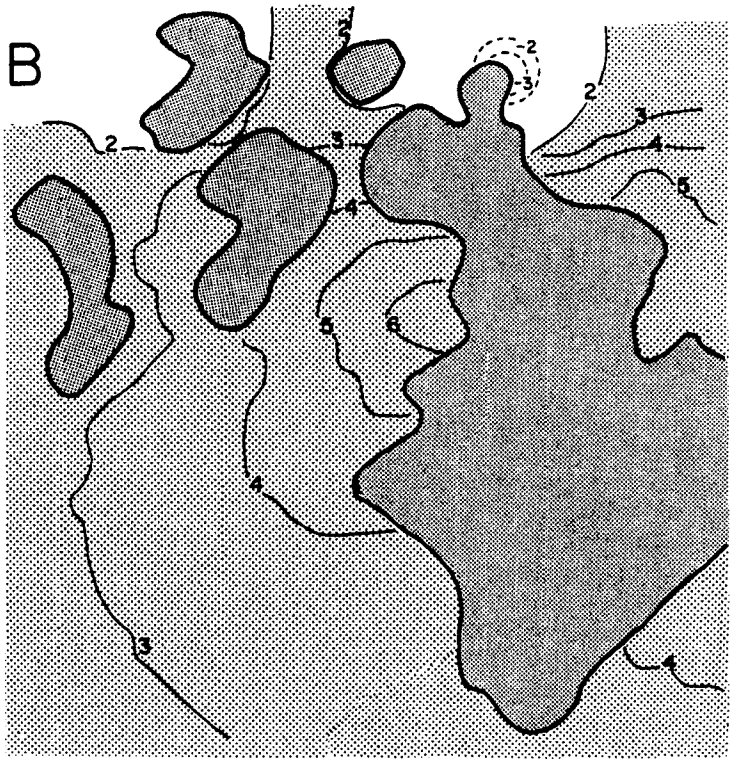

Figure 8B

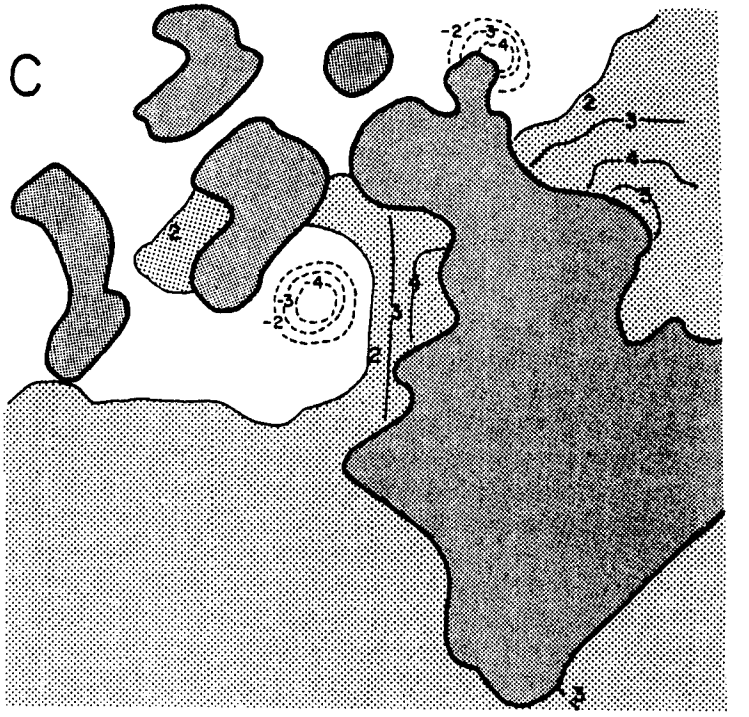

Figure 8C

plots of the electrostatic potential at the RNase S surface show two sites with exceptionally high positive potential at pH 6.0 (Figure 8B). This number increases to five by pH 4.0. The ion site coordinates are accordingly included in the charge site list. Their occupancy or net partial charge is determined in each iteration by the electrostatic potential of the site and a specified ion concentration:

$$Z_{ion} = K_a [Ion]/(1 + K_a [Ion]) \quad (10)$$

where $K_a = 10^{(\epsilon\psi/kT)}$. Thus, the proton sites influence the ion occupancy, which in turn influences the proton site pK_i values, and the ion-site cross interactions are taken into account. In the case of an ion whose binding is enhanced by specific electronic or other interactions with the protein site, further terms will enter.[13,37,38,56,62,66]

E. Summary of Computational Sequence

Figure 9 summarized in flow chart format the relationships between variant and invariant parameters and the calculated quantities discussed before.

If one wishes to explore an alternative dielectric model a new set of work factors could easily be substituted. For example, a microscopic dielectric model, if computationally feasible, could prove useful. These calculations of protein coulombic interactions, in which details of the molecular structure are explicitly employed, could allow the evaluation of effective dielectric values for unique local geometries that depend heavily on the relative positions and types of the interacting atoms.

F. Macromolecular Assembly

The overall free energy of association, ΔG_{assoc}, may be taken[74] as the sum of contributions as follows:

$$\Delta G_{assoc} = \sum_{i}^{n} (\Delta G_{i,el} + \Delta G_{i,h} + \Delta G_{i,conf} + \Delta G_{i,vw} + \Delta G_{i,hb}) + \Delta G_{buried} + \Delta G_{S-S} + \Delta G_{vib} \quad (11)$$

Here the terms within the summation over all residues refer, respectively, to electrostatic, hydrophobic, conformational, van der Waals, and hydrogen bonding contributions. $\Delta G_{S\text{-}S}$, the contribution from disulfide linkages,[76] is rarely an important term for protein-protein association.[77] ΔG_{buried} refers to contributions from changes in burial of titratable groups from the solvent interface. ΔG_{vib} is the free energy contributed by the additional vibrational states in a protein assembly.

The most important purely destabilizing contribution, $\sum_{i}^{n} \Delta G_{i,conf}$, represents the effect of freezing out translational and rotational motions. Following the method of Page and Jencks,[78] Chothia and Janin[79] estimate this contribution to be in the range of 20 to 30 kcal/mol in the formation of the insulin dimer, the trypsin-pancreatic inhibitor complex, and the hemoglobin $\alpha\beta$ dimer. The main counterbalancing contribution is the hydration or solvent layer release, often referred to as hydrophobic free energy of association, $\sum_{i}^{n} \Delta G_{i,h}$. This factor for protein-protein association has been correlated with the extent of burial of protein surface on as-

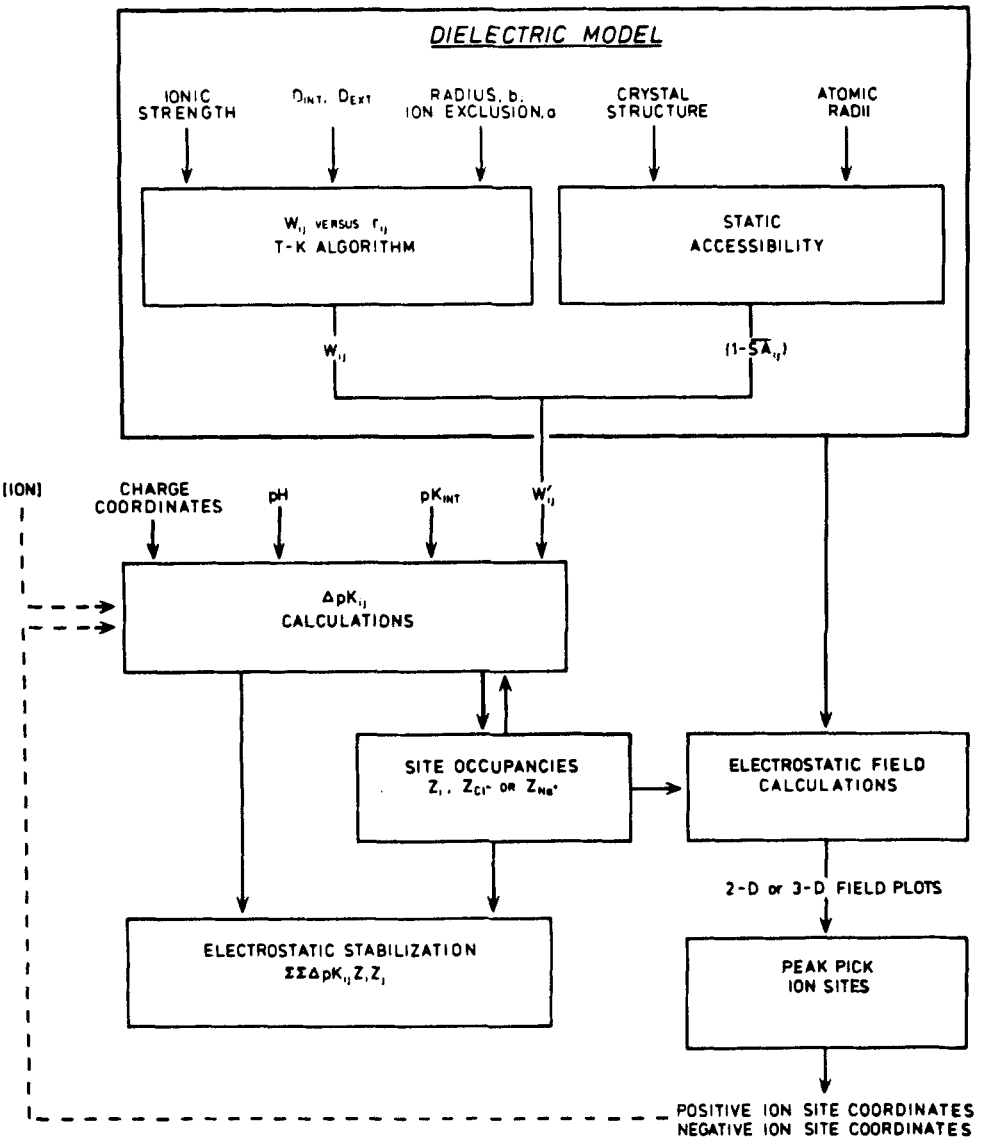

FIGURE 9. This figure describes the flow of the computations involved in the calculations that have been presented in the text. All the calculations stem from the computations that take place within the dielectric model box. Two separate computations take place at this level. (1) Computation of the $\overline{SA}_{ij}$ terms. The input for these computations consists of the X-ray crystallographic coordinates of the protein being studied and the atomic radii of the various atoms in the protein molecule. (2) Computations of W_{ij} vs. r_{ij} table. For a given protein, a radius b and an ion exclusion radius a are defined. Using D_{int}, D_{ext}, and the Tanford-Kirkwood algorithm, a numerical table of W_{ij} values is calculated. At every chosen ionic strength, a W_{ij} value corresponds with one r_{ij}. The charge coordinates, pK_{int} of various amino acid side chains, and the pH range over which the calculations are performed are entered at the next stage of the calculations. The charge coordinates are used to calculate r_{ij} for all pairs of charges. Each r_{ij} corresponds to a W_{ij} value in the previously calculated W_{ij} table. The W_{ij} values that are selected from the table are modulated by the previously calculated term as described in the text. The resulting W'_{ij} values are the core of the further calculations that are described in the text.

sociation.[55,79,80] These two terms are often viewed as almost completely counterbalancing each other.

The discrete charge electrostatic model provides a quantitative method of calculating the contribution of ΔG_{el} to ΔG_{assoc}. The electrostatic contribution to association may be estimated at each pH value from the difference in the summed electrostatic free energy terms for all

charge sites $\sum_{i}^{n} \Delta G_{i,el}$, in the assembled complex minus those for the isolated subunits according to the modified Tanford-Kirkwood theory,[64,81,82] equivalent to the expression in Equation 9.

G. Structural Dynamics; Hydrogen Exchange

The importance of charge interactions in modulating hydrogen exchange in model compounds has been recognized for some time.[83-85] Current models for proton exchange incorporate the dynamic nature of the structure to explain exchange data from the interior of a protein. Protons on the protein surface (freely exposed to solvent) have exchange rates similar to small model compounds, while buried exchangable protons (lacking solvent contact in the static structure) are considerably slowed. In contrast to model compounds, the slowly exchanging protons have a more basic pH_{min} and deviate from first order kinetics with respect to catalytic ion concentration. The fact that completely internalized amide protons in a native protein have slow, but measurable, exchange with solvent implies that in solution the protein undergoes internal motions which render buried protons accessible to solvent.[42,63]

The rate of chemical exchange, k_{obs}, for a single amide proton is given by:

$$k_{obs} = k_a [10^{-pH}] + k_b [10^{pH-pK_w}] (10^{0.05t}) \quad (12)$$

where pK_w (0°C) = 14.94 with temperature correction $10^{0.05t}$, where t is the temperature in °C.[86] For model compounds, such as poly-DL-alanine, k_{obs} is first order in the acidic and basic pH regions with the pH of minimum rate (pH_{min}) occurring at 3.1.[87] The hydrogen exchange reaction at a protein amide can be described by the same kinetic scheme. Each pseudo-first-order rate constant k_a and k_b can be expressed in terms of the intrinsic rate for the model compound and a modifier term reflecting the influence of the protein on the kinetic process:

$$k_a = k_{int}^{H+} A (e^{(\Delta G_\alpha^\ddagger/kT)}) \quad (13)$$

$$k_b = k_{int}^{OH-} A (e^{(\Delta G_\beta^\ddagger/kT)}) \quad (14)$$

where k_{int}^{H+} and k_{int}^{OH-} are the intrinsic rates for the acid and base catalyzed chemical step from the model compound, A is a preexponential factor accounting for the non-pH-dependent effects of the protein conformation, and $\Delta G_\alpha^\ddagger$ and $\Delta G_\beta^\ddagger$ are the apparent activation energies conferred by the protein charge array on the acid and base catalyzed steps. These free energy terms, in turn, can be written as a sum of separate free energy contributions to the barriers:

$$\Delta G_a^\ddagger = \Delta G_{el} + \Delta G_q^+ ; \quad \Delta G_b^\ddagger = \Delta G_{el} + \Delta G_q^- \quad (15)$$

where ΔG_{el} is the pH-dependent electrostatic component of the overall protein stability and ΔG_q^+ and ΔG_q^- are the calculated free energies required to bring the catalytic anion or cation to a particular amide, k, in the presence of the electrostatic field of the formal charge arrays. For the computation of the field effects at specific protons, a charge + (for acid catalysis) or − (for base catalysis) is placed at the position of the amide N. The interaction of this charge with all other protein charges is summed to get ΔG_q^+ or ΔG_q^-:

$$\Delta G_q^{+/-} = \sum_{i=1}^{n} W_{ik} (1 - \overline{SA}_{ik}) Z_i (^{+/-}1) \quad (16)$$

The static accessibility of internal amides, SA_k, is normally zero. Whether 0 or finite, this value is averaged with SA_i to get SA_{ik}. The parameters for estimating W_{ik} are the same as those used for the formal charge W_{ij} for the appropriate distance r_{ik}.

The kinetics of deuteration of imidazole,[88] histidine, and related compounds[89] in aqueous solutions have been reported as a function of pH. The slow step involved the attack of hydroxide ion on the positively charged form of the imidazole ring leading to an ylide intermediate followed by the fast reaction of the ylide with D_2O. The kinetic scheme is expressed as follows:

$$k_{obs} = k_b K_w/(K_i + H^+) \quad (17)$$

where k_{obs} is the first-order rate constant determined from the exchange experiment, K_i is the apparent dissociation constant of the imidazole, K_w is the ion product of water, and k_b is a second-order rate constant:

$$k_b = (k_{int}^{OH^-}) A (e^{\Delta G_q^-/kT}) \quad (18)$$

where $k_{int}^{OH^-}$ is the intrinsic rate constant for free imidazole A and ΔG_q^- is defined above. There is no ΔG_{el} term required if the reactive imidazole protons are accessible to solvent in the native structure and it is assumed that no overall conformational change of the protein is required for exchange to occur within certain time limits.

III. INDIVIDUAL pK VALUES AND OVERALL TITRATION CURVES

All the characteristics of the pH-dependent phenomena in proteins stem from changes in the formal charge array that are determined by proton site occupancy and specific ion binding. The pH dependence of the proton site occupancy is described in terms of appropriate intrinsic pK values, pK_{int}, modulated by the field of the formal charge array. In some cases stabilization or destabilization by hydrogen bonding interactions may be acknowledged by formal adjustments of pK_{int} by ± 0.50 unit to reflect interaction energies of approximately ± 700 cal/mol.[61,81,90,91]

This section deals with the direct comparison with theory of titrations of individual groups and of overall titration curves. It will be followed by sections emphasizing one or another inherent aspect of the electrostatic behavior of certain proteins specifically illuminating their structure and function.

A. Myoglobins

The initial work published in 1974 and 1975 by Shire and co-workers[56,92,93] in developing the solvent-accessibility treatment was based on information much of which has since been revised. For example, the crystal coordinates from sperm whale myoglobin published by Watson in 1969[94] were replaced by higher resolution data of Takano in 1977.[22] Also, the original sequence of Edmundson[95] defined residue 122 as Asn rather than Asp as now accepted.[96] The assumed absence of a required charge on residue 122 led Shire et al. to make an ad hoc compensating assumption[56] that temporarily discouraged the progress of this work until the correct assignment came to our attention. The titration behavior of a few individual groups in myoglobins was known, but correct assignments were not yet fully established.[27,39,93]

The initial formal treatment also differed in a number of details from that which evolved shortly thereafter. The pK_{int} values for the classes of dissociable groups were based initially

on small molecule models but were adjusted by iterative curve fitting.[56] The adjusted pK_{int} values remained within rational limits, indicating that the broad outlines of the treatment were coherent and reasonable. However, it was felt that systematic errors could be propagated by this procedure, and it was set aside in all subsequent work. The locations of charges in carboxyl, imidazole, and guanidyl groups were taken at average positions intermediate between the particular electronegative atoms.[56] However, alkylation studies of imidazole groups had shown selectivity between N^{τ} and N^{π} in a number of instances.[32,97,98] Furthermore, in a polarizable group, access to solvent and counterions would be expected to direct the formal charge to the more exposed potential site or to the one more compatible with impinging electrostatic fields from neighboring protein groups. In subsequent work, therefore, the degree of static solvent accessibility has been taken as the primary criterion of charge site location with a secondary criterion of dominant interaction with another polar or charged protein group, such as one forming an ion pair with the group in question.[81,82,91]

1. Histidine Titrations

Before the work of Shire and co-workers had been completed, an ambitious project was launched to study the titration behavior of a series of myoglobins homologous with sperm whale myoglobin. The experimental venture consisted of three parts. First, the determination was made of each myoglobin sequence to establish the highly conservative patterns of evolutionary substitution and to provide charge site loci with reference to the sperm whale myoglobin structure.[99] Second, full titration curves for each myoglobin available up to 1975 were determined for the observable histidine C^{ϵ} proton NMR resonances in D_2O.[27] Third, assignment of NMR signals to specific residues was based in part not only on comparisons between myoglobin species but also, to an essential degree, on observations of carboxymethylated and other chemical derivatives.[27] The observable proton-NMR signals were assigned to the more mobile external ones in distinction to the masked or buried residues.[9,100]

The carboxymethylation of histidine residues of sperm whale myoglobin in solution and in the crystalline state had been worked out previously to show patterns consistent in many but not all details with the crystalline protein structure.[32,100] The assignments of the four invariant titrable histidine residues 36, 48, 81, and 119 were so based. For example, residues 36 and 48 are distinguishable by comparison of carboxymethylation products in the dissolved and crystalline states.[32,100] Residue 119 forms the N^{π}-carboxymethyl derivative only slowly in the crystalline state. Residue 81 was identified by a separate modification of the amino terminus in such a way as to perturb the C^{ϵ} resonance of this nearby histidine residue.[27] All other assignments of histidine residues were made by suitable comparisons between species, helped by the conservation of both the chemical shift limits and the pK ranges of given residue positions. The NMR measurements,[39] the complete set of sequences, and the new crystal coordinates[22] could not be brought together until 1977.

The characteristic C^{ϵ} proton titration behavior of the four invariant histidine residues is illustrated in Figure 10 for human myoglobin in which no other titratable histidine residues are present.[27] The titrations of residues 48 and 81 span normal chemical shift limits and fit normal patterns. In general, the same may be said of all titrations of variable histidine residues encountered in the other myoglobins.

The titration curves for residues 119 and 36 are atypical at the higher pH values. A reversal of chemical shift trend is seen clearly for residue 119 in Figure 10. The high pH range for residue 36 is also affected, as analyzed for the case of sperm whale myoglobin in Figure 11. The pK for the secondary process is 8.6 which is close to the hemic acid (heme-bound water) titration value.[91] Both these residues, therefore, sense a propagated conformational change probably driven by the hemic acid dissociation which may also be associated with some widespread structural changes revealed by crystallography at high pH.[42]

Residue 36 stands apart from the others in two further respects. The first is that it is

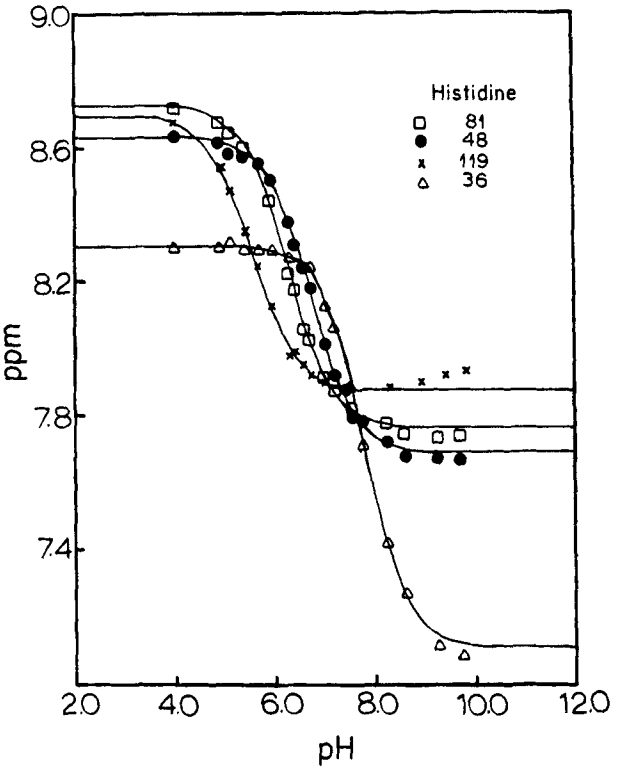

FIGURE 10. Titration curves for human myoglobin with histidine residues identified on the figure. (From Botelho, L. H. and Gurd, F. R. N., *Biochemistry*, 17, 5188, 1978. With permission.)

subject to carboxymethylation at a finite rate only under conditions of high salt concentration either in the crystalline state[100] or in solution.[39] By contrast, the carboxymethylation is negligible in solution under the normal low salt conditions of the NMR study.[32,39,97] Hence, the crystalline structure is clearly not retained in solution with respect to residue 36, but appears to be so for the other histidine residues[32,39,100] under experimental conditions. The crystalline structure was accordingly adjusted by side-chain rotation to bring Glu-38 within a suitable hydrogen bonding configuration with His-36. This close interaction could contribute to the lack of reactivity towards bromoacetate under conditions in which the proton titration takes place, as well as to the relatively high pH range in which the titration occurs.

The second special characteristic is that residue 36 does not titrate over any part of the pertinent pH range if the ferric iron is complexed in a low spin form such as with azide or cyanide, or in a diamagnetic complex of the ferrous iron. The latter two forms differ crystallographically in numerous details from the ferrimyoglobin form.[101,102] In the case of the azide derivative, it was possible to identify the C^{ϵ} proton resonance of residue 36 and so to show directly that its chemical shift was insensitive to pH.[39] The observations suggest that heme ligand state controls the structure in the region of residue 36 in all-or-none manner through strong conformational linkage, but not necessarily in a manner comparable to the control by high salt concentration.

Figure 12 illustrates the variety of titration relationships to be found among the histidine residues substituted between one myoglobin species and another.[91] For every residue, both the characteristic chemical shift limits and the titration pattern were well conserved from

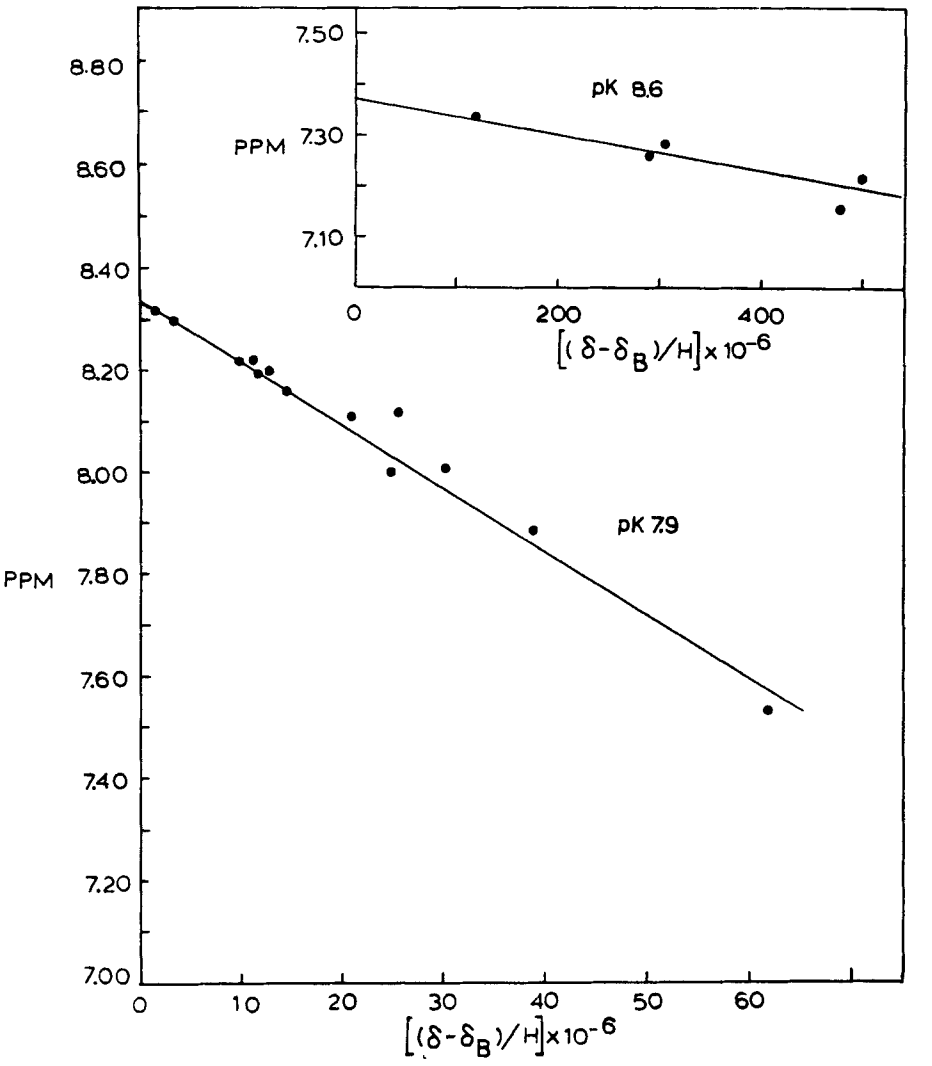

FIGURE 11. Linearized plots to determine pH dependence of chemical shift of histidine-36 C-2 proton of sperm whale myoglobin in terms of dominant processes in the lower and higher (inset) pH ranges. (From Botelho, L. H. and Gurd, F. R. N., *Biochemistry*, 17, 5188, 1978. With permission.)

one myoglobin to the next, adding strength to the evidence from reactivity patterns,[98] ^{13}C-NMR observations,[103] and immunologic reactions[104,105] that the protein structures are closely similar. Figure 13 shows, moreover, that the pK value for a particular histidine residue position is conserved between the myoglobin species.[27] In all cases, except for residues 36 and 119, discussed before, the change of chemical shift value over the pH range was normal.

Figure 14 shows the relations between the observed pK_{obs}, and computed, $pK_{1/2}$, values (Equation 8) for all titratable histidine residues in 12 different myoglobins.[91] Four other species, corresponding closely to one or another panel,[91] were not included.

The open circles in Figure 14 represent the pK_{int} of 6.00 and the closed that of 6.60 according to the discrimination between N^{π} and N^{τ} based on SA (see Section II). The computations were based on structural data for sperm whale myoglobin in which substitutions were adjusted by graphic projections of the immediate regions involved.[91] The success of the correlations between the observed and computed pK values is obvious. The correlation

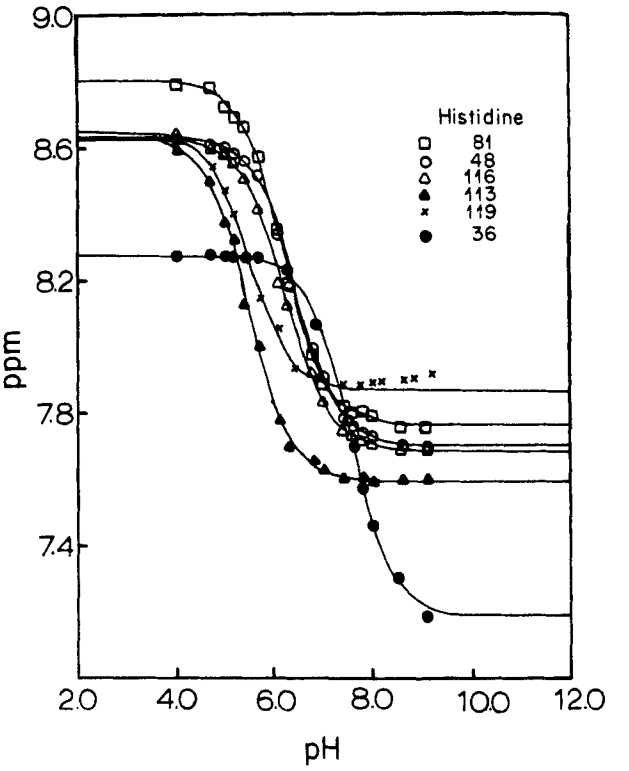

FIGURE 12. Titration curves for gray whale myoglobin with histidine residues identified on the figure. (From Botelho, L. H., Friend, S. H., Matthew, J. B., Lehman, L. D., Hanania, G. I. H., and Gurd, F. R. N., *Biochemistry*, 17, 5197, 1978. With permission.)

coefficients for the plots range from 0.94 (Figure 14A) to 0.99 (Figure 14L), in contrast with the correlation coefficients for $pK_{1/2}$ with pK_{int} that fall near 0.35. Note that the higher and the lower pK_{int} values lead in particular instances to the opposite order for $pK_{1/2}$.

More recent work to be described below[71] has applied the $(1 - \overline{SA}_{ij})$ formulation (Equation 7) in place of the $(1 - SA_j)$ formulation used by Shire, Botelho, and co-workers. In the new work some changes were made to test more fully for side-chain accommodation in modeling substitutions between myoglobin species that produced no radical differences.[71] The correlation coefficients between $pK_{1/2}$ and pK_{obs} computed for slightly different conditions were as follows: sperm whale, 0.865; pilot whale, 0.906; minke whale, 0.923. The results in Table 1 show that the calculated values for residue 36 are somewhat low, unless Glu-38 is repositioned to form a salt bridge with His-36.[106] As described before, the solution structure of this region of myoglobin is moot.

The NMR titrations of histidine residues in the myoglobins were obtained in D_2O adjusted with small amounts of DCl and NaOD with 0.10 *M* NaCl at 17°C. The computed results shown in Figure 14 and Table 1 were for I = 0.01 and 25°C in water. The computation conditions were chosen to correspond with earlier overall titration results.[56] Allowing for enthalpy of dissociation, ionic strength effects, and the solvent isotope effect, the $pK_{1/2}$ value may be underestimated by about 0.21 units.[91,106] These individual factors are probably of comparable magnitude to the expectable uncertainties in pK_{int} values from the small variations in titration values of model compounds. Consistent treatments of computations under various constraints are summarized in Table 1.

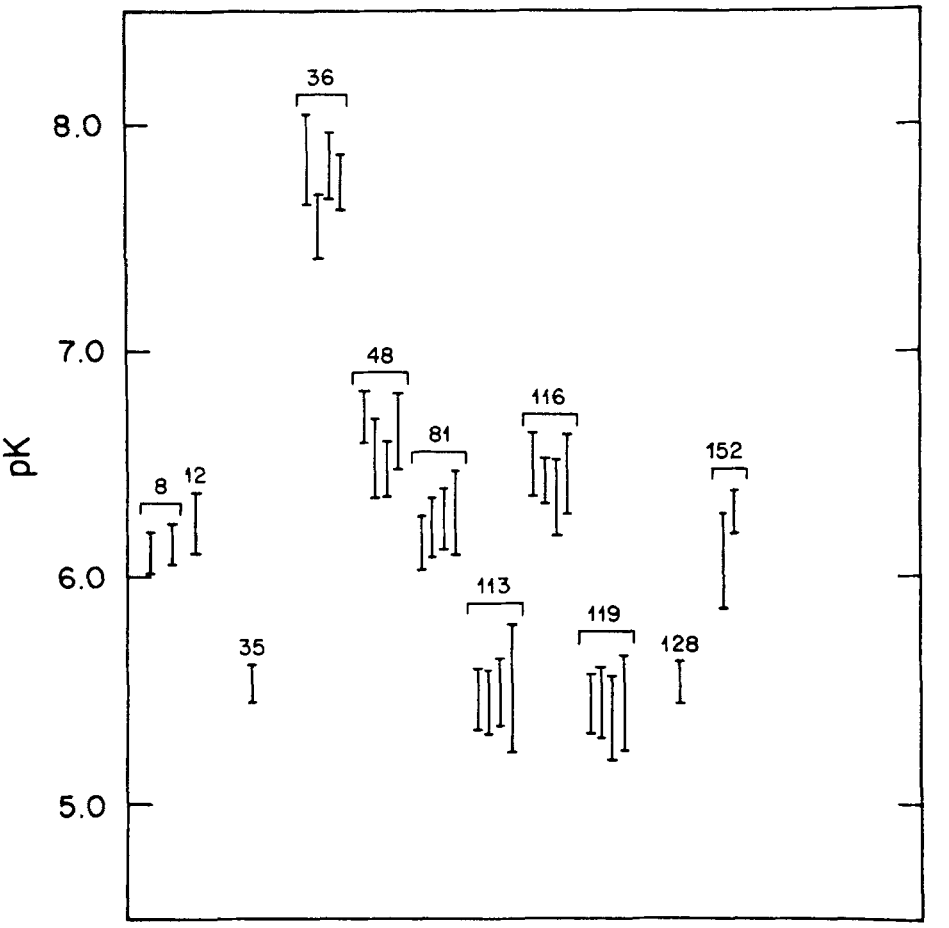

FIGURE 13. Ranges of pK values for each residue observed, shown as bars extended at the limits by 0.05 unit, with a minimum range of 0.15 unit for clarity. The myoglobins are grouped into four related sets, and certain residues are represented in 1, 2, 3, or all 4 such sets. (From Botelho, L. H. and Gurd, F. R. N., *Biochemistry*, 17, 5188, 1978. With permission.)

2. Other pK Values

Figure 15 shows a comparison of computed and observed pK values for sperm whale myoglobin that includes, besides the histidine results already discussed,[91] values for three tyrosine residues for which the correlations are nearly as satisfactory.[107] The computed value for Tyr-103 falls between two alternative observed values[108] that may reflect the tendency for multiple products to form at high pH.[109] Figure 15 shows good correlations with the same treatment applied to horse heart ferricytochrome c.

The dissociation of hemin-bound water in myoglobin can be followed with great accuracy by absorbance spectroscopy to show the effects of I and pH on this pK. Figure 16 shows a plot of the computed $pK_{1/2}$ against a function of I for sperm whale myoglobin.[92] The experimental points fall on the upper curve which represents the then standard treatment incorporating the $(1 - SA_j)$ term. A few pK_{int} values have since been modified without significant effect in the pH range in question. As Figure 16 shows, omitting the SA term produces an overestimate of the effect on the $pK_{1/2}$ caused by increasing I. The ionic strength function used here was adopted as standard. Figure 17 shows a satisfactory comparison with computed values[92] of the observed dependence of the pK_i on pH at approximately $I = 0.001$ *M*.

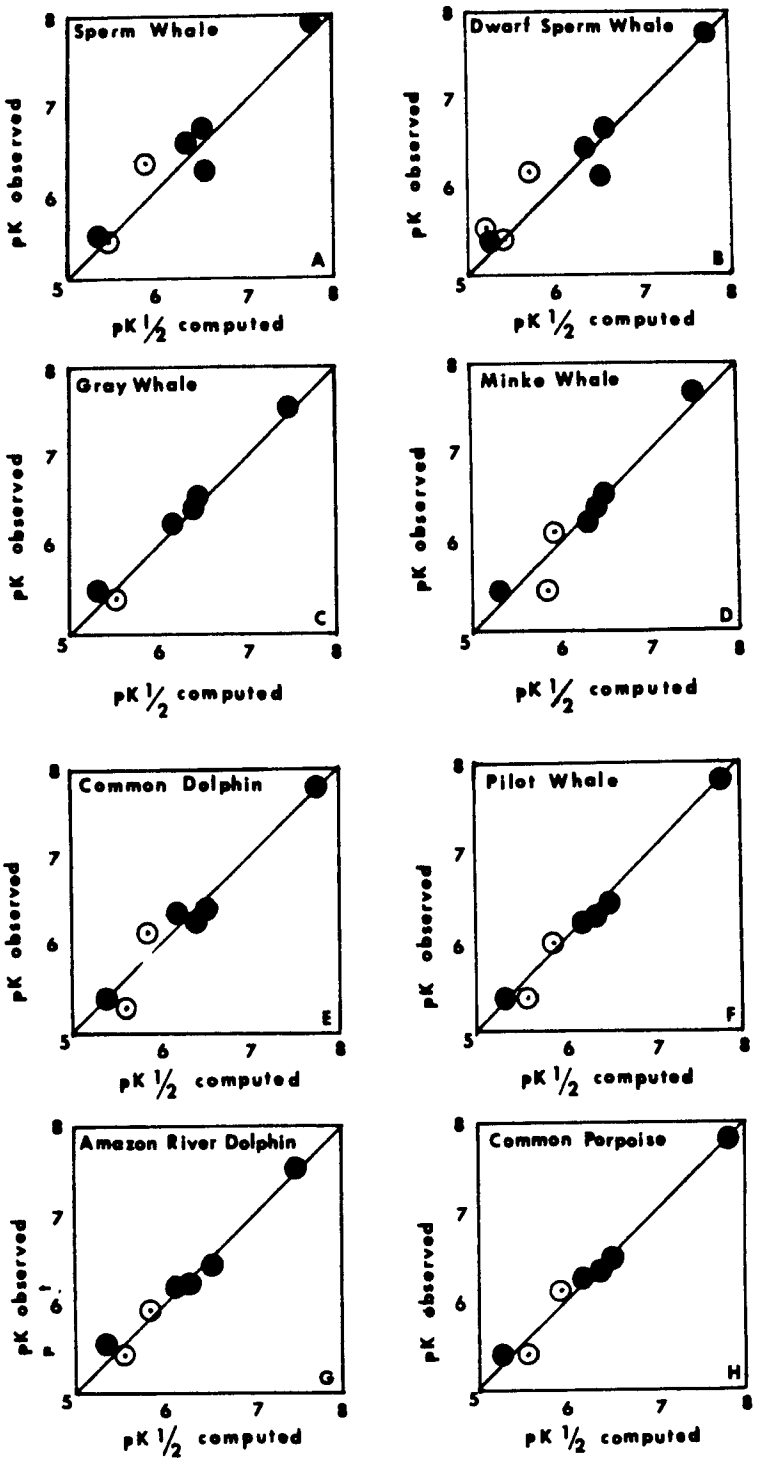

FIGURE 14. Comparison of computed $pK_{1/2}$ values with the corresponding observed pK values for a series of myoglobins indicated in each part, A through L. The histidine pK values were computed on the basis of assumed pK_{int} values of 6.60 (closed circles) or 6.00 (open circles). (From Botelho, L. H., Friend, S. H., Matthew, J. B., Lehman, L. D., Hanania, G. I. H., and Gurd, F. R. N., *Biochemistry*, 17, 5197, 1978. With permission.)

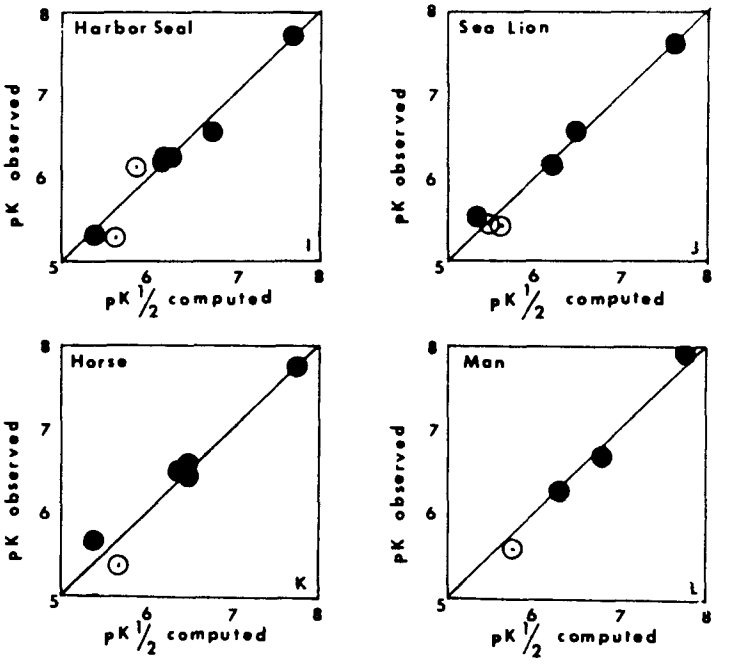

FIGURE 14

Table 1
COMPARISON OF EXPERIMENTAL HISTIDINE $pK_{1/2}$ VALUES WITH THOSE CALCULATED BY THE $(1 - SA_j)$ AND $(1 - SA_{ij})$ FORMALISMS FOR MYOGLOBINS[a]

Histidine residues	Experimental values[b]	Calculated values[c]	
		$(1 - SA_j)$[d]	$(1 - SA_{ij})$[e]
His 12	6.28	5.70	5.79
His 36	7.97	7.77	7.50
His 48	6.73	6.53	6.62
His 64	<5.00	4.20[f]	4.10
His 81	6.17	6.55	6.70
His 113	5.49	5.35	5.47
His 116	6.55	6.36	6.57
His 119	5.46	5.42	5.42

[a] See text for a description of the $(1 - SA_j)$ and $(1 - \overline{SA_{ij}})$ formalisms.
[b] Experimental solution conditions were 17°C, 0.10 *M* NaCl.[91]
[c] Calculations performed at 25.0°C, I = 0.01 *M*. Add 0.21 pK units to compare to experimental values.[91]
[d] Taken from Reference 91.
[e] Unpublished data of B. Garcia-Moreno E., 1984.
[f] Taken from References 81 and 82.

Adapted from Flanagan, M. A., Role of Electrostatic Interactions in the Structure and Function of Myoglobin, Lysozyme and Hemoglobin, Ph.D. thesis, Indiana University, Bloomington, 1983.

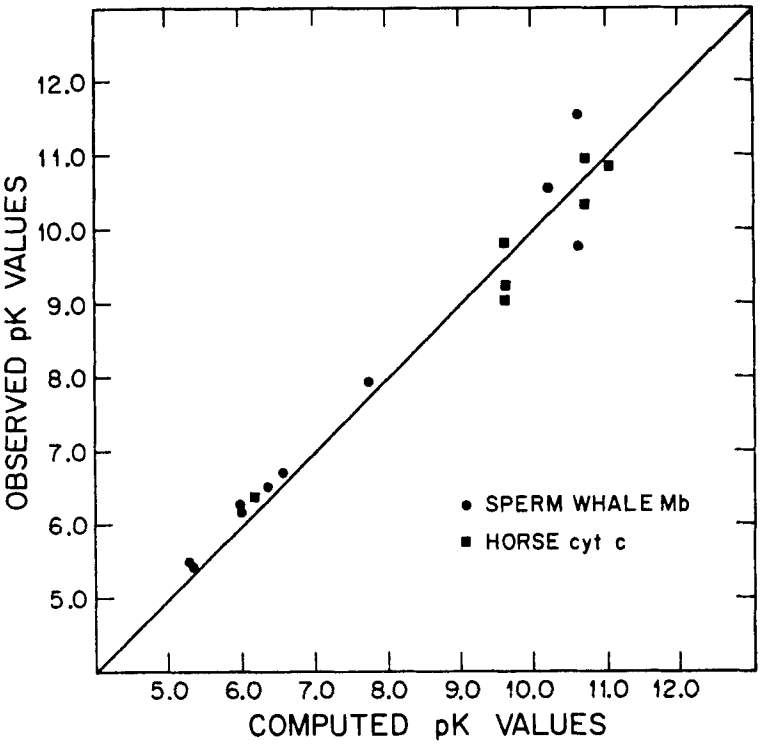

FIGURE 15. Comparison of observed and computed pK values. (From Matthew, J. B., Friend, S. H., Botelho, L. H., Lehman, L. D., Hanania, G. I. H., and Gurd, F. R. N., *Biochem. Biophys. Res. Commun.*, 81, 416, 1978. With permission.)

3. Full Titration Curves

The computations of the pK_i value for a given site under given conditions reflect summed contributions of all the other charged sites under those conditions. Therefore, the agreement of computed and observed overall titration curves will also constitute a key test for the electrostatic treatment.[56,93] Figure 18 shows experimental points and computed titration curves for sperm whale myoglobin, 0.2 m*M*, I = 0.01 *M*, 25°C.[107] Curve A is representative of the treatment used by Botelho et al.[91] for the histidine titration described above, employing the $(1 - SA_j)$ formulation. In curve B, SA is always taken as 1, which has the effect of equating pK_i with pK_{int} under all conditions so that the electrostatic effects are neglected. In curve C, SA is always taken as 0, which ignores the moderating effect of solvent accessibility. In curve D, the assumption of curve C is retained and in addition all groups are placed 1 Å inside the low dielectric medium. The treatment of curve A is clearly superior. Figure 19 shows that the use of the $(1 - \overline{SA}_{ij})$ formalism to correspond with curve A in Figure 18 produces essentially as good a match with experiment.[106]

B. Hemoglobins

Hemoglobins are constructed on the same architectural plan as myoglobins and are believed to have a shared ancestry.[110,111] The individual chains are adapted to form very stable αβ heterodimers which in turn combine to form the familiar $\alpha_2\beta_2$ tetramer. As an adaptation to oxygen delivery to the tissues, alternative forms of the tetramer structure itself are linked to the combination with the ligand, the preferentially oxygenated form of the tetrameric protein differing from the deoxygenated form. As oxygen is released from the protein, the relative stability of the preferentially oxygenated form is decreased, facilitating further

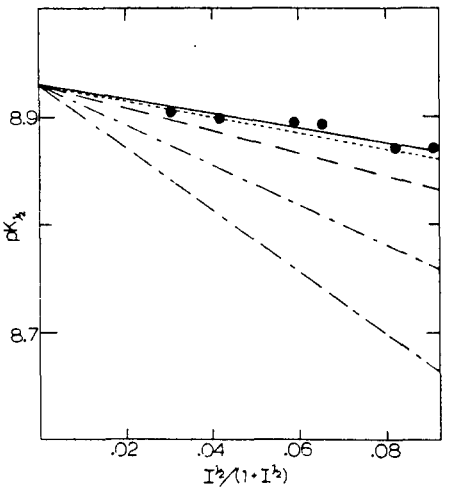

FIGURE 16. Plots of the pK values for half-titration, pK_{1-2}, against the ionic strength function, $I^{1/2}/(1 + I^{1/2})$, for the ionization of the iron-bound water molecule in sperm whale ferrimyoglobin at 25°C. Experimental data are given in full circles, with an uncertainty of ±0.005 pH unit. Computations with solvent acessibility factors included for d = 0 (——) and d = 1.0 Å (– – –); solvent accessibility factors not included, for d = 0 (-·-·-) and d = 1.0 Å (-··-··-); according to the Linderstøm-Lang treatment described in the text (——). (From Shire, S. J., Hanania, G. I. H., and Gurd, F. R. N., *Biochemistry*, 13, 2974, 1974. With permission.)

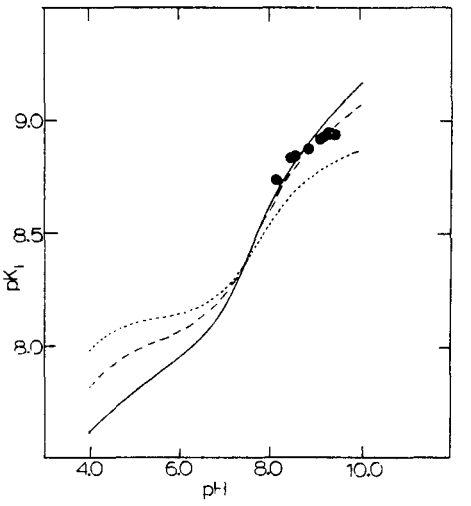

FIGURE 17. Variation with pH of the computed pK_1 for the iron-bound water in sperm whale ferrimyoglobin at 25°C. Ionic strength 0 (——), 0.01 (— —), and 0.10 *M* (– – –); full circles represent experimental values obtained at approximately 0.001 *M* ionic strength. (From Shire, S. J., Hanania, G. I. H., and Gurd, F. R. N., *Biochemistry*, 13, 2974, 1974. With permission.)

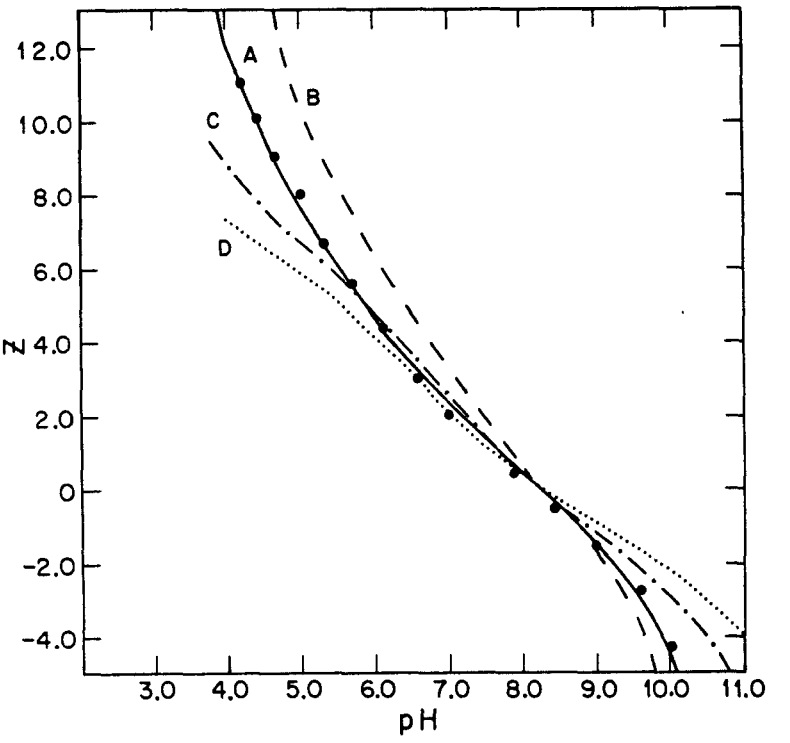

FIGURE 18. Computed titration curves for ferrimyoglobin 0.2 *mM*, 25°C, as described in the text. (From Matthew, J. B., Friend, S. H., Botelho, L. H., Lehman, L. D., Hanania, G. I. H., and Gurd, F. R. N., *Biochem. Biophys. Res. Commun.*, 81, 416, 1978. With permission.)

release. Although functionally important distinct structural forms exist bearing intermediate numbers of oxygen molecules, it will be sufficient to illustrate here the pH-dependent properties of the system in terms of the fully oxygenated oxyhemoglobin and the fully deoxygenated deoxyhemoglobin.

The structural transition to ligand binding affects pH-dependent properties by altering values of r_{ij} and SA. These alterations are generally adaptive and illustrate the great functional importance of electrostatic interactions. Best known are differences in hydrogen ion affinity, the Bohr effect, in carbamino formation expecially with NH_2-terminal residues, and in ion binding affinity ranging from simple anions to the regulator molecule DPG.[64,68,74]

1. Histidine Titrations

When Matthew et al.[61] reported in 1979 the calculation of $pK_{1/2}$ values and overall titration curves for deoxy and liganded conformations of adult human hemoglobin, the coordinates for the former were available at 2.5 Å resolution[110] but the corresponding coordinates for the human oxyhemoglobin were not available. Therefore, a hypothetical liganded structure was generated by rigid rotation of the deoxyhemoglobin α and β chains into the oxyhemoglobin quaternary structure suggested from comparison with a low resolution structure for horse oxyhemoglobin.[112] Although several tertiary structural changes had been implicated in the stereochemical mechanism for hemoglobin function,[113] no attempt was made to introduce these rearrangements in the rigid rotation quaternary structure.

The computed $pK_{1/2}$ values are listed in Table 2,[61] and the titration results for the deoxyhemoglobin and liganded hemoglobin in Figures 20 and 21, respectively.[61] Table 2 correlated the $pK_{1/2}$ values determined by ^{13}C- and ^{1}H-NMR with the respective computations.

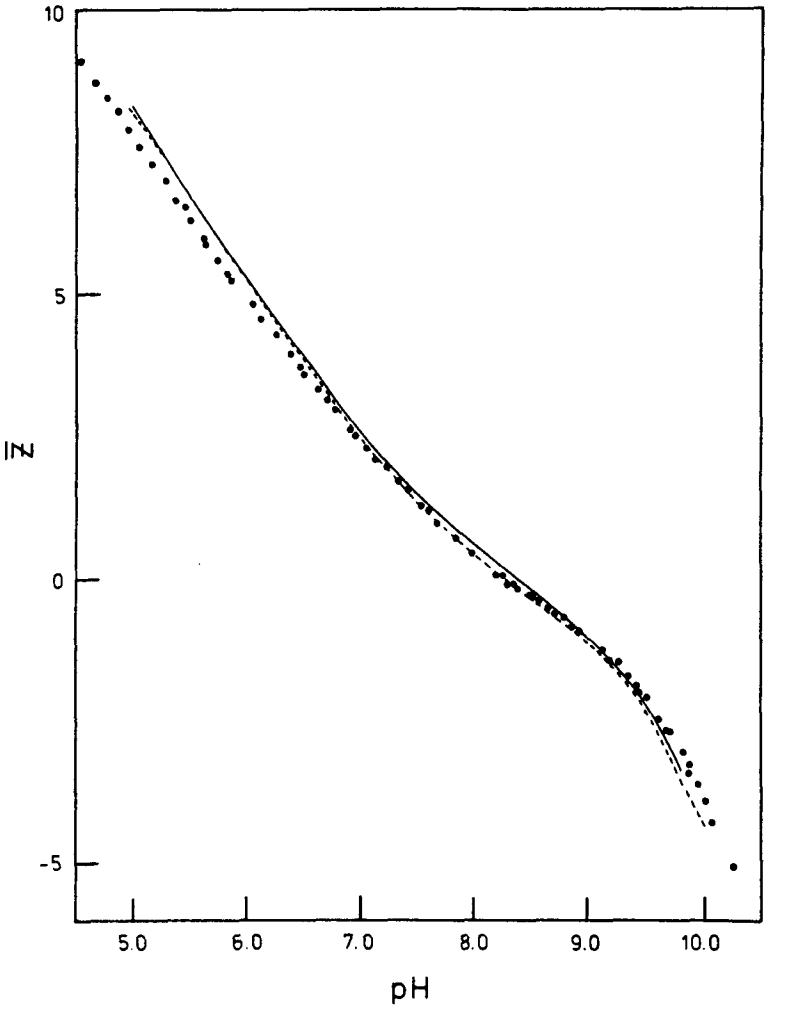

FIGURE 19. Comparison of experimentally determined proton titration points for 25°C in 0.01 *M* KCl[30,56] with the $(1 - \overline{SA}_{ij})$ formalism (solid curve) and the $(1 - SA_j)$ formalism (dashed curve). (From Flanagan, M. A., Role of Electrostatic Interactions in the Structure and Function of Myoglobin, Lysozyme and Hemoglobin, Ph.D. thesis, Indiana University, Bloomington, 1983.)

Of the 26 $pK_{1/2}$ values determined for the titrating histidines[118] and amino-terminals[116] of liganded and unliganded forms, only 9[116,118] were assigned to specific residues at that time. These assigned $pK_{1/2}$ values are indicated with arrows, and the remaining histidine values are aligned with the computed pK values. While this alignment represents no attempt at pK assignment, reasonable correspondence does result. The good agreement between computation and measurement in both Figures 20 and 21[61] is tantamount to the correct prediction of the alkaline Bohr effect,[67] referring to the excess binding of protons by deoxyhemoglobin relative to oxyhemoglobin. These results led to the conclusion that tertiary structural rearrangements in liganded hemoglobin relative to deoxyhemoglobin were not required to account for proton titration behavior and the Bohr effect.

Subsequently, structures have become available for two forms of liganded hemoglobin: a refined oxyhemoglobin at 2.1 Å resolution[119] and a carbonmonoxyhemoglobin at 2.7 Å resolution.[120] In both structures tertiary rearrangements are reported relative to the deoxy-

Table 2
INDIVIDUAL SITE $pK_{1/2}$ VALUES: THEORETICAL AND EXPERIMENTAL,[a] ACCORDING TO THE $(1 - SA_j)$ FORMALISM

Residue and chain	Oxyhemoglobin			Deoxyhemoglobin		
	Theoretical			Theoretical		
	I = 0.01	I = 0.10	Experimental	I = 0.01	I = 0.10	Experimental
His-146β	8.52	8.21 ⟷	7.9[b,c]	9.00[d]	8.48[d] ⟷	8.1[b,c]
His-117β	7.98	7.72	8.0[b]	8.08	7.75	8.2[b]
His-112α	8.04	7.68	7.5[b]	8.14	7.71	7.6[b]
His-50α	7.67	7.43	7.5[b]	7.87	7.47	7.2[b]
His-89α	7.46	7.20	7.2[b]	7.50	7.15	7.18[b]
His-45α	7.00	6.83	7.0[b]	7.11	6.84	7.18[b]
His-20α	6.86	6.74	6.7[b]	6.90	6.75	6.95[b]
His-77β	6.43	6.53	6.6[b]	6.58	6.58	6.75[b]
His-72α	6.46	6.31	6.0[b]	6.52	6.32	6.60[b]
His-2β	6.43	6.52 ⟷	6.51[b,c]	6.53	6.53 ⟷	6.38[b,c]
His-143β	3.73	4.00	Not observed[b]	6.03	6.07 ⟷	6.25[b,c]
Val-1α	7.64	7.29 ⟷	7.16[e]	8.10	7.56 ⟷	7.83[e]
Val-1β	6.60	6.80 ⟷	7.00[e,f]	7.13	7.00 ⟷	6.91[e]

[a] Deoxy- and oxyhemoglobin theoretical $pK_{1/2}$ values at two ionic strengths are compared with experimentally observed $pK_{1/2}$ values. Theory and experimental values are correlated with specifically assigned sites indicated with an arrow. Ionic strength of 0.10 most closely compared with experimental conditions.

[b] Observed by proton NMR.[114]

[c] Assigned by variant and chemical modification with proton NMR.[114]

[d] His-146 ... Asp-94 salt bridge distance of 2.8 Å may be stretched in solution yielding a slightly lower $pK_{1/2}$.

[e] Observed and assigned by carbon-13 NMR.[115,116]

[f] Observed by kinetic methods.[117]

Taken from Matthew, J. B., Hanania, G. I. H., and Gurd, F. R. N., *Biochemistry*, 18, 1919, 1979. With permission.

hemoglobin structure.[110] To evaluate the effect, calculations were carried out on the oxyhemoglobin structure of 2.1 Å resolution, as well as on the carbonmonoxy structure at 2.7 Å resolution, and the resulting $pK_{1/2}$ values are compared in Table 3 with those based on the rigid rotation conformation. To facilitate comparison with Table 2, the results of computations for both $(1 - SA_i)$ and $(1 - SA_{ij})$ formalisms are included. For historical reasons, many of the hemoglobin calculations in the following are based on the $(1 - SA_j)$ treatment. When available, the corresponding $(1 - SA_{ij})$ results are included to demonstrate their near equivalence as exemplified in Table 3.

With the exception of the special case of His-143β (Table 2), most entries for the three liganded structures in Table 3 match relatively well. Isolated points of disagreement may reflect rather subtle side-chain rearrangements. They may likewise reflect some effects of high salt concentration or ion binding in the crystalline forms that affect the portrayal of the behavior of the protein in low salt solution conditions. The large change for His-146β is attributable to an ion pair with Asp-94β in the deoxy structure which is broken in the liganded structure. This histidine, which has been implicated as a key residue in the stereochemical mechanism of the Bohr effect,[113] has been studied extensively by proton NMR[28] which is the basis for showing that the ion pair is salt-labile. In 0.4 *M* chloride, the $pK_{1/2}$ drops from 8.0 in deoxyhemoglobin to 7.1 in oxyhemoglobin,[121] while at 0.1 *M* ionic strength, the corresponding change was only a slight drop from 8.0 to 7.9.[28,118] Likewise, the observed

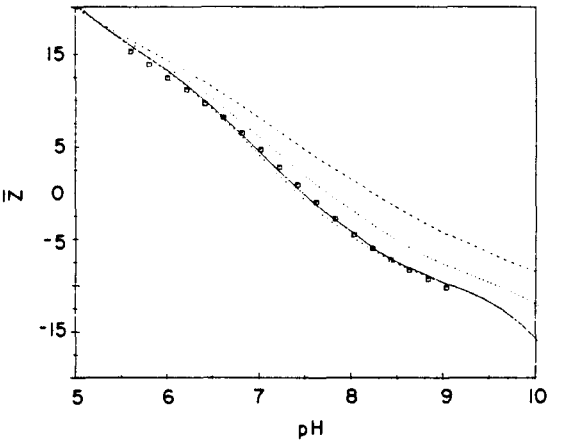

FIGURE 20. Comparison for human deoxyhemoglobin of experimental results[61] as points with computed titration curves at 25°C. The full curve allows for Cl^- binding to the Val-1α.... Arg 141α site at I = 0.10 *M*. Broken curves, from above, are for I = 0.0, 0.01, and 0.10 *M*, respectively. (From Matthew, J. B., Hanania, G. I. H., and Gurd, F. R. N., *Biochemistry*, 18, 1919, 1979. With permission.)

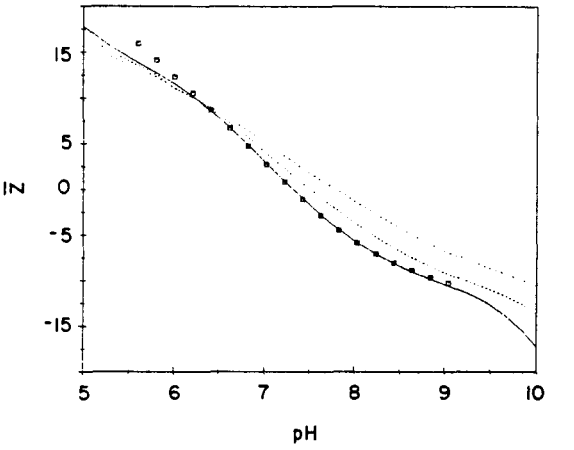

FIGURE 21. Plot for human oxyhemoglobin corresponding to conditions of Figure 20 except that no bound Cl^- was assumed in the computations. (From Matthew, J. B., Hanania, G. I. H., and Gurd, F. R. N., *Biochemistry*, 18, 1919, 1979. With permission.)

pK in carbonmonoxyhemoglobin in 7.85 in 0.1 *M* bis-Tris-HCl buffer at 27°C[113,118] but is 7.1 in the presence of 0.2 *M* phosphate and 0.2 *M* NaCl at 30°C.[121]

In Table 4 the titration behavior of the liganded and unliganded forms is shown over a range of pH, with experimental values of net charge compared with computations in which both SA formalisms are represented. For the oxyhemoglobin and carbonmonoxyhemoglobin structures, the ion pair His-146β ... Asp-94β is included to correspond with the low salt conditions.[121] Note that this latter format produces excellent agreement with observation.

Table 3
$pK_{1/2}$ OF HISTIDINES AND AMINO TERMINI IN LIGANDED AND UNLIGANDED FORMS OF HEMOGLOBIN AT I = 0.10 *M*

Residue	Rigid rotation structure[a] $(1 - SA_j)$	Oxyhemoglobin[b] $(1 - SA_j)$	Oxyhemoglobin[b] $(1 - \overline{SA_{ij}})$	Carbonmonoxyhemoglobin[c] $(1 - SA_j)$	Carbonmonoxyhemoglobin[c] $(1 - \overline{SA_{ij}})$	Deoxyhemoglobin[d] $(1 - SA_j)$	Deoxyhemoglobin[d] $(1 - \overline{SA_{ij}})$
His-146β	8.21	5.91	6.25	5.86	6.00	8.48	8.30
His-117β	7.72	7.35	7.38	7.52	7.56	7.75	7.88
His-112α	7.68	6.78	6.90	6.58	6.74	7.71	7.75
His-50α	7.43	7.57	7.67	7.66	7.77	7.47	7.28
His-89α	7.20	6.89	6.80	6.74	6.60	7.15	7.00
His-45α	6.83	7.41	7.50	7.42	7.45	6.84	6.87
His-20α	6.74	6.41	6.62	7.65	7.77	6.75	6.67
His-77β	6.53	6.50	6.58	6.48	6.55	6.58	6.60
His-72α	6.31	6.67	6.64	6.79	6.70	6.32	6.25
His-2β	6.52	6.43	6.52	6.36	6.47	6.53	6.53
His-143β	4.00	5.83	5.98	5.89	6.15	6.07	5.92
Val-1α	7.29	8.22	8.04	7.27	7.14	7.56	7.40
Val-1β	6.80	6.79	6.63	6.55	6.75	7.00	6.81

[a] From Reference 61, Table 2.
[b] From Reference 119.
[c] From Reference 120.
[d] From Reference 110.

The results with deoxyhemoglobin are also satisfactory, and in that case correspond directly with those in Figure 20.[61] Note the parallelism between the salt sensitivity of His-146β in liganded hemoglobin and that of His-36 in myoglobin (Section III.A.1).

Since specific treatments have been made of ion binding in solution involving the regions of Val-1α and Val-1β in the deoxy state, these residues will be discussed in the special section on ion binding to follow. In a more general sense, it is worthwhile to draw attention to the possible effects of high salt, 2 to 4 *M*, and the relatively extreme pH values used in preparing the various hemoglobin crystals.[119,120,123] Specific salt bridges have been shown to be more salt sensitive in liganded hemoglobin,[118] and the tetramer to dimer dissociation constant of oxyhemoglobin is both acid-driven[124,125] and strongly favored by high salt concentrations;[125-127] transitions to oxyhemoglobin under these conditions involve behavioral discontinuities in the presence of β-chain carbamino adduct,[116,128] and the infrared spectrum of CO stretching frequencies of carbonmonoxyhemoglobin crystals is substantially different from the spectrum obtained on the dissolved crystals.[129]

2. Comparison of Titration Behavior of Hemoglobin and Myoglobin

The pK values for histidine residues in both forms of human hemoglobin fall within a higher range of pH than is the case for myoglobin in which only one histidine residue has a $pK_{1/2}$ over 7. Figure 22 shows observed[118] and computed[106,130] values for the titratable histidines per αβ dimer in the tetramer forms corresponding to the fully deoxygenated and fully oxygenated hemoglobins. Not all the observed values from proton NMR are assignable to a given residue, although much more information has been provided by this excellent work than can be dealt with here.[118] The computed values, in contrast, are based on specific residues. The two independent types of results are ranked in order without arbitrary omissions, and regress together according to a consistent pattern. Similarly ranked values usually agree within 0.25 pK units. The conditions are shown for 0.1 *M* ionic strength, 25°C.

Table 4
EXPERIMENTAL[a] AND COMPUTED TITRATION DATA FOR LIGANDED AND UNLIGANDED FORMS OF HEMOGLOBIN AT 25°C, I = 0.10 *M*

	Oxyhemoglobin[b]					Carbonmonoxyhemoglobin[c]			Deoxyhemoglobin[d]		
		Computed				Computed				Computed	
		Formed		Broken		Formed	Broken				
pH	Experimental Charge	$(1 - SA_j)$	$(1 - \overline{SA}_{ij})$	$(1 - SA_j)$	$(1 - \overline{SA}_{ij})$	$(1 - \overline{SA}_{ij})$	$(1 - SA_j)$	$(1 - \overline{SA}_{ij})$	Experimental Charge	$(1 - SA_j)$	$(1 - \overline{SA}_{ij})$
6.0	12.3	12.00	12.24	10.98	10.71	12.74	11.23	11.76	12.4	12.95	12.36
6.6	6.7	6.64	6.90	5.30	4.99	7.35	5.60	6.07	8.1	7.68	7.08
7.0	2.7	2.55	2.86	1.24	0.82	3.14	1.45	1.82	4.6	3.61	3.03
7.4	−1.1	−1.37	−1.02	−2.50	−2.86	−0.94	−2.46	−2.13	0.8	−0.37	−0.83
7.6	−2.9	−3.14	−2.80	−4.11	−4.42	−2.82	−4.20	−3.87	−1.1	−2.18	−2.56
8.0	−5.9	−6.13	−5.92	−6.76	−6.97	−6.06	−7.08	−6.76	−4.6	−5.30	−5.54
8.6	−8.9	−9.38	−9.30	−9.60	−9.72	−9.51	−10.08	−9.77	−8.4	−8.47	−8.71

Note: Ion pair between His-146β and Asp-94β is computed to be either formed or broken in the given structure.

[a] Data taken from Reference 122.
[b] From Reference 119.
[c] From Reference 120.
[d] From Reference 110.

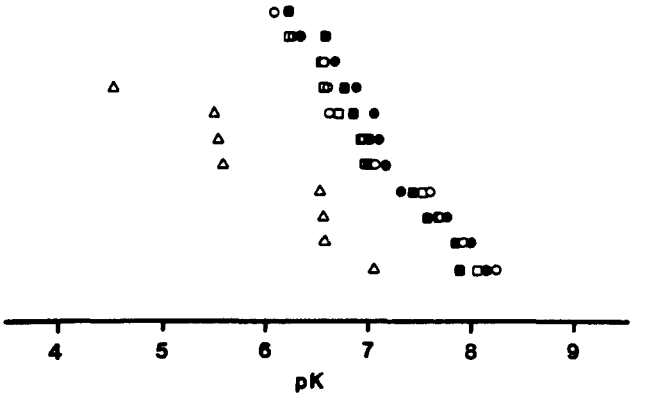

FIGURE 22. Rank order of observed (closed symbols) and computed (open symbols) histidine pK values at I = 0.1 *M* for myoglobin (Δ), oxyhemoglobin (□), and deoxyhemoglobin (○).[106,118,130]

The results for hemoglobin in Figure 22 show that almost all histidine pK values in hemoglobin fall above the higher pK_{int} value of 6.60, i.e., that their sites experience net negative electrostatic fields. These results are in strong contrast with those for sperm whale myoglobin which also appear in Figure 22, with a prominent grouping of sites that experience net positive electrostatic fields. For the myoglobin, the assignments of titrating NMR resonances are all experimentally based.[27] The contrasting pK values in the two cases are suited to their buffering functions in different environments.[61] A second consequence of the interaction of the hemoglobin histidine residues with net negative fields is that the predominant interactions are stabilizing in the functional pH range, with a continuous loss of stabilizing interactions as the pH rises. A further point apparent from Figure 22 is that pK values are generally somewhat higher for the deoxy than for the oxy tetramer.

The histidine titrations in deoxy- and oxyhemoglobins overlap the Val-1α and Val-1β amino group titrations. The computed titration curves show, in first derivative form, that their ranges are less closely overlapped with other groups.[61] The agreement is each case between computation and measurement is shown to be good over the pH range of 6 to 9 (Figures 20 and 21).[61] As already shown in Figure 22, the electrostatic contributions are substantial throughout this range.

In determining the titration curve from the values of pK_i for every group at all pH values, Equation 8 shows how each pairwise interaction W'_{ij} is taken into account to arrive at the pK_i. The individual contributions of $\Delta pK_{ij}Z_j$ terms (Equation 8) are illustrated in Figure 7A for residue Val-1α in the deoxyhemoglobin tetramer and in Figure 7B for His-117β. In each case, the accumulated pairwise contributions are illustrated for a range of pH values as described in the legend.

Hemoglobin differs from myoglobin and indeed most other proteins in the pattern of titration as the ionic strength is varied.[67] The effect which is seen experimentally is predicted by the electrostatic treatment as illustrated in Figures 20 and 21. In Figure 23, single residues, Val-1α in deoxyhemoglobin α-chain monomer and Val-1 in sperm whale myoglobin, are taken as examples at three ionic strength values. The steepest curves are at lowest ionic strength in each case, but the two cases are sharply contrasted with the crossover point for the hemoglobin residue occurring at the very low pH near 4, about four units below the isoionic conditions. The crossover point for the myoglobin group occurs very close to the isoionic point. In this comparison, the α-chain monomer is used because it is representative of the behavior seen in the whole tetramer.[67]

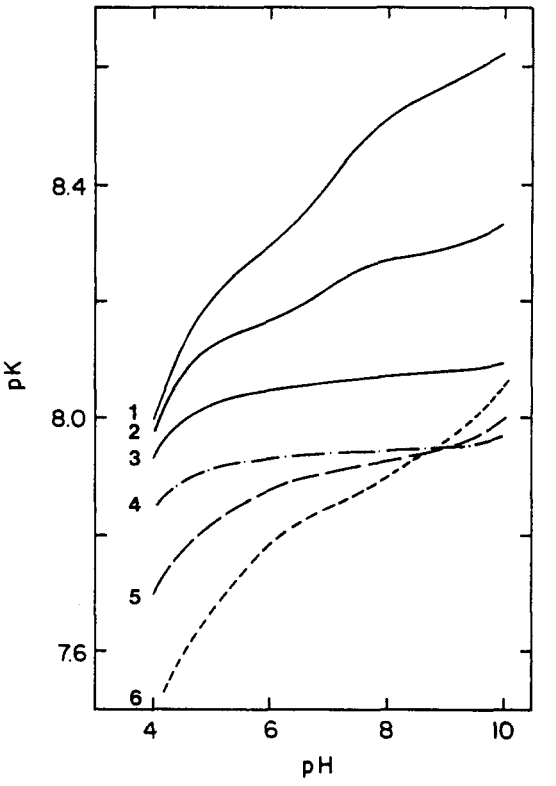

FIGURE 23. Comparison of ionic strength effect on the electrostatically calculated pK_i values for a single amino acid residue, the amino-terminal valine group, in human ferrihemoglobin A α-chain monomer (solid curves, 1, 2, and 3) and sperm whale ferrimyoglobin (broken curves, 4, 5, and 6). The pH variation at 25°C is shown at three levels of ionic strength: 0 *M*, curves 1 and 6; 0.01 *M*, curves 2 and 5; and 0.1 *M*, curves 3 and 4. (From Matthew, J. B., Hanania, G. I. H., and Gurd, F. R. N., *Biochemistry*, 18, 1928, 1979. With permission.)

The difference illustrated in Figure 23 can be shown to reflect differences in spatial distribution and solvent accessibility of the charged groups in the two proteins, as summarized in Table 5. If uniform charge distributions were assumed for the hemoglobin α chain and the myoglobin, r_{ij} between nearest neighbors would average to 10 and 8.3 Å, respectively.[67] However, in both proteins the r_{ij} between nearest neighbors bearing opposite charges is less than the distance prescribed by uniform charge distribution. Table 5 lists all the acidic functions with their positively charged neighbors wherever $r_{ij} < 7.0$Å. The histidine residues in hemoglobin α chain are generally much closer to acid groups than they are in myoglobin, in keeping with the results and computations in Figures 22 and 23. The distinction between the proteins applies also to the mean static solvent accessibilities, SA, of the different classes of charge-bearing groups, so that the hemoglobin has lower SA values for acidic and the more neutral basic groups, and higher for the strongly basic residues. The mutual interaction of the first two categories accords with their sharing lowered SA_{ij} values and expressing strong interactions with consequently elevated histidine pK values (Tables 1 and 5).

Figure 24 shows a hypothetical manipulation of the electrostatic characteristics of hemoglobin α chain as expressed by the pK_i values, calculated for two residues, Val-1α (above)

Table 5
CHARGE-PAIR RELATIONSHIPS IN SPERM WHALE FERRIMYOGLOBIN AND HEMOGLOBIN α CHAIN[a]

Sperm whale myoglobin			Hemoglobin α chain		
AA	r_{ij}	Base	AA	r_{ij}	Base
Glu-4	2.4	Lys-79	Asp-6	3.1	Lys-127
Glu-6	2.8	Lys-133		6.8	Val-1
Glu-18	3.5	Lys-77	Glu-23	5.7	His-112
Asp-20	4.1	Arg-118		6.5	His-20
Asp-27	3.3	Arg-118	Glu-27	3.2	Arg-31
Glu-38	2.8	His-36		3.3	His-112
Glu-41	5.4	Lys-47	Glu-30	2.4	His-50
	5.5	Lys-50	Asp-47		
Asp-44	3.3	Lys-47	Asp-64	6.8	Lys-60
Glu-52	4.6	Lys-56	Asp-74	2.8	Lys-7
	5.2	Lys-34		6.2	Lys-11
Glu-54			Asp-75	6.0	His-72
Glu-59	5.5	Lys-62	Asp-85	2.9	Lys-139
Asp-60	3.1	Arg-45		4.2	His-89
Glu-83	6.5	His-81	Asp-94		
	6.6	Lys-78	Glu-116	3.9	Lys-16
Glu-85			Asp-126	6.2	His-112
Glu-105	3.8	Lys-102			
Glu-109			C term		
Asp-122	3.4	Lys-16	Heme PR1	4.5	Lys-61
Asp-126	6.2	His-122	Heme PR2	3.7	His-45
Glu-136	5.5	Arg-139			
Asp-141	3.3	Lys-140			
	5.1	Lys-141			
Glu-148					
C term					
Heme PR1	6.1	Lys-96			
Heme PR2	6.2	Arg-45			

[a] r_{ij} denotes the separation in ångströms between point charges.

Taken from Matthew, J. B., Hanania, G. I. H., and Gurd, F. R. N., *Biochemistry*, 18, 1928, 1979. With permission.

and His-112α (below), each varying with pH and with ionic strength. The left hand set represents the unadjusted computations. The central set represents the effect of altering the charge configuration by arbitrarily splitting apart the histidine-carboxyl ion pairs to 10 Å distance.[67] The result is a lowering of pK_i values and a decreased ionic strength dependence for interposition of shielding ions. The right hand set represents the result, in addition, of reducing the SA value of each lysine and arginine point charge from an average of 0.73 to 0.50 which is characteristic of myoglobin. The two steps altering the characteristic charge pattern of hemoglobin α chain render it in stages similar to that of myoglobin.

3. Binding of Ions

Deoxyhemoglobin preferentially binds Cl^- and other ions relative to oxyhemoglobin.[74,122] The result is that the charge array of the former is augmented relative to the latter, in addition to the changes accompanying the quaternary transition. An illustration of the locations of charge sites postulated in the β-cleft region of deoxyhemoglobin is shown in Figure 25.[64]

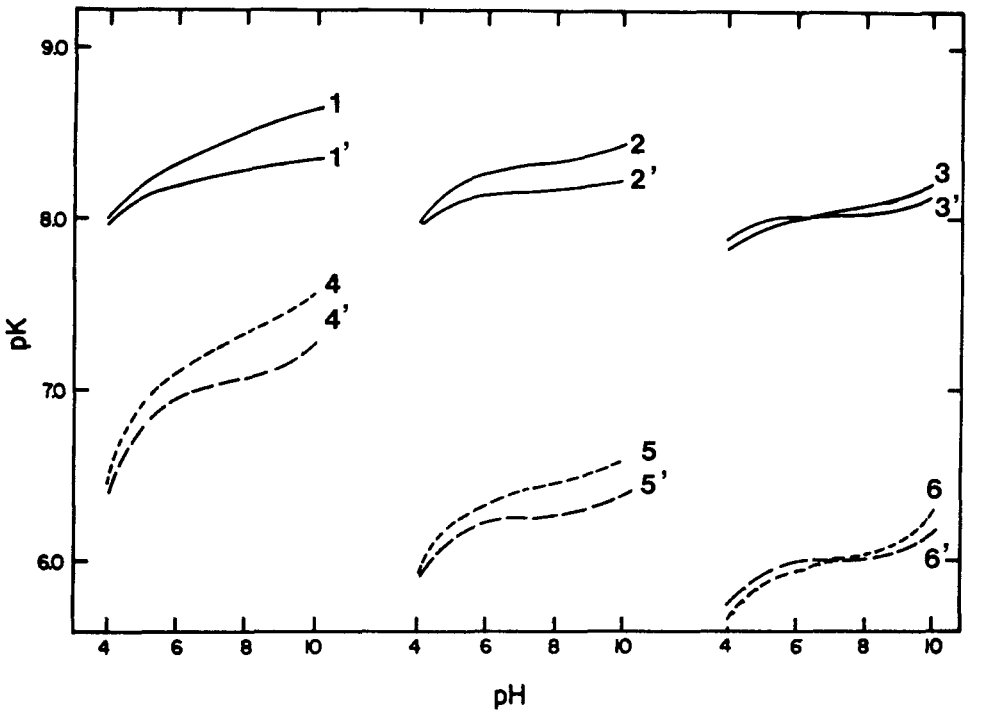

FIGURE 24. Shown are the pH and ionic strength dependences of two groups in the hemoglobin α chain: Val-1α (curves 1 to 3) and His-112α (curves 4 to 6). Unprimed and primed numbers indicate the 0 and 0.01 ionic strength calculations, respectively. The two sets of curves designated 1 and 4 show predicted pK, behavior in hemoglobin α chain for Val-1α and His-112α, respectively. Curves 2 and 5 show the predicted behaviors when the α-chain charge configuration is altered by splitting the histidine-carboxyl ion pairs to 10 Å distance. Finally, curves 3 and 6 show the predicted behaviors for Val-1α and His-112α when, in addition, the static accessibility of each lysine and arginine point charge is reduced from an average of 0.73 to 0.50. The two steps in altering the characteristic charge pattern of hemoglobin α chain render it in stages similar to that of myoglobin. (From Matthew, J. B., Hanania, G. I. H., and Gurd, F. R. N., *Biochemistry*, 18, 1928, 1979. With permission.)

Alternative positions for Cl^- are shown as well as that of diphosphoglycerate.[64,68] A more tenaciously bound Cl^- is considered to be located at Val-1α. Effects of chloride and DPG binding in enhancing the protonation state of certain residues have been estimated.[64,68]

Figure 26 shows computed electrostatic contributions to the alkaline Bohr effect, $\Delta\bar{Z}$, vs. pH in the range of 6 to 9 at 25°C, in human hemoglobin A_o, I = 0.10 *M*. The trend of the results is that the occupancy of each of several sets of four chloride sites will account for the observed maximum of ΔZ, with some distribution of such occupancies to account for the pH dependence.[64] As described previously (see Reference 68), partial occupancy of any given simple anion site is most probable. According to the computations, the observed Bohr effect results from the changes in protonation state of approximately ten groups.[67,106] Paralleling the change producing the alkaline Bohr effect that is based on the quaternary transition is another, the oxidation of oxy to ferrihemoglobin producing the residual oxidative Bohr effect. Here the quaternary states are similar and differences result mainly from the introduction of positive charges at each heme iron. The computed changes in proton binding, distributed among ten or more residues per dimer,[64] agree well with the available experimental results.[131]

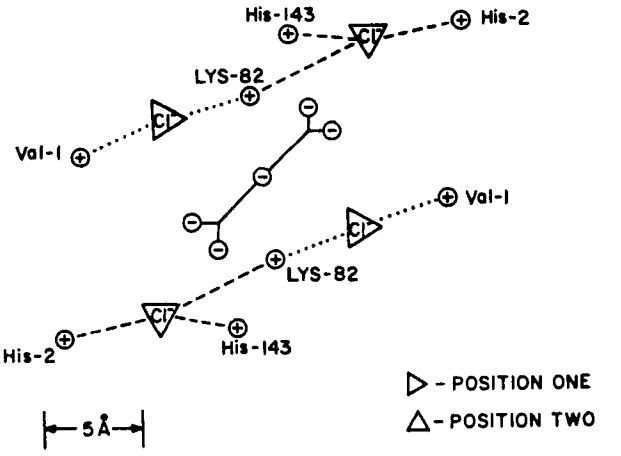

FIGURE 25. Diagram illustrating the locations of charge sites in the β-cleft region of human hemoglobin A_0. The alternative positions 1 and 2 for pairs of chloride sites on either side of the dyad axis are shown. The position of the diphosphoglycerate polyanion is shown in skeletal form. (From Matthew, J. B., Friend, S. H., and Gurd, F. R. N., in *Hemoglobin and Oxygen Binding*, Ho, C., Ed., Elsevier/North Holland, Amsterdam, 1982, 231. With permission.)

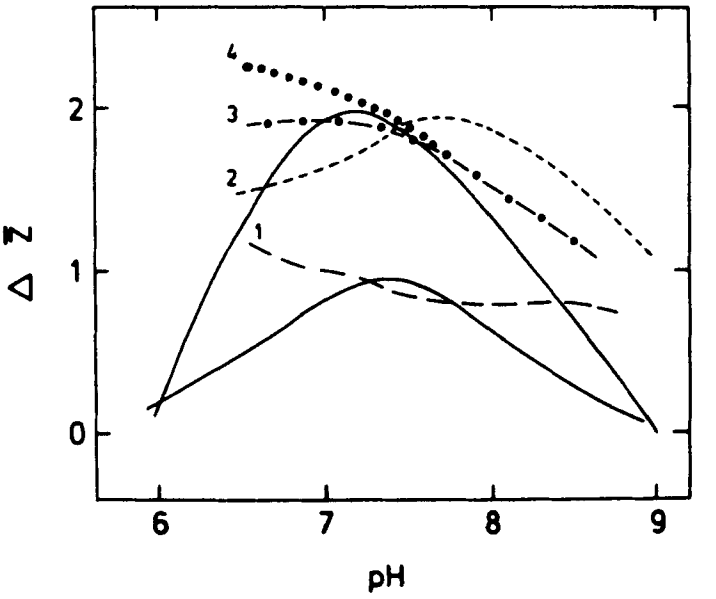

FIGURE 26. Computed electrostatic contributions to the alkaline Bohr effect, $\Delta\bar{Z}$ vs. pH 6 to 9 at 25°C, in human hemoglobin A_0, I = 0.10 *M*. Broken curves indicate cases of (1) no bound chloride; (2) chloride bound at Val-1α and His-117β sites; (3) chloride bound at Val-1α and position 1 (Figure 25); (4) chloride bound at Val-1α and position 2 (Figure 25). Full curves were drawn through the experimental data of Rollema et al.,[122] the upper in 0.10 *M* KCl and the lower in 0.01 *M* KCl. (From Matthew, J. B., Friend, S. H., and Gurd, F. R. N., in *Hemoglobin and Oxygen Binding*, Ho, C., Ed., Elsevier/North Holland, Amsterdam, 1982, 231. With permission.)

4. Temperature Dependence of Titration Behavior

Recent data on the contribution of protons to the thermodynamic linkage between oxygenation and dimer-tetramer assembly,[132] taken with calorimetric observations and estimates of the heat of binding of Bohr protons,[133] lead to the conclusion that the enthalpic component of the cooperative transition on oxgenation is due in its entirety to the alkaline Bohr effect. The good correspondence of the computed and experimental Bohr effect at 25°C discussed above,[61,64] implies that tertiary structural changes contribute little compared with the quaternary changes in determining the differential proton binding. The possible effects of the quaternary structural change on the proton binding behavior at several temperatures have been explored.[106]

The computations call first for including the variation of the dielectric constant of water with temperature in the computation of W_{ij}, and second, the adjustment of the pK_{int} values by use of heats of ionization determined for free amino acids. These latter data were little sensitive to either temperature or ionic strength. The location of chlorides chosen for modeling corresponds to those at the α-chain terminals and β-chain positions 1 in Figure 25. The $(1 - SA_{ij})$ formalism, was used. The individual electrostatic contributions to the enthalpy expressed at each titratable site were calculated by computing the slope of the plot of pK_i at a reference pH, usually pH 7.4, vs. 1/T. The slope then equals $\Delta H/2.303R$.

Figure 27 shows observed and computed curves for the difference in the number of bound protons between 10 and 20°C for the deoxy and liganded forms. The correspondence is satisfactory at this and other temperature intervals explored. Furthermore, both computed and observed effects varied little with temperature, an example of the conservation of a key functional characteristic.[106]

Table 6 lists apparent enthalpies and pK_i values for individual histidine and amino terminal residues of deoxy- and oxyhemoglobin for pH 7.4, $I = 0.10\ M$ and 25°C. It is striking that in no case does the computed enthalpy reach the standard values used to adjust the pK_{int} value, 7.14 and 10.6 kcal/mol H^+ for histidine and amino terminal residues, respectively. The pK_i values of residues with the lower enthalpies will decrease less per unit temperature change, facilitating retention of the protonic charges and assuring that buffering characteristics and electrostatic stabilization are relatively insensitive to temperature. The cited characteristics result from the temperature dependence of the W'_{ij} summations as well as of the $(pK_{int})_i$ values (Equation 8), and as such represent qualities of the charge site lattices.[106]

IV. ELECTROSTATIC FREE ENERGY CONTRIBUTIONS

In the last section the energy of interaction between pairs of discrete charges was summed for each site to define its effective pK_i under given conditions according to Equation 8. The point was made that the control of pK_i by impinging electrostatic fields represented in itself the net effect of stabilizing or destabilizing free energy contributions. The latter are evaluated directly by summing the W'_{ij} terms for pairwise interactions according to Equation 9.

In this section the electrostatic free energy contributions are analyzed in two stages. The first deals with individual protein molecules in terms of both stabilizing and destabilizing interactions and their known and surmised functional importance. Questions raised in the context of one protein or another concern, for example, the magnitudes and pH dependence of ΔG_{el} values, evidence from effects of ionic strength variation or substitution of amino acids, roles of specific groups or ion pairs, and indications of functional adaptation of given SA_j values.

The second stage of the analysis deals with assembly processes involving the hemoglobin tetramers, the docking of BPTI with trypsin, and myoglobin folding. Among the topics raised are net changes in free energy between reactants and products in the assembly proc-

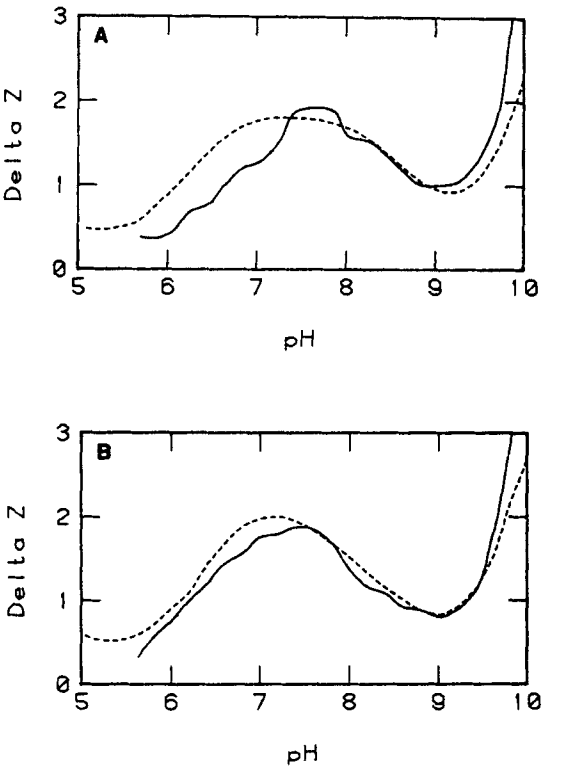

FIGURE 27. The difference in number of bound protons, Delta Z, between proton titration curves at 10 and 20°C. The solid curves are those computed from the Antonini et al.[134] data at 0.25 *M* NaCl; the dashed curves are those computed from the theoretical curves calculated at I = 0.10 *M*. (A) Deoxyhemoglobin; (B) liganded hemoglobin. (From Flanagan, M. A., Role of Electrostatic Interactions in the Structure and Function of Myoglobins, Lysozyme and Hemoglobin, Ph.D. thesis, Indiana University, Bloomington, 1983.)

esses, relation of docking orientation to component dipoles and monopoles, and relative importance of electrostatic and nonelectrostatic contributions to the processes.

A. Stabilizing and Destabilizing Interactions

1. Myoglobins

Figure 28 plots the value of $\Delta G_{i,el}$ for the individual groups in sperm whale myoglobin as a function of pH. The distinct contours represent the summed interactions between the site in question and all others of like and unlike charge, varying degrees of charge occupancy, SA_{ij} and r_{ij}. The three panels cover, first, the acidic groups which all provide stabilizing interactions under all conditions but with marked quantitative distinctions. Second, the histidine residues vary widely in contribution, with several proving distinctly destabilizing at low pH. Third, the strongly basic residues show a wide variety of behavior, in that many sites change little whereas others become destabilized in certain pH ranges. All these latter sites retain their positive charge and thus respond passively to changes in occupancy of other sites. The three panels illustrate vividly the distinctive roles of each site.[82]

The variety of roles illustrated in Figure 28 suggests a highly developed adaptation in which electrostatic interactions provide part of the basis for biological functional diversity.

Table 6
APPARENT ENTHALPIES AND pK_i VALUES FOR HISTIDINE AND AMINO TERMINAL RESIDUES OF DEOXY- AND OXYHEMOGLOBIN, pH 7.4, I = 0.10 *M*, 25°C

	Deoxyhemoglobin		Oxyhemoglobin	
Residue	ΔH	pK_i	ΔH	pK_i
Val 1	9.67	7.95	9.85	7.24
His 20	6.69	6.71	6.68	6.71
His 45	6.71	6.90	6.73	6.94
His 50	5.86	7.53	5.92	7.49
His 72	6.84	6.29	6.79	6.28
His 89	6.60	7.04	6.54	7.20
His 112	5.83	7.67	5.82	7.65
Val 1	9.38	7.53	9.74	6.80
His 2	6.14	6.63	6.44	6.63
His 77	6.80	6.63	6.91	6.60
His 117	6.40	7.88	6.40	7.86
His 143	5.96	6.28	5.39	4.73
His 146	5.92	8.22	5.72	8.08

Taken from Flanagan, M. A., Role of Electrostatic Interactions in the Structure and Function of Myoglobin, Lysozyme and Hemoglobin, Ph.D. thesis, Indiana University, Bloomington, 1983.

A somewhat simpler but vivid illustration of the distinctive adaptation of the charge lattice in sperm whale myoglobin is found in Figure 29. Here the strongest single stabilizing (A) or destabilizing (B) interaction is plotted for each site, rather than the summed terms as in Figure 28. The primary W'_{ij} values are plotted against r_{ij}. The points are numbered and can be keyed from Figure 28. In several cases, numbers are paired as both members of an interacting pair recognize the other as the single most stabilizing or destabilizing influence to which it is subjected. Figure 29 shows (A) how important such primary stabilizing interactions are and (B) how minimized are the primary destabilizing interactions. Overall, the discrete charge lattice is strongly biased towards stability in terms of SA characteristics and distances of separation.[82]

Table 7 summarizes the information on $\Delta G_{i,el}$ values for individual groups in Figure 28 for pH 7.50, I = 0.01 *M* and 25°C and extends it to show the frequencies of substitution with given residues in 53 mammalian myoglobins. Invariant residues are marked X. The residues within a particular class are listed in the order of decreasing stabilization (compare with Figure 28). Strong conservation is the rule, with charges being retained in many cases where substitutions are observed.[82] Table 7 shows clearly the ranges of (1 − SA) values for each residue as well as the corresponding $\Delta G_{i,el}$ values.

Table 8 summarizes the W'_{ij} values in kcal/mol relating members of charge pairs such as those emphasized in Figure 29. The table lists the paired residues in sperm whale myoglobin, computed values of W'_{ij}, r_{ij}, and the structural regions involved in the protein according to helical or interhelical segments. Finally, an index of retention is shown, comprising the percentage of both charge types retained in the pair among 53 varieties of mammalian myoglobins. Omitting the heme entry, 11 charge pairs account for nearly 80% of the total

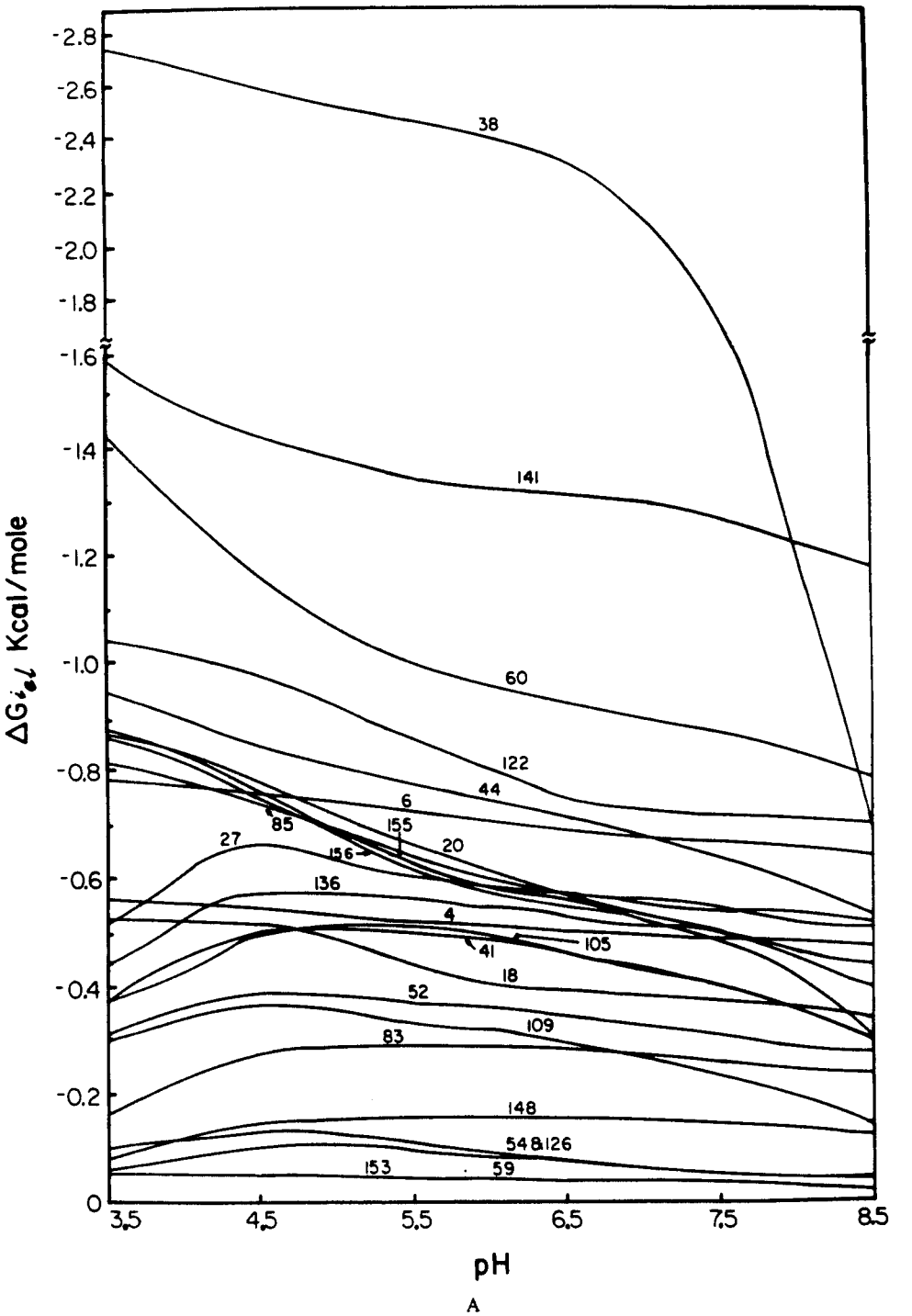

FIGURE 28. (A) Computed free energy contributions, $\Delta G_{i,el}$ in kilocalories per mole, for acidic groups over the pH range from 3.5 to 8.5. The COOH terminal is denoted by 153. Residues 20, 27, 44, 60, 122, 126, and 141 are aspartic acid. All others are glutamic acid. Note that the scale is condensed beyond −1.6 kcal/mol in the ordinate. The ionic strength is 0.01 *M* and the temperature is 25°C. (B) Corresponding plot for histidine residues. Note that the negative ordinate is condensed. (C) Corresponding plot for basic residues. The NH_2 terminal is denoted by 1. Residues 31, 45, 118, and 139 are arginine. The iron atom is denoted by 154. All others are lysine. (From Friend, S. H. and Gurd, F. R. N., *Biochemistry*, 18, 4620, 1979. With permission.)

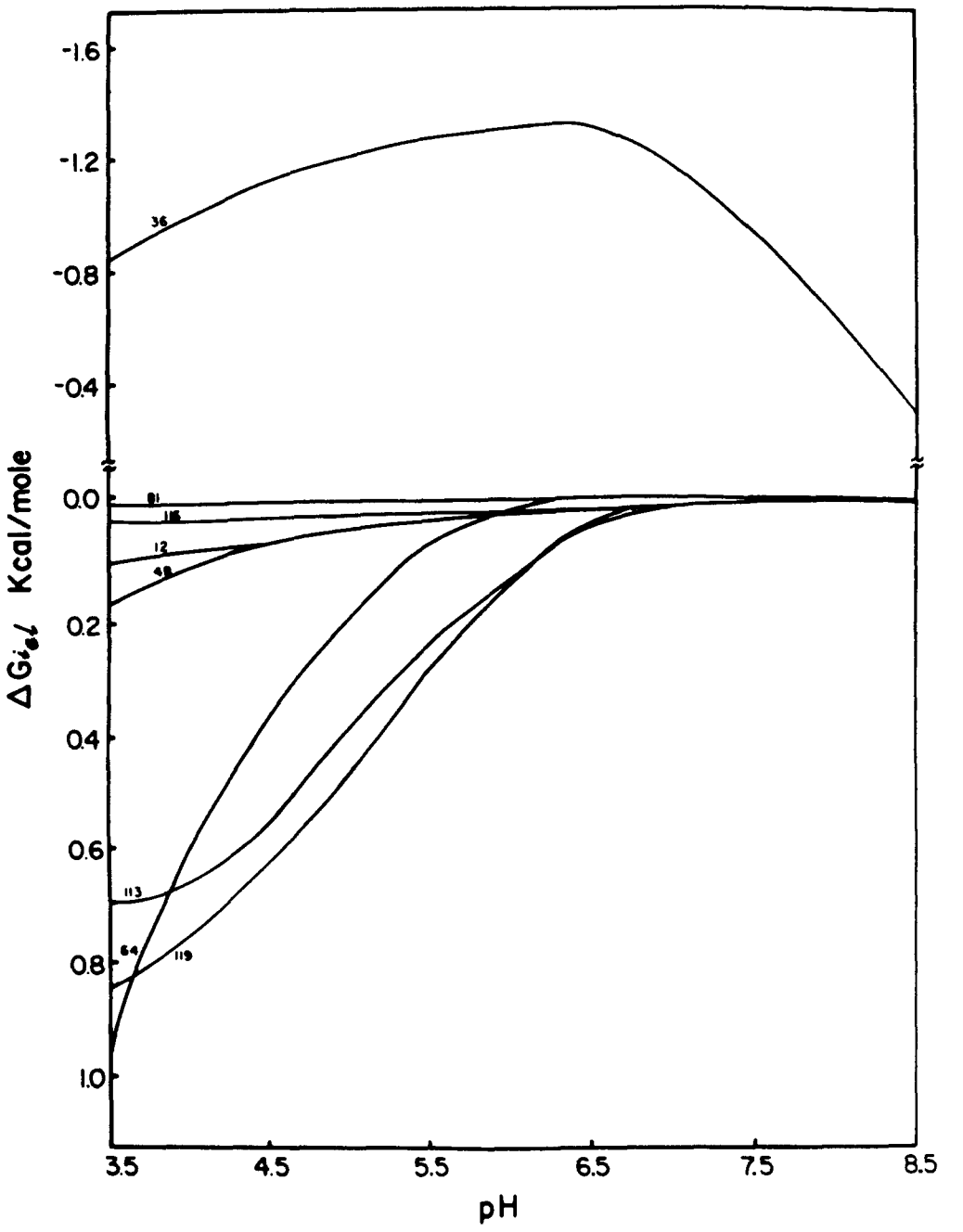

Figure 28B

electrostatic stabilization.[82] The retention index is convincingly high. The strongly stabilizing interactions are nearly evenly distributed between those that will stabilize a given local structural element and those that will attach two separate structural elements. Presumably the intraelement stabilizations could contribute to nucleation stages and interelement stabilizations to final folding, with both being responsible for significant stabilization of the complete structure.

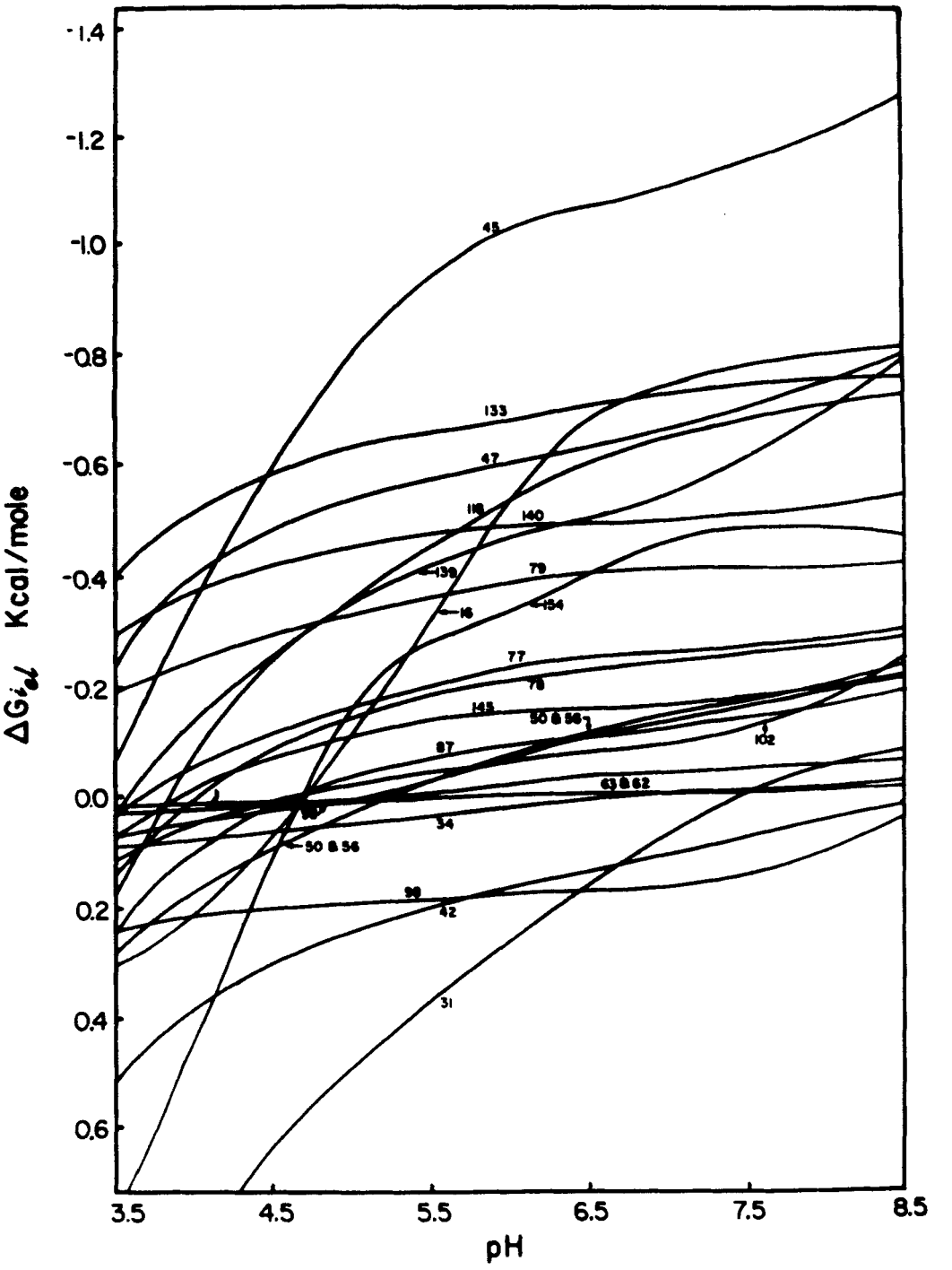

Figure 28C

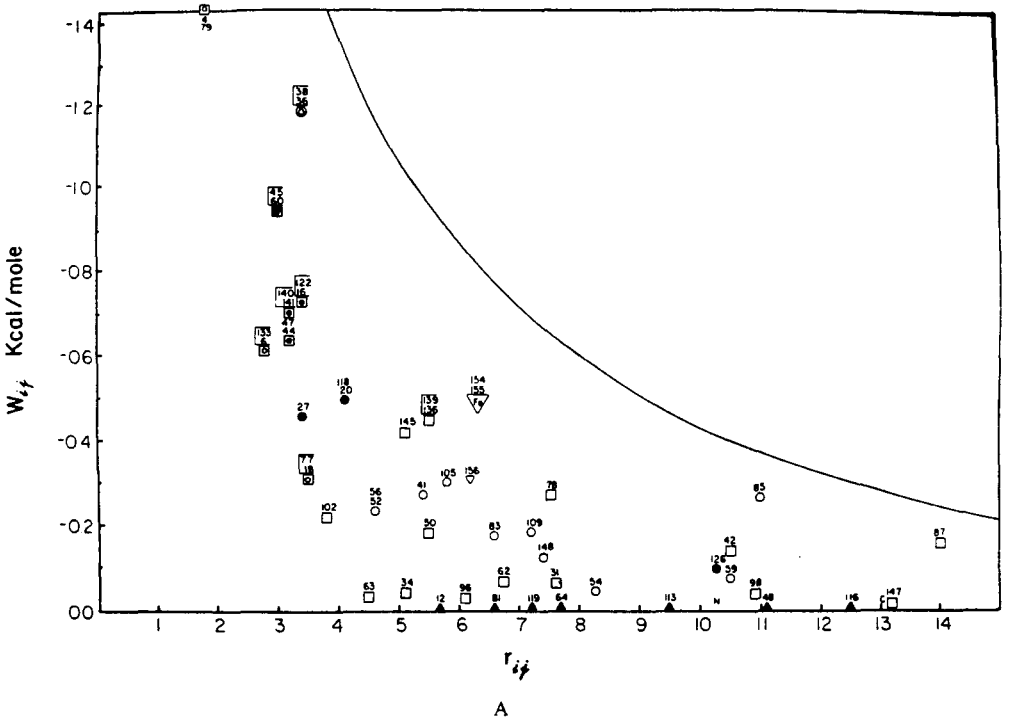

A

FIGURE 29. (A) Computed maximum stabilizing interaction, W_{ij}, in kilocalories per mole, experienced by each charged site plotted against the distance in angstroms, r_{ij}, between the numbered site and the oppositely charged site with which that maximum interaction occurs. In the case of the 11 charge pairs in which the same interaction holds top rank for both members of each pair, both site numbers are shown together. The classes of sites are denoted as follows: (■) Arg; (□) Lys; (Fe) iron atom; (N) NH_2 terminal; (▲) His; (○) Glu; (●) Asp; (C) COOH terminal; (▽) propionic acid. The curve denotes the computed stabilization between fully occupied, oppositely charged sites, each assigned (1 − SA) of 0.95. The conditions are for pH 7.50, an ionic strength of 0.01 *M*, and 25°C. (B) The corresponding destabilizing interactions for all charged sites. (From Friend, S. H. and Gurd, F. R. N., *Biochemistry*, 18, 4620, 1979. With permission.)

The free energy computations of the type in Figure 28 are summed in Figure 30 as a function of pH for three ionic strength values.[81] The pH of maximum stabilization at each ionic strength occurs near 6.5, well below the isoionic point near pH 8.30. Substantially the same pH profile was obtained by Acampora and Hermans[135] when they plotted the midpoints of thermal denaturation transitions against pH. This result provides very strong support for the general correctness of the electrostatic treatment.[81] The computations in Figure 30 were based on the $(1 - SA_j)$ formulations. As shown in Figure 31,[106] the $(1 - SA_{ij})$ formalism results in somewhat higher values of $\Sigma\Delta G_{el}$ with the same pH dependence.

The systematic decrease in stability with increasing ionic strength reflects the shielding of preferentially stabilizing interactions (Figure 32). The loss of stabilization also results from changes in the charge array, more easily observed at low pH.[9,71,81,106] The acid denaturation profiles of several species of myoglobins are shown in Figure 33. The curves shown are representative of myoglobins of several suborders of Cetacea containing characteristic patterns of substitution. The less stable species undergo the transition at the higher pH values. On the acid limbs of Figure 30, asterisks mark the pH values of the midpoints of the transition under the particular conditions.[81] It is significant that under these conditions the native structure is stabilized to a considerable extent by the electrostatic interactions. The point has been made that, although electrostatic lattice effects will be weaker in the disordered, denatured structure, the release of masked histidine side chains from the interior

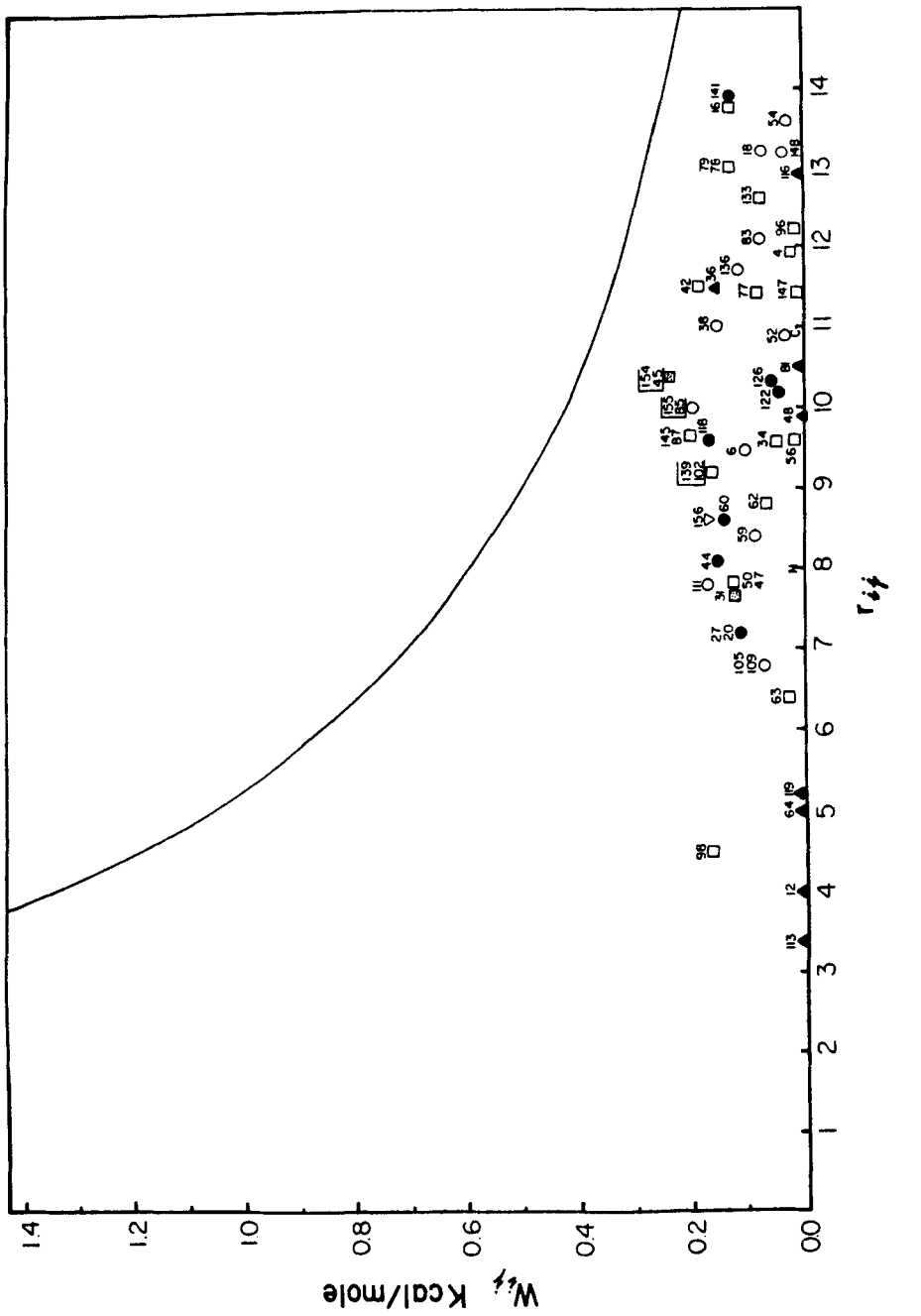

FIGURE 29B

Table 7
SUMMED ELECTROSTATIC FREE ENERGY CONTRIBUTION OF INDIVIDUAL CHARGE SITES AND THEIR SUBSTITUTION FREQUENCIES IN MYOGLOBIN

			Substitution[b]	
Residue	**(1 − SA)**	**$\Delta G_{i,el}$[a]**	**Residue**	**Frequency**
		Acidic Residues		
Glu-38	0.55	−1.73	x	
Asp-141	0.80	−1.31	x	
Asp-60	0.60	−0.88	Glu	2
Asp-122	0.45	−0.75	Glu	8
			Asn	6
			Gln	1
Glu-6	0.50	−0.69	x	
Asp-44	0.60	−0.66	x	
Asp-20	0.50	−0.55	x	
Glu-85	0.75	−0.55	Gln	2
			Asn	1
Asp-27	0.35	−0.55	Glu	36
Glu-136	0.50	−0.52	x	
Glu-4	0.25	−0.49	Asp	49
Glu-105	0.35	−0.43	x	
Glu-41	0.50	−0.42	Ser	2
			Asp	1
Glu-18	0.40	−0.39	x	
Glu-52	0.30	−0.32	Pro	2
			Ala	2
Glu-109	0.30	−0.29	Asp	17
			Gly	1
Glu-83	0.40	−0.29	Asp	8
Glu-148	0.20	−0.14	Val	3
Glu-54	0.25	−0.07	Asp	10
Asp-126	0.30	−0.07	Glu	1
Glu-59	0.30	−0.05	Ala	2
Prop-155	0.70	−0.52	x	
Prop-156	0.50	−0.26	x	
Gly-153	0.10	−0.04	x	
		Histidine Residues		
His-36	0.85	−0.61	x	
His-64	0.95	0.00	x	
His-81	0.05	0.00	Gln	8
His-12	0.15	0.00	Asn	45
His-116	0.05	+0.01	Gln	21
His-48	0.30	+0.02	Asn	2
His-113	0.35	+0.06	Gln	15
His-119	0.80	+0.06	x	

Table 7 (continued)

Residue	(1 − SA)	$\Delta G_{i,el}$[a]	Substitution[b] Residue	Frequency
		Basic Residues		
Arg-45	0.75	−1.14	Lys	54
Lys-16	0.90	−0.75	x	
Lys-133	0.60	−0.70	x	
Lys-47	0.55	−0.69	x	
Arg-118	0.70	−0.66	Lys	41
Arg-139	0.95	−0.59	x	
Lys-140	0.45	−0.49	Asn	33
Lys-79	0.45	−0.42	x	
Lys-77	0.45	−0.24	x	
Lys-78	0.60	−0.22	x	
Lys-145	0.50	−0.16	Asn	6
			Gln	3
			Glu	1
Lys-56	0.65	−0.15	Arg	3
Lys-50	0.40	−0.13	x	
Lys-87	0.95	−0.10	Ala	1
Lys-102	0.40	−0.10	Gln	1
Lys-63	0.05	−0.08	x	
Lys-62	0.20	−0.08	Arg	2
Lys-96	0.05	−0.02	x	
Lys-34	0.15	−0.01	Thr	10
Arg-31	0.40	+0.05	Ser	1
Lys-42	0.75	+0.09	x	
Lys-98	0.20	+0.17	x	
Fe-154	0.95	−0.45	x	
Val-1	0.05	−0.01	Gly	49

Note: x denotes invariant residue.

[a] pH 7.50, ionic strength 0.01 *M*, 25°C.
[b] Substitutions among 57 mammalian myoglobins.

Taken from Friend, S. H. and Gurd, F. R. N., *Biochemistry*, 18, 4620, 1979. With permission.

of the molecule will account for a substantial stabilization to be attributed to protonation phenomena.[9,81,135] The masked histidine residues are conserved between species.

The electrostatic basis of the anchoring of structural elements in myoglobin was raised in connection with the charge pairs in Table 8. It was found that alterations in the anchoring of the A helix could be observed through changes in circular dichroism at 295 nm attributable to the only two tryptophan residues in the protein at positions 7 and 14.[136] The pH dependence of these changes is illustrated in Figure 34. Figure 35 shows the pH dependence of the molar ellipticities at 295 (open symbols) compared with that of overall structure reflected in the Soret absorbance at 409 nm. Parts A and B refer to the sperm whale and harbor seal myoglobins, respectively, at more than one ionic strength value. Clearly, the precise anchoring of the A helix undergoes a certain degree of change above the pH at which the overall change commences.

Table 8
ELECTROSTATIC STABILIZATION THROUGH CHARGE PAIRS

Paired residues		W_{ij} Kcal/mol	r_{ij} Å	Pairing by region	Charge-pair retention index
Glu-4	Lys-79	−1.44[a]	1.8	A-EF[b]	100[c]
Glu-38	His-36	−1.20	3.4	C-C	100
Asp-60	Lys-45	−0.96	3.0	E-CD	100
Asp-122	Lys-16	−0.74	3.4	GH-A	88
Asp-141	Lys-140	−0.71	3.3	H-H	42
Asp-44	Lys-47	−0.65	3.2	CD-CD	100
Glu-6	Lys-133	−0.62	2.8	A-H	100
Asp-20	Arg-118	−0.50	4.1	B-G	100
Prop-155	Fe-154	−0.48	3.5	Heme-Heme	100
Glu-136	Arg-139	−0.46	5.5	H-H	100
Glu-18	Lys-77	−0.32	3.5	A-EF	100
Glu-52	Lys-56	−0.24	4.6	D-D	93

[a] pH 7.50, ionic strength 0.01 *M*, 25°C.
[b] In accordance with the standard nomenclature, a single letter refers to a given helical segment, whereas two letters are used to denote an interhelical segment between the corresponding two helixes.
[c] Percentage retention of both charge types among varieties of mammalian myoglobin.

Taken from Friend, S. H. and Gurd, F. R. N., *Biochemistry*, 18, 4620, 1979. With permission.

On examining the pH dependence of pairwise interactions in sperm whale myoglobin it was found that Lys-16 shows stabilization especially with respect to Asp-122 (Table 9) but destabilization with respect to His-119, Arg-118, and His-12. Of these, His-119 shows the appropriate $pK_{1/2}$ of 5.42 to provide the main destabilizing interaction with Lys-16.[82] A like pattern exists for the seal myoglobin in which there are effects of substitutions of Glu-122 and Lys-118. The different patterns are illustrated in Table 9 and Figure 36.[136]

The sensitivity of the stabilization of the A helix to a subset of charge site interactions has a counterpart in the titration behavior of a preparation of sperm whale myoglobin in which both tryptophan residues were converted to oxindolylalanine residues.[137] The effect of this conversion is twofold. First, the stereochemistry of C^{γ} is converted from trigonal to tetrahedral to alter the relation between aromatic nucleus and the C^{α}-C^{β} axis. Second, the $C^{\delta 1}$, vicinal to C^{γ}, is oxidized to the ketone level to confer added bulk and polarity.

The altered protein is considerably less heat stable than the unmodified protein.[137] The oxindolylalanine residues, monitored by circular dichroism at 264 nm, sense a change that precedes the overall measures of acid denaturation, in a way very reminiscent of the tryptophan probes in the unmodified protein (Figure 34). This observation implies a loosening of the A helix anchoring. Despite the absence of a direct alteration in the number of charge loci, Figure 37 shows that the titration curve in the native region, pH range 5.5 to 9.0, reflects a small, consistent decrease in protons bound relative to the unmodified protein.[137] This observation is an example of the interconversion of different classes of stabilizing or destabilizing energy categories in which packing and polarity changes are rendered as titration changes. A site-specific example of the change propagated beyond the immediate contacts of the A helix is provided in Figure 38.[137] Here the hemic acid dissociation is determined for the derivative (I) and the unmodified myoglobin (II).

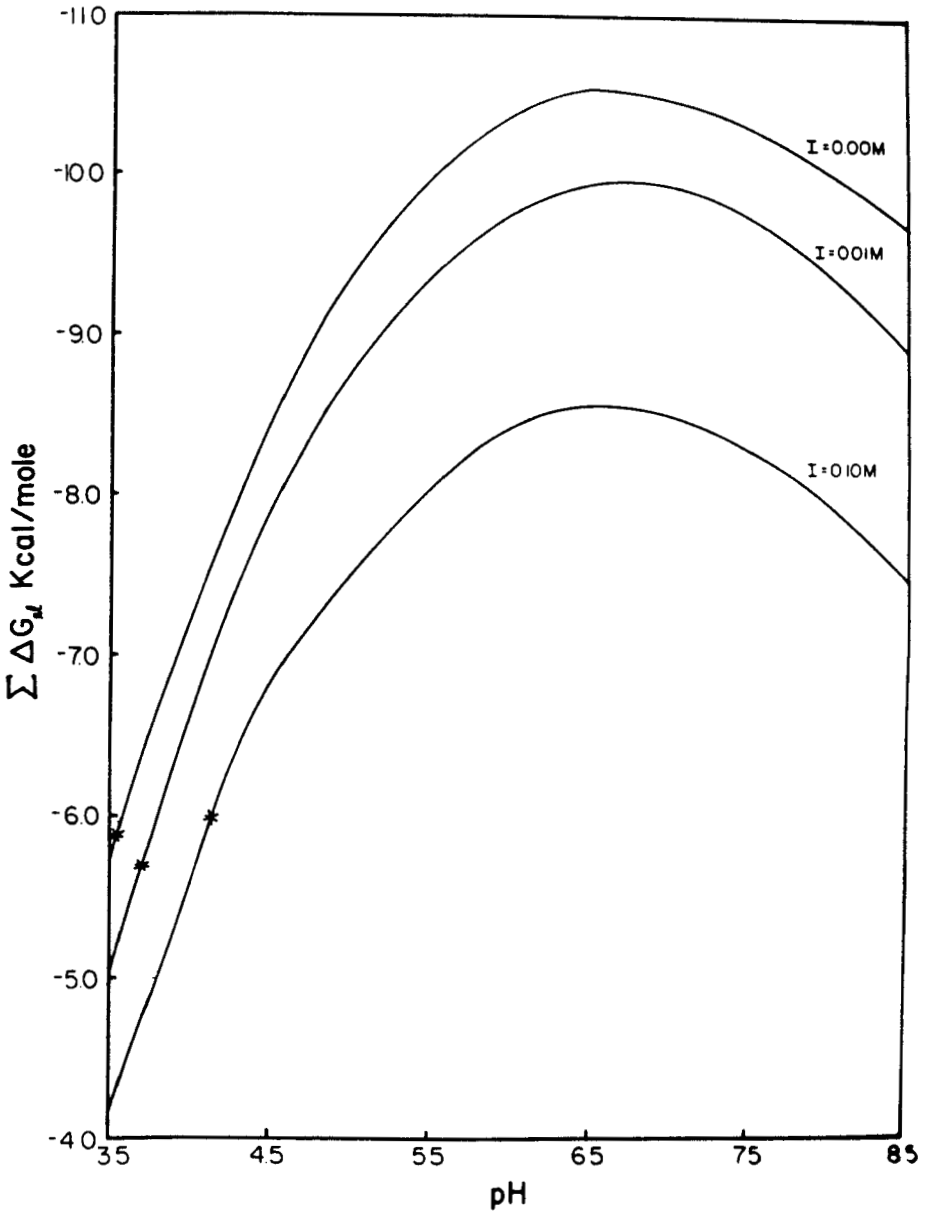

FIGURE 30. Dependence of summed electrostatic free energy terms, in kilocalories per mole, between individual charged sites as a function of pH at ionic strength values of 0.00, 0.01, and 0.10 *M*. These calculations were done with the $(1 - SA_j)$ formalism. The asterisked point on each curve at low pH represents the midpoint pH for the unfolding transition at the particular ionic strength. (From Friend, S. H. and Gurd, F. R. N., *Biochemistry*, 18, 4612, 1979. With permission.)

The results of the oxindolylalanine myoglobin studies imply various structural adaptations relative to the unmodified protein as would be expected on stereochemical grounds. By circular dichroism the modified side chains show continued constraints, whereas Figures 37 and 38 illustrate how small changes in electrostatic characteristics have been recruited as part of the process of overall adaptation to the new composition. Focusing on the A helix, it is striking that the electrostatic contribution to its anchoring to the rest of the myoglobin

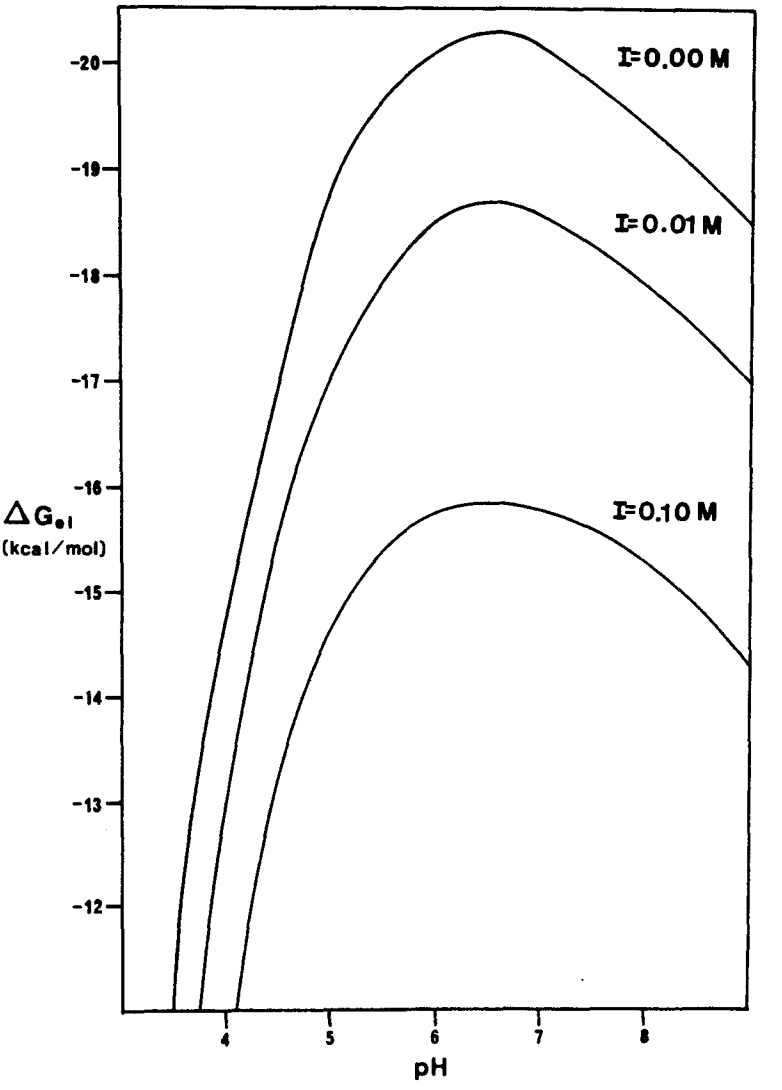

FIGURE 31. Dependence of summed electrostatic free energy terms, in kilocalories per mole, between individual charged sites as a function of pH at ionic strength values of 0.00, 0.01, and 0.10 *M*. These calculations were done with the $(1 - \overline{SA}_{ij})$ formalism.

is computed to be especially strong relative to any other structural element in the protein.[139] Given that electrostatic interactions are relatively forgiving of small changes in r_{ij} compared to other stabilizing interactions, it follows that they are well suited to provide ample stabilization despite the substantial local perturbation produced by the oxindolylalanine residues.

2. Hemoglobins

The stabilizing and destabilizing electrostatic interactions in hemoglobins have made themselves felt in Section III in the guise of asymmetries of charge and special SA distributions in which histidine-carboxyl interactions and binding of external ions are especially prominent characteristics (Figures 22 and 25 to 27 and Table 8).

Because the different states of assembly of hemoglobins, monomers, dimers, tetramers, and liganded or effector-complexed forms reflect different responses of the charge site

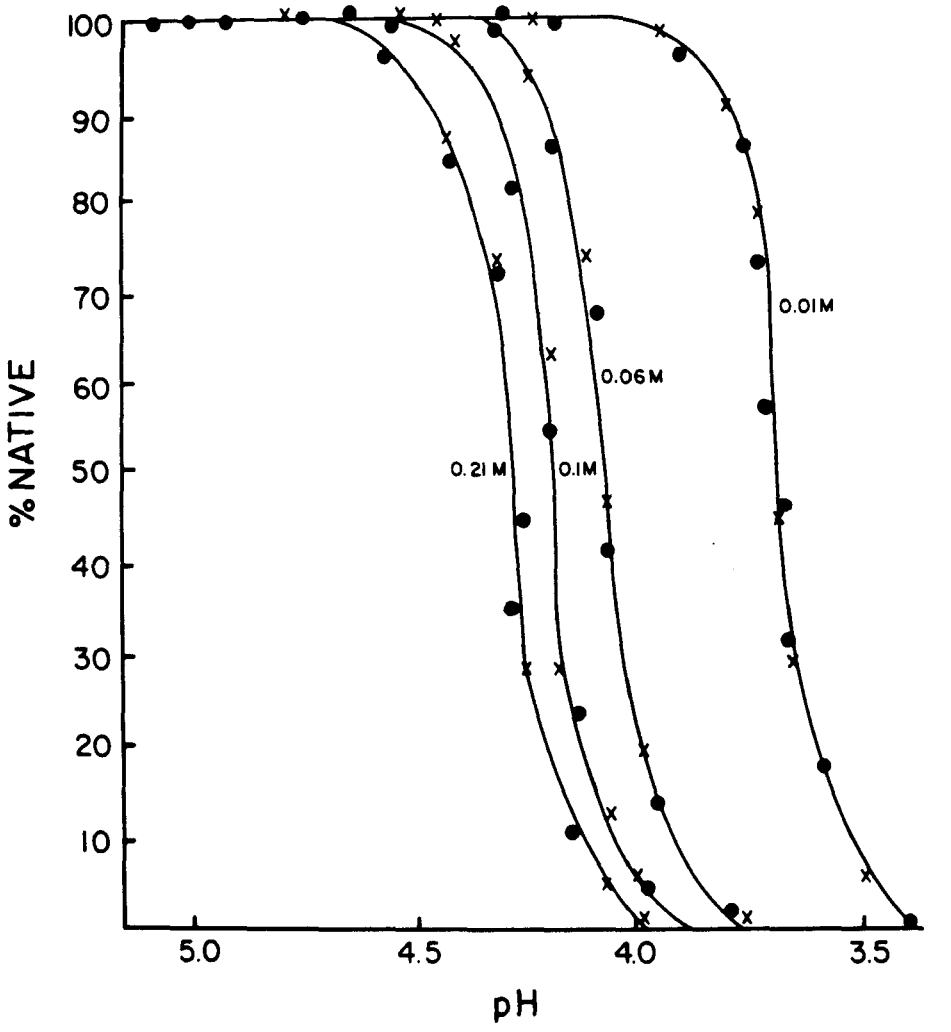

FIGURE 32. Dependence of the unfolding transition of sperm whale ferrimyoglobin on pH. The ordinate shows the percent of the native form. The curves show results for ionic strength values of 0.21, 0.10, 0.06, and 0.01 *M*, respectively: (●) 409 nm: (X) 222 nm. (From Friend, S. H. and Gurd, F. R. N., *Biochemistry*, 18, 4612, 1979. With permission.)

lattices, each has special electrostatic characteristics. The various examples will be dealt with systematically later. However, it is useful to illustrate with the example of the assembly of the αβ dimer from the monomers the roles of particular groups in promoting or hindering the assembly process. Table 10 lists all electrostatic interaction energies greater than 50 cal/mol for monomer-dimer assembly at pH 7.6.[106] The entries indicate the change in $\Delta G_{i,el}$ for the given residue realized by subtracting the monomer value from the dimer value. The table shows broad but selective participation by residues in both chains. Net involvement of histidine or aminoterminal groups titrating in this pH range is minimal, which may explain why this assembly step is inferred from experimental evidence to be independent of pH between pH 7 and 9.[125] As will be shown in Part B (this section), the patterns of higher order assembly are qualitatively and quantitatively different.

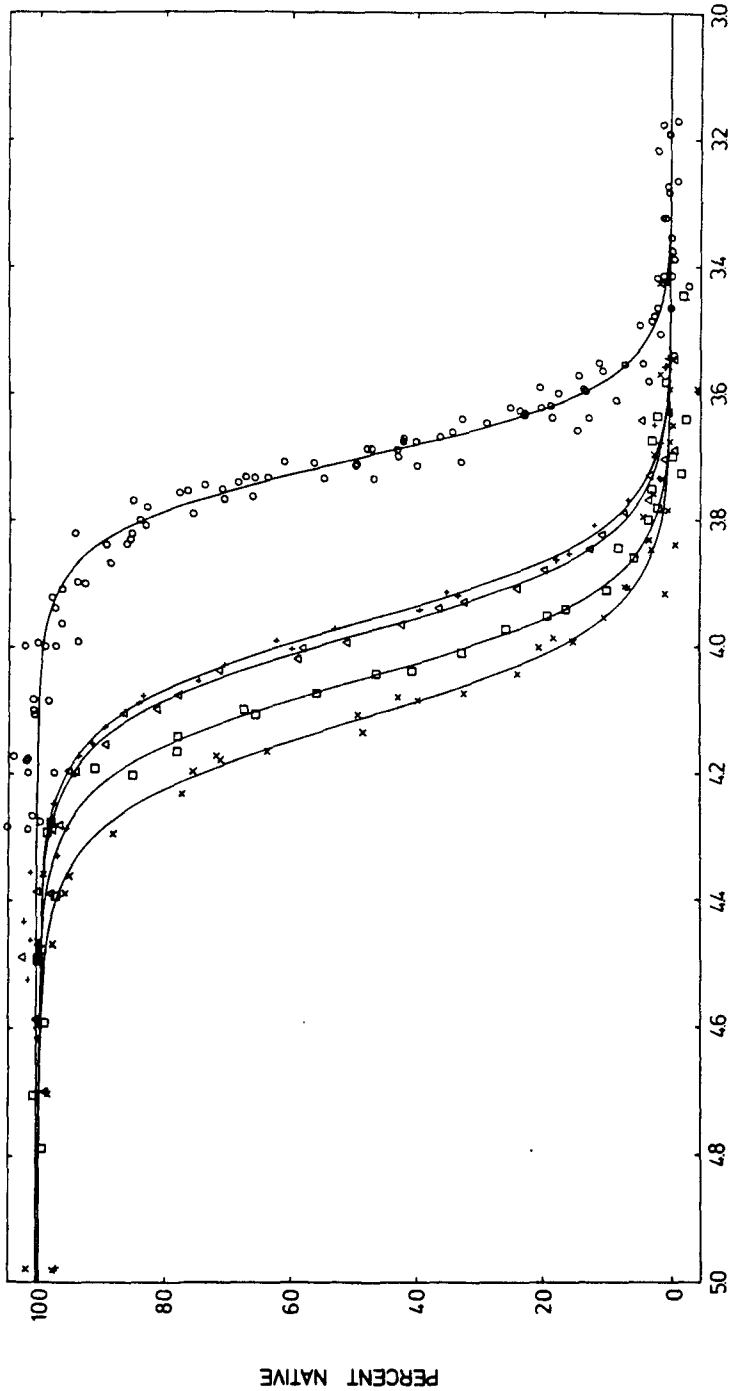

FIGURE 33. Acid-denaturation profiles of representative species of cetacean myoglobin at I = 0.01 *M*, 25°C. The percent native structure is plotted as a function of pH for the myoglobins of sperm whale (○), goose-beaked whale (+), killer whale (△), minke whale (□), and Hubb's beaked whale (X). Increasing hydrogen ion activity is to the right. (From Flanagan, M. A., Garcia-Moreno E., B., Friend, S. H., Feldmann, R. J., Scouloudi, H., and Gurd. F. R. N., *Biochemistry*, 22, 6027, 1983. With permission.)

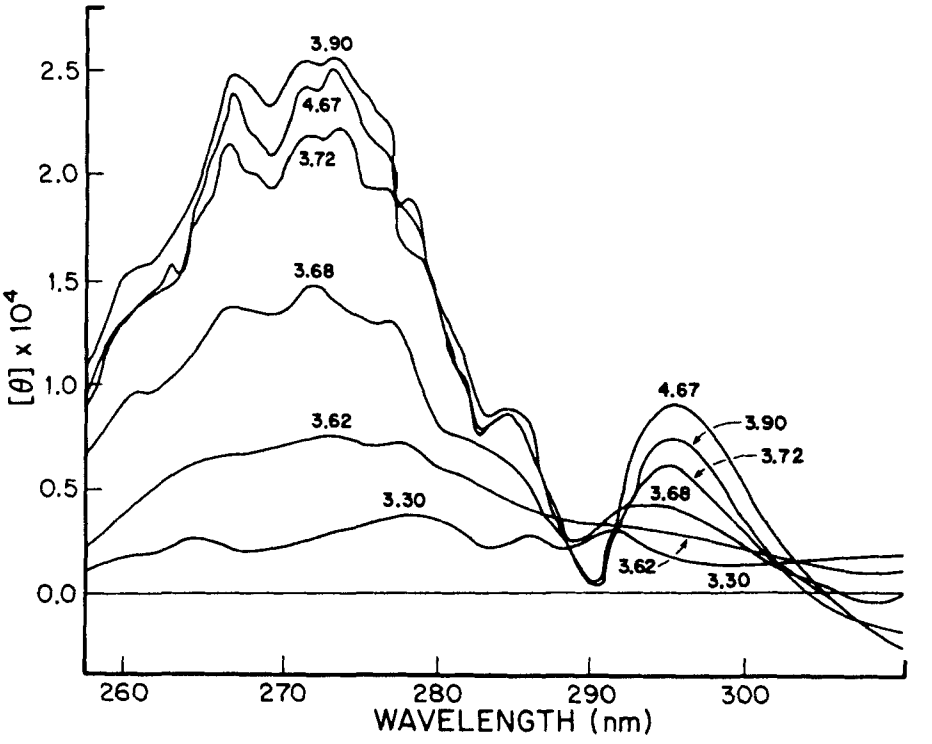

FIGURE 34. Near ultraviolet CD spectra of sperm whale ferrimyoglobin, 10 μ*M*, at various pH values. The spectra were recorded in acetate buffers at an ionic strength of 0.01 *M*. Each curve is an average of 12 spectra. (From Gurd, F. R. N., Friend, S. H., Rothgeb, T. M., Gurd, R. S., and Scouloudi, H., *Biophys. J.*, 32, 65, 1980. With permission.)

3. Bovine Pancreatic Trypsin Inhibitor (BPTI)

The examples of myoglobin and hemoglobin represent, respectively, a symmetrical effective charge lattice and one that has a certain inherent dissymmetry. A final example to illustrate stabilizing and destabilizing interactions concerns the adaptation to a different asymmetry in the structure of BPTI and a pH-dependent conformational transition that can be traced experimentally and theoretically.

BPTI is small enough that the titration behavior of all charge-bearing groups can be observed by ^{13}C-NMR.[29] The composition is heavily weighted towards strongly basic amino acids. Apart from the N-terminal and C-terminal groups, the titrating groups are four carboxyl groups, three phenoxyl, four lysine amino, and six arginine guanidino. The most intriguing question concerns how can the large imbalance of charge be accommodated at neutral conditions without excessive destabilization and interference with disulfide bond matching? The answer has two parts. The first deals with the charge site lattice characteristics of the molecule as specified by the crystallographic structure determined at high pH in the isoionic range.[140] The second deals with a pH-driven conformational change involving the juxtaposition of the terminal residues 1 and 58.[141] Evidence for the latter change was confirmed and extended, and the consequences for electrostatic stabilization evaluated.[29]

Figure 39 shows the dependence on pH of summed ΔG_{el} in kcal/mol for the native BPTI structure at I = 0.00 in curve A and I = 0.01 in curve B. Some stabilization extends into and beyond the neutral pH range. Curve C shows the significant broadening of the region of stability for the structure involving the juxtaposition of the termini. The latter increment arises first from site occupancy of the positive terminal amino group as the pH is lowered,

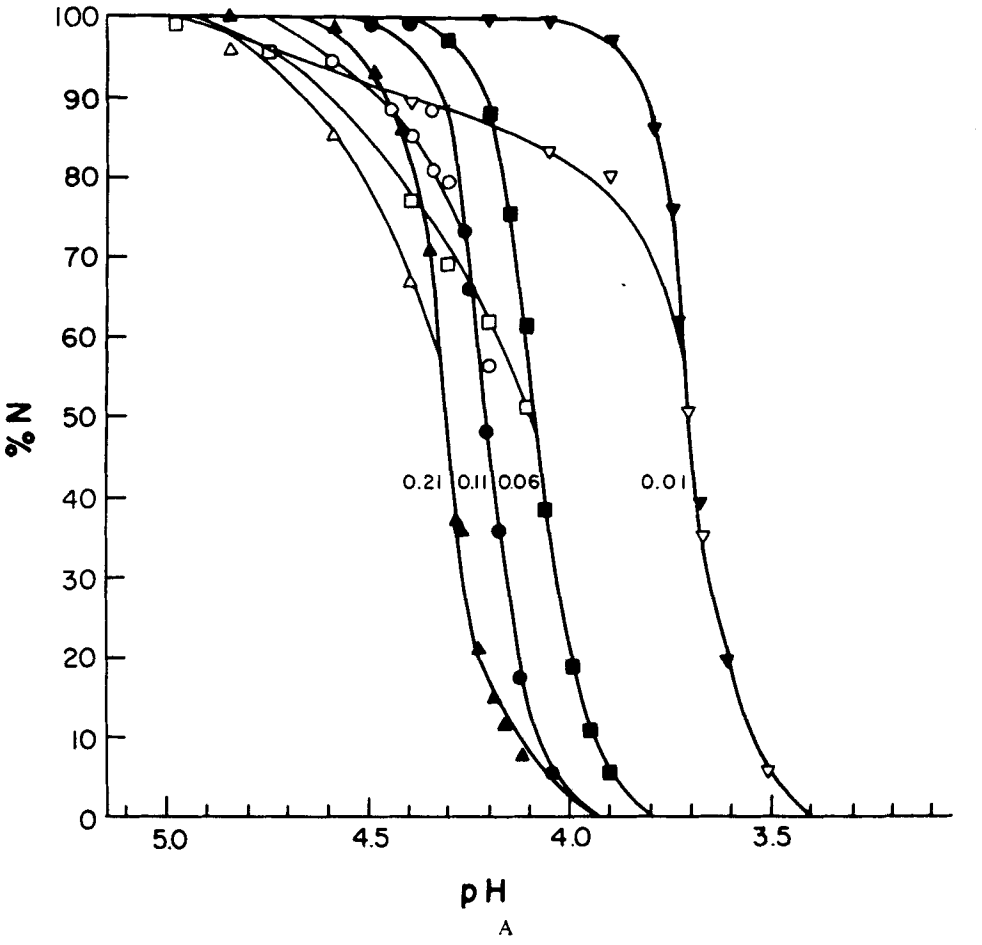

FIGURE 35. (A) Profiles for acid denaturation of sperm whale ferrimyoglobin in terms of percent native values at various ionic strengths. The thick lines and darkened symbols represent the 409-nm Soret band absorbance changes, while the thin lines and open symbols represent the change in molar ellipticities at 295 nm. The symbols (▼,▽), (■,□), (●,○), (▲,△) indicate ionic strengths of 0.01, 0.06, 0.11, and 0.21 *M*, respectively. (B) Similar unfolding profiles for seal myoglobin; (■,□), (●,○) indicate ionic strengths of 0.01 and 0.10 *M*, Gurd, F. R. N., Friend, S. H., Rothgeb, T. M., Gurd, R. S., and Scouloudi, H., *Biophys. J.*, 32, 65, 1980. With permission.)

second from the local spatial rearrangement to bring the interacting residues together, and third from the change in SA_{ij} accompanying the rearrangement. Examination of the individual contributions of other sites shows that the lattice distribution exploits the negative charges with relatively low SA values and provides efficient stabilizing interactions, with minimized destabilizing interactions between the positively charged sites achieved with high SA values. Comparison of curves A and B shows the effect of ionic shielding in lessening the destabilizing interactions; we have stressed before that increased ionic strength preferentially shields the relatively more distant charges. The importance of the specific SA values to compensate for the numerical imbalance in anionic and cationic sites is brought out by curve D in which every group is arbitrarily assigned for the purpose of calculation to the overall average SA value of 0.76. In this example, as soon as the tyrosine residues are protonated, the small net stabilization approaches nil.[29]

Since BPTI is a very stable protein indeed, the overall role of the electrostatic stabilization is small.[142-145] The role of the electrostatic lattice in the folding sequence may be especially

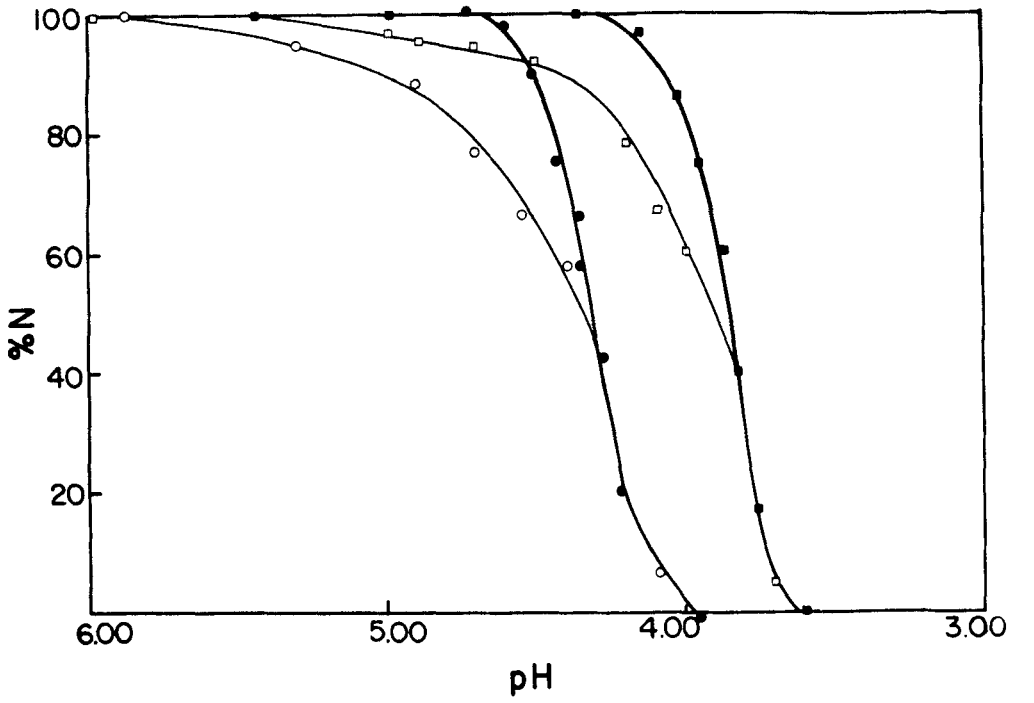

Figure 35B

important, however, because it can provide guidance to the folding pathway out of proportion to the energy differences in the overall process. We shall see in the following section that the charge lattice does appear to influence the docking process with trypsin.

B. Assembly Processes

1. Hemoglobin: Electrostatic and Nonelectrostatic Factors

Electrostatic free energy contributions to assembly processes are computed by subtracting the summed contributions of the reactants from that of the product. In the case of the hemoglobins, such analyses can be particularly revealing. As noted above, the formation of the $\alpha^1\beta^1$ dimer is so strongly favored that over the physiological range of conditions, and indeed the practical range for experimental measurement, the assembly processes of dimer to tetramer can be isolated. The interface formed between one dimer and another involves both like and unlike monomeric units, e.g., $\alpha^1\alpha^2$ or $\alpha^1\beta^2$. Either the deoxy or the oxy dimer-tetramer assembly requires the juxtaposition of substantial surfaces in the contact that were previously exposed to solvent. The contacts are somewhat different for the deoxy and oxy systems, offering the opportunity to sample the application of similar principles to two distinct cases. Furthermore, both assembly processes can be analyzed and defined experimentally for numerous natural variants bearing single substitutions in either the α or β chain.

The electrostatic free energy for the assembly of tetramer from dimer is defined as:

$$\Delta G_{2,el} = (\Delta G_{el})_{Tet} - 2\,(\Delta G_{el})_{Dim} \tag{19}$$

where $\Delta G_{2,el}$ for deoxy and oxy assemblies are denoted at $^{o}\Delta G_{2,el}$ and $^{4}\Delta G_{2,el}$, respectively. By substracting the deoxy assembly free energy from that for oxy assembly, the regulatory

Table 9
INTERACTIVE ELECTROSTATIC FREE ENERGIES IN CAL/MOL BETWEEN POSITION 16 AND POSITIONS 118, 119, AND 122 IN SPERM WHALE AND SEAL MYOGLOBIN AS A FUNCTION OF pH AT I = 0.01 *M* AND I = 0.10 *M* AT 25°C

Ionic strength	pH	ΔG_{el} 16-118	ΔG_{el} 16-119	ΔG_{el} 16-122
Sperm Whale Myoglobin				
r_{ij} (Å)		10.25	5.21	3.41
I = 0.01 *M*	4.00	138	720	−734
	4.50	138	662	−734
	5.00	138	542	−734
	5.50	138	360	−734
	6.00	138	173	−734
I = 0.10 *M*	4.00	63	662	−619
	4.50	63	567	−631
	5.00	63	475	−637
	5.50	63	331	−648
	6.00	63	173	−648
Seal Myoglobin				
r_{ij} (Å)		10.42	2.30	6.74
I = 0.01 *M*	4.00	66	310	−130
	4.50	66	220	−160
	5.00	66	120	−170
	5.50	66	51	−180
	6.00	66	19	−200
I = 0.10 *M*	4.00	39	320	−77
	4.50	39	250	−110
	5.00	39	160	−120
	5.50	39	71	−130
	6.00	39	26	−130

Taken from Gurd, F. R. N., Friend, S. H., Rothgeb, T. M., Gurd, R. S., and Scouloudi, H., *Biophys. J.*, 32, 65, 1980. With permission.

energy, $\delta\Delta G_{04,el}$, is obtained.[125] For a particular site the contribution to the electrostatic free energy of assembly is

$$\delta\Delta G_{i,el} = (\Delta G_{i,el})_{Tet} - (\Delta G_{i,el})_{Dim} \quad (20)$$

When summations of all groups are made, both members of the identical pair of sites in the tetramer are considered (Equation 19). A difference between $\delta\Delta G_{i,el}$ for hemoglobin A_o and for a given mutant is denoted as $\delta\Delta G_{i,el}$.

The summations considered here correspond to the pairwise interaction terms used to construct titration curves for normal liganded and unliganded hemoglobin A_o (Figures 7 and 20 to 27 and Tables 5, 6, and 10) and specifically follow the assumptions concerning Cl^- occupancy applied to curve 3 of Figure 26. The procedures for placement of substituting side chains retained as much as possible of the initial stereochemistry and sought to minimize packing or polarity conflicts with neighboring side chains.[71,130,140]

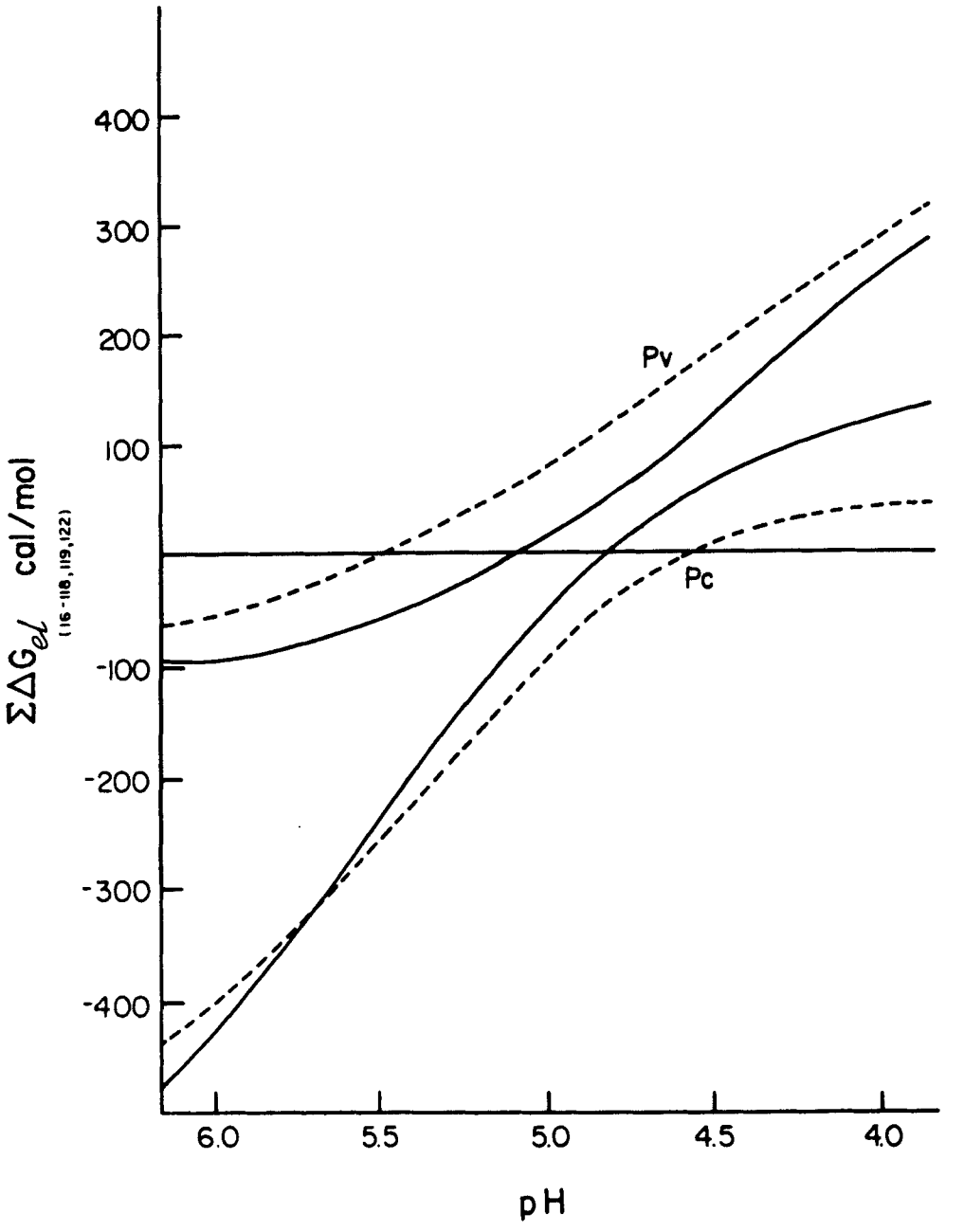

FIGURE 36. Summed electrostatic free energy between residues 16 and 118, 119, 122, $\Sigma\Delta G_{el(16\text{-}118,119,122)}$, in sperm whale myoglobin (lower curves) and seal myoglobin (upper curves) as a function of pH between 6.0 and 4.0. Computed values at 25°C are shown for I = 0.01 *M* (——) and I = 0.01 *M* (- - - -). (From Gurd, F. R. N., Friend, S. H., Rothgeb, T. M., Gurd, R. S., and Scouloudi, H., *Biophys. J.*, 32, 65, 1980. With permission.)

As recognized for assembly of hemoglobin A_o[146] and in the present calculations,[130] as well as in other systems,[147,148] changes in ΔG_{el} upon molecular association reflect contributions both from direct formation of intermolecular charge interactions and indirect potentiation of intramolecular charge interactions from the reduction of local effective dielectric

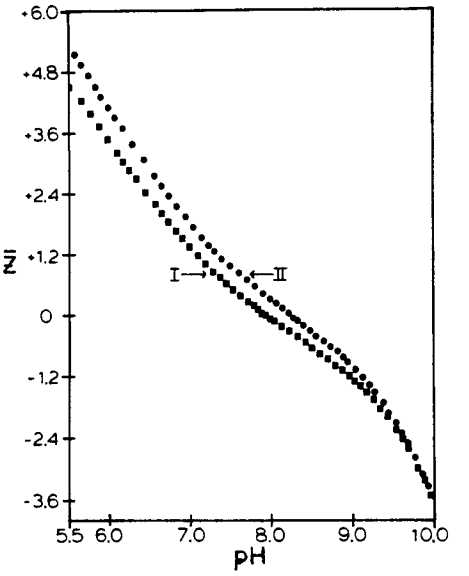

FIGURE 37. Potentiometric hydrogen ion titration of aquoferri derivatives of (I) (7,14-*bis*-oxindolylalanine) myoglobin and (II) sperm whale myoglobin in 0.01 *M* KCl. (From Radding, J. A., The Chemical Modification of Tryptophans in Sperm Whale Myoglobin, Ph.D. thesis, Indiana University, Bloomington, 1983. With permission.)

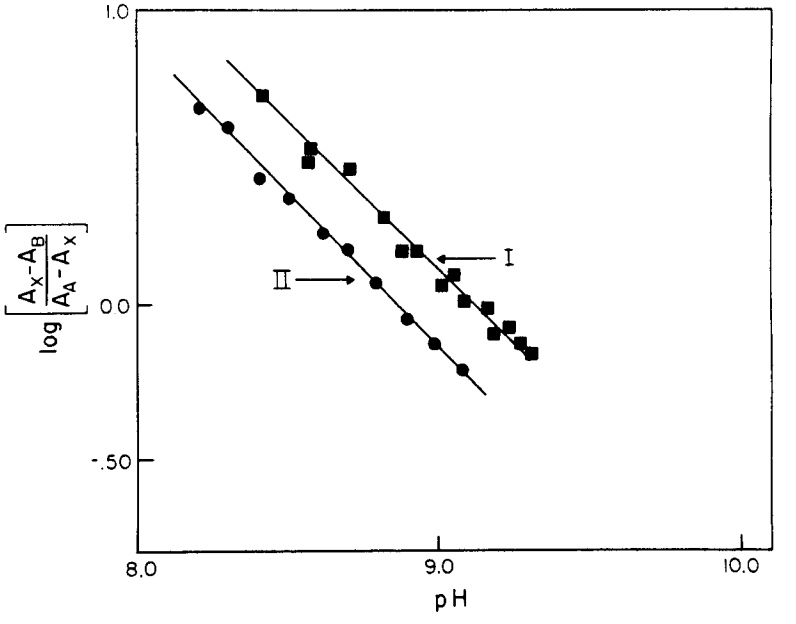

FIGURE 38. Hemic acid dissociation constant determination for (7,14-*bis*-oxindolylalanine) myoglobin (I) and sperm whale myoglobin (II) as determined by Nakhleh[138] at an ionic strength of 0.01 *M*. (From Radding, J. A., The Chemical Modification of Tryptophans in Sperm Whale Myoglobin, Ph.D. thesis, Indiana University, Bloomington, 1983. With permission.)

Table 10
ELECTROSTATIC CONTRIBUTION OF INDIVIDUAL CHARGED RESIDUES IN HEMOGLOBIN TO MONOMER-DIMER ASSEMBLY, pH 7.6, I = 0.10 *M*, 25°C

	Alpha chains			Beta chains	
Residue	ΔG_{el} (cal/mol)	$pK_{1/2}$[a]	Residue	ΔG_{el} (cal/mol)	$pK_{1/2}$[a]
Val 1	−50	8.2	Glu 7	−97	
Asp 6	115		Glu22	−58	
Lys 7	−77		Glu 26	−315	
Glu 27	−610		Arg 30	−644	
Glu 30	−115		Asp 94	−78	
Arg 31	−727		His 117	−55	7.7
Arg 40	−81		Glu 121	−66	
His 50	−54	7.4	His 146	−114	8.0
Asp 85	−56				
Lys 99	−82		Total	−1427	
His 112	146	7.7			
Asp 126	100				
Lys 127	−90				
Total	−1581				

[a] The $pK_{1,2}$ values listed are for the monomeric form.

Taken from Flanagan, M. A., Role of Electrostatic Interactions in the Structure and Function of Myoglobin, Lysozyme and Hemoglobin, Ph.D. thesis, Indiana Univeristy, Bloomington, 1983.

constant as solvent is displaced on apposition. This effect appears in the calculations as an increase in the $(1 - SA_{ij})$ term. The indirect potentiation characteristically affects the α subunits more than the β subunits.

The dimer-tetramer assembly processes in hemoglobin offer a unique opportunity to distinguish between free energy changes of electrostatic and nonelectrostatic origins. The latter are estimated by difference for cases in which the overall processes have been measured experimentally by Ackers and his colleagues as $^{\circ}\Delta G_2$ and $^{4}\Delta G_2$, and their difference the regulatory energy $\delta\Delta G_{04}$ defined analogously with the electrostatic terms above.[149] In the following illustrations in Table 11 the terms $^{\circ}\Delta G_{2,non\text{-}el}$ and $^{4}\Delta G_{2,non\text{-}el}$, obtained by difference from the experimental values and the computed electrostatic values, are listed next to the related $^{\circ}\Delta G_{2,el}$ and $^{4}\Delta G_{2,el}$ entries to bring out the distinctions between the two classes of free energy changes.

Table 11 lists normal hemoglobin A_o and nine mutant forms in which the substitutions are located at or near the $\alpha^1\beta^2$ contact except as noted.[130] The substitutions are described according to residue number and the amino acid residues involved. The ΔG values are expressed in kcal/mol. The conditions chosen for analysis are pH 7.4, 25°C, with I = 0.10 *M* for the electrostatic calculations[130] and 0.1 *M* Tris-HCl/1 m*M* Na_2 EDTA at 21.5°C for the experimental measurements except as noted.[149]

The first listing for normal hemoglobin A_o shows the comparable magnitudes of electrostatic and nonelectrostatic contributions to the overall free energies of assembly. The first two variant examples are β99 mutants. The substitution Asp → Asn in hemoglobin Kempsey affects the $^{\circ}\Delta G_{2,el}$ favorably because it removes a negative charge site from the net negative field imposed by the charge lattice as a whole. However, the much more striking consequence

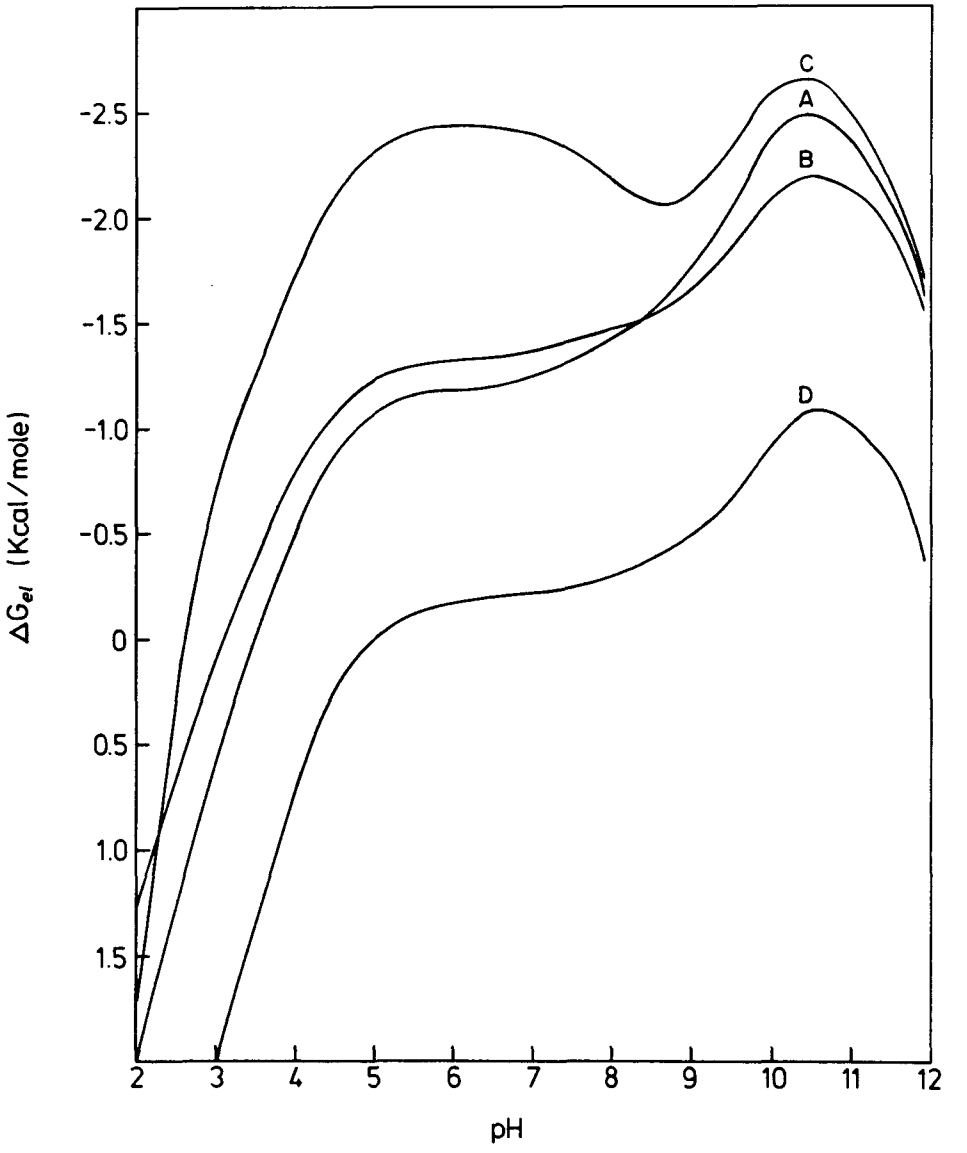

FIGURE 39. Dependence upon pH of summed electrostatic free energies in kilocalories per mole is shown for the native BPTI structure at I = 0.00 in curve A and I = 0.01 in curve B. Curve C shows the significantly broadened region of stability calculated for the structure involving juxtaposition of the termini. Curve D applies to a hypothetical system at I = 0.00 in which all SA values are set to 0.76. For clarity, the curves for I = 0.10 are omitted. (From March, K. L., Maskalick, D. G., England, R. D., Friend, S. H., and Gurd, F. R. N., *Biochemistry*, 21, 5241, 1982. With permission.)

is the cost in $^{\circ}\Delta G_{2,non\text{-}el}$. In this nearly isomorphous substitution, the replacement of the carboxylate by the carboxamide weakens the hydrogen bond acceptor role both by the reduction of electronegativity and the limitation to a single oxygen atom with the other being converted to the potential donor role as the amide. The results indicate that such dipolar interactions outweight the disadvantage of the negative charge site in hemoglobin A_o, and that the functional value of this residue derives from the other characteristics of the carboxylate group that express themselves at short range. This is not to rule out the possibility that a local electrostatic labilization may have functional value. The substitution Asp → His

Table 11
ELECTROSTATIC AND NONELECTROSTATIC COMPONENTS OF FREE ENERGY OF DIMER-TETRAMER ASSEMBLY

Hemoglobin	Modification	$^{\circ}\Delta G_{2,el}$	$^{\circ}\Delta G_{2,non\text{-}el}$	$^{d}\Delta G_{2,el}$	$^{d}\Delta G_{2,non\text{-}el}$
A_o	—	−7.9	−6.4	−4.4	−3.6
Kempsey	β99 Asp-Asn	−9.3	+0.9	−4.5	−4.2
Yakima	β99 Asp-His	−9.8	0.0	−4.4	−5.1
Barcelona	β94 Asp-His	−7.8	−6.2	−4.8	−3.2
Rush	β101 Glu-Gln	−8.7	−6.3	−3.3	−4.5
British Col.	β101 Glu-Lys	−11.7	+0.3	−3.5	−2.4
Legnano	α141 Arg-Leu	−2.8	−7.3	−0.5	−8.5
Chesapeake	α92 Arg-Leu	−7.3	−4.4	−4.2	−5.4
Créteil	β89 Ser-Asn[a]	−7.9	−0.6	−4.4	−3.3
Kansas	β102 Asn-Thr[a]	−7.6	−6.0	−4.3	−1.5

[a] Near $\alpha^1\beta^2$ interface.

Prepared by M. Crowl-Powers[130] incorporating unpublished data of G. K. Ackers; prepared expressly for this manuscript.

in hemoglobin Yakima, with another variant of the β-fork side chain, produces a further computed improvement in $^{\circ}\Delta G_{2,el}$, but the unfavorable change in $^{\circ}\Delta G_{2,non\text{-}el}$ is fully as marked. Hemoglobin Barcelona, β94 Asp → His, contains the same substitution as hemoglobin Yakima without differing significantly from hemoglobin A_o in the assembly parameters. Unlike the β99 mutants in the sensitive interfacial region, the β94 site produces little net effect on the free energy components of either assembly process. Stabilization by electrostatic interactions is reduced by 5 to 10% relative to hemoglobin A_o for all the four protein species. Compensating effects of this sort have been observed for five additional mutant hemoglobin species (not shown) sharing small deviations among the various free energy categories from the behavior of hemoglobin A_o.[130] These latter substitutions are also distant from the $\alpha^1\beta^2$ interface.

The pair of β101 substitutions represented by hemoglobins Rush and British Columbia, Glu → Gln and Glu → Lys, respectively, illustrate a number of minor changes in assembly free energy categories. The one really striking change is in $^{\circ}\Delta G_{2,non\text{-}el}$ for British Columbia. The change in the charge lattice as such is stabilizing for the deoxy assembly in both cases, although somewhat unfavorable for the oxy assembly. However, Gln at this location exacts no cost in the nonelectrostatic category, implying that the retention of shape and, in part, of polarity characteristics is energetically acceptable in this case (compare with hemoglobin Kempsey). The strong effect of the Glu → Lys change in hemoglobin British Columbia is another vivid example, as with Kempsey, of a nonelectrostatic consequence of the substitution of a charged residue.

The substitution of Arg → Leu is shared by hemoglobins Legnano, α141, and Chesapeake, α92. The consequences are much greater in the former case in which the loss of electrostatic stabilization is very marked for both assembly processes. Especially with respect to the oxy assembly process there is, conversely, a strong increase in the nonelectrostatic component of stabilization in hemoglobin Legnano. In this case, the effects may be amplified because α141 is located in both the $\alpha^1\alpha^2$ and $\alpha^1\beta^2$ contacts. The results for hemoglobin Chesapeake which is altered in the $\alpha^1\beta^2$ contact are less stringent because of very few changes in $\delta G_{i,el}$ terms (see text following Equation 20) relative to hemoglobin A_o, leaving distinct but relatively moderate changes in the nonelectrostatic terms. To illustrate the extent of the electrostatic perturbations introduced by the identical substitutions at different sites, the

numbers of sites with $\delta G_{i,el}$ values exceeding 100 cal/mol in the deoxy and oxy assembly processes are three and one for hemoglobin Chesapeake and five and ten for hemoglobin Legnano, respectively.[130] The actual values in the latter case are also much larger on the average, and produce the large net effects (Table 11).

Lastly, hemoglobins Créteil and Kansas, β89 Ser → Asn and β102 Asn → Thr, respectively, offer cases in which uncharged residues are involved. Table 11 shows that the computed electrostatic contributions undergo little or no change because the charge lattice is deemed to be susceptible only to changes in SA. Note the very large effect of the substitution in hemoglobin Créteil on the nonelectrostatic terms, particularly that for the deoxy assembly. In the case of hemoglobin Kansas, the effect is directed specifically to the nonelectrostatic term for the oxy assembly.

Since the $\Delta G_{2,el}$ terms specifically allow for the effects of the interface formation, the $\Delta G_{2,non\text{-}el}$ terms obtained by difference will reflect directly the nonelectrostatic changes in the docking process including the immediate interfaces and any other regions of the molecule that may be involved. Because the nonelectrostatic interactions involve short-range effects of dipoles, nonpolar clustering, motility, packing characteristics, and so on, it is reasonable that their effects will be most felt in the docking interfaces of the tetramers. Various illustrations of these points have been provided above. Because of unspecifiable structural consequences of the substitutions, some redistribution between ΔG_{el} and $\Delta G_{non\text{-}el}$ terms may occur (compare with oxindolylalanylmyoglobin[137]).[130]

2. Association of Trypsin with BPTI

Although the driving force for the very strong association between the trypsin and the inhibitor arises almost entirely from nonelectrostatic sources, the observed pH dependence of K_{assoc} may be explained in terms of the electrostatic interactions.[150] Despite the high net positive charge of each component molecule, the association is electrostatically nearly isoenergetic at neutral pH because the approach to the docking berth where specific interactions can make the pair fast is not overcome by the longer range electrostatic repulsive effects. This adaptation depends on the presence of a small number of intermolecular electrostatic stabilizations which compensate for the many repulsive, destabilizing interactions between the scattered positive charges. The following discussion deals with the relations of the individual charge distributions of the reactants as they dock in the assembly, the computed ΔG_{el} of the reactants and product as functions of pH in the conformation characteristic of the complex, equipotential contours around BPTI, presentations of monopole and dipole treatments, and computations of intermolecular electrostatic free energies of approach according to the discrete charge Tanford-Kirkwood theory.

Figure 40 represents trypsin (T) and BPTI (I) by model spheres of the appropriate radius in the relationship found in the complex[151] as seen in a YZ plane. The axis connecting the centers of mass (shown as dots) was used for docking calculations. The arrows connect the centers of positive and negative mass (pH 7, I = 0.00) projected onto the plane, the point representing the positive pole. The approximate locations of charge sites of special importance are marked. The most obvious indication from this diagram is that the dipole of each molecule as well as its equivalent monopole would interact with the other in a destabilizing way.[150]

In considering the electrostatic stabilization of the complex, the two separate components were taken as being in their conformations in the complex which differ somewhat from those determined on the separate proteins.[140,151] This assumption need not reflect the actual pathway but helps define initial and final states. It is significant that the electrostatic stabilities in the complex conformations T′ and I′ are somewhat greater. Thus, the transition to the combining geometry is made at some expense measured in electrostatic terms. In Figure 41, ΔG_{el} is plotted against pH for the T′ and I′ structures as derived above from the complex structure T′I′. The differences T′I′ − (T′ + I′) are small, ranging from a destabilizing

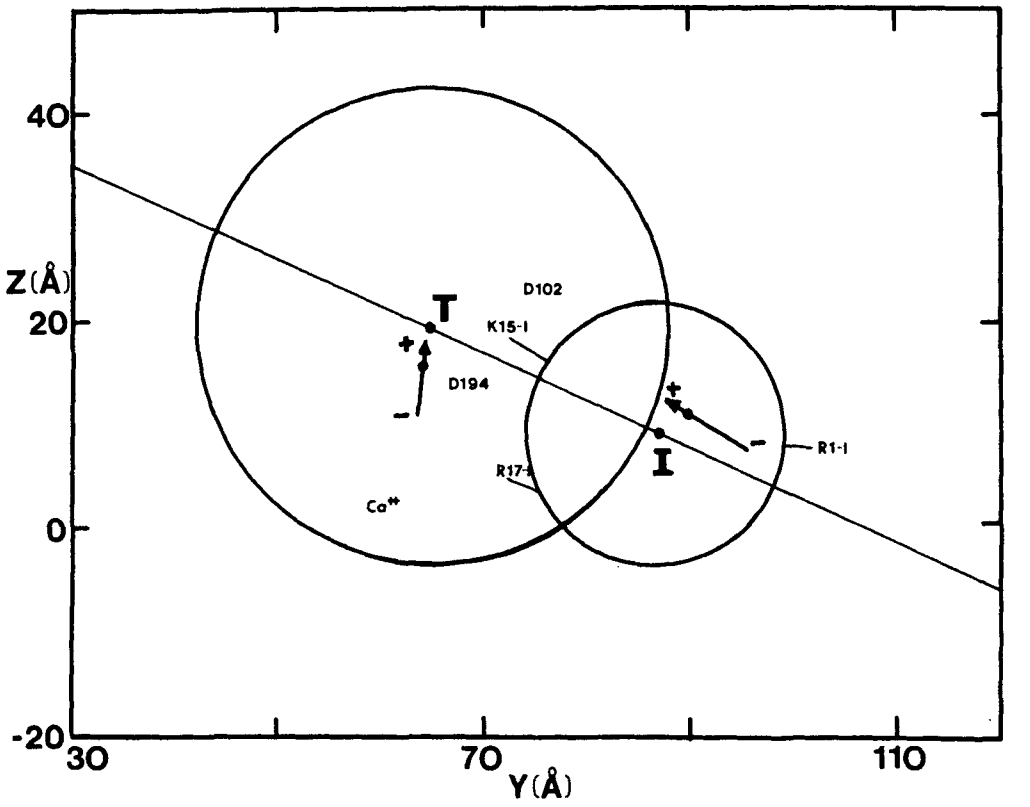

FIGURE 40. Representation of trypsin (T) and BPTI (I) by model spheres of the appropriate radius in the relationship found in the complex as seen in a YZ plane. The axis connecting the centers of mass (shown as dots) was used for docking calculations. The arrows connect the centers of positive and negative mass (pH 7, I = 0.00) projected onto the plane, the point representing the positive pole. The approximate locations of charge sites of special significance are marked using the one-letter code. (From March, K. L., Electrostatic Interactions and Ion Binding in Trypsin, Bovine Pancreatic Trypsin Inhibitor, and Other Proteins, Ph.D. thesis, Indiana University, Bloomington, 1983.)

interaction of 2 kcal/mol at low pH and ionic strength to a stabilization of 3 kcal/mol at pH 9. The cost of the assembly in electrostatic terms is thus seen to be small. Consideration of the individual $\delta\Delta G_{i,el}$ terms[150] clarifies the patterns of effects of ionic strength shown in Figure 41. Exceptions to the usual shielding effects of higher ionic strength in reducing the summed electrostatic stabilization are encountered for I′ and for the complex because the numerous relatively distant destabilizing interactions are proportionately more shielded than the more proximate stabilizing interactions. The pH dependence of the net stabilization follows experimental trends.[150,152,153]

In considering the energetic requirements for the approach of the two protein molecules along the docking coordinate it is useful to portray the equipotential contours around BPTI. Figure 42 represents a section with protein atoms defined by bold outlines. The solid curves represent equipotentials in units of kT calculated for a uniform dielectric medium which prescribes no attenuation according to the SA formulation. The dashed curve represents the kT/2 equipotential calculated with SA attenuation. The consequences of the attenuation effect are to reduce sharply the barrier to the approach of the other macrocation and to minimize the probability of specific attraction or binding of small counterions.[150]

The earlier analyses of the interactions between molecules bearing more than one type of charge were expressed not simply with a smeared or localized monopolar approximation,[11]

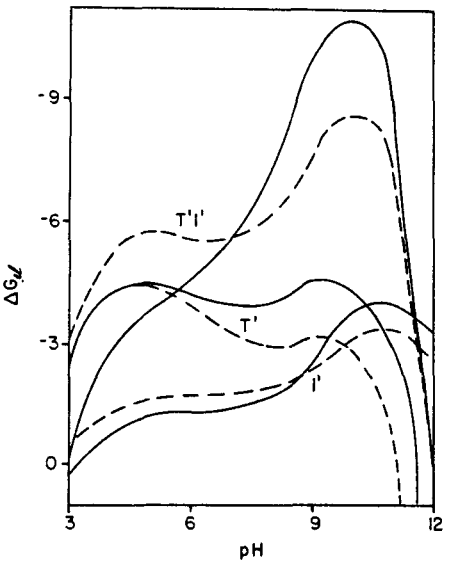

FIGURE 41. The summed electrostatic free energy (kcal/mol) for the isolated T′ and I′ molecules (in the complex conformation) as well as the complex T′I′, as a function of pH for both I = 0.01 *M* (—) and I = 0.10 *M* (- - -) at 25°C. (From March, K. L., Electrostatic Interactions and Ion Binding in Trypsin, Bovine Pancreatic Trypsin Inhibitor, and Other Proteins, Ph.D. thesis, Indiana University, Bloomington, 1983.)

but also in terms of dipolar characteristics.[7] These alternative treatments serve to stress the roles of net charge and charge array asymmetry in various potential functions including protein-protein assembly. The discrete charge arrays of the protein molecules are not represented in the approximations. In the following, these alternative formulations are tested.

Figure 43 shows the computed electrostatic free energy change, $(\delta\Delta G_{el})_{assoc}$, as T′ and I′ approach along the docking axis, for the examples of the monopole and dipole approximations, as well as for an "inverted" approach along the same axis but with the reverse orientation of the dipole of I′. Clearly, the association of these systems bearing high charges of like sign is very disfavored, especially if the charge polarization of the reactants represented by the dipole is taken into account.[150]

In Figure 44, the results of considering the individual charges with the full electrostatic treatment at I = 0.00 are shown. The results at pH 7 are qualitatively entirely different from those just discussed.[150] As the molecules approach in the correct orientation, the system passes through a maximum instability at a distance of 6 Å and then the trend changes so that net destabilization is small at final contact. The inverted dock pathway is consistently disfavored. The dashed curve marked SA (∞) indicates that if all charge sites in the normal approach mode were to retain the SA values for completely separated T′ and I′, then the stabilization would be improved relative to the partial reduction in SA_{ij} for mainly positively charged groups during actual complex formation. This effect slightly overweighs that involving stabilizing interactions. Such behavior is in contrast with the calculations for the cytochrome c: flavodoxin complex.[148] The results of calculations for pH 5 and pH 9 fit with the principles discussed.

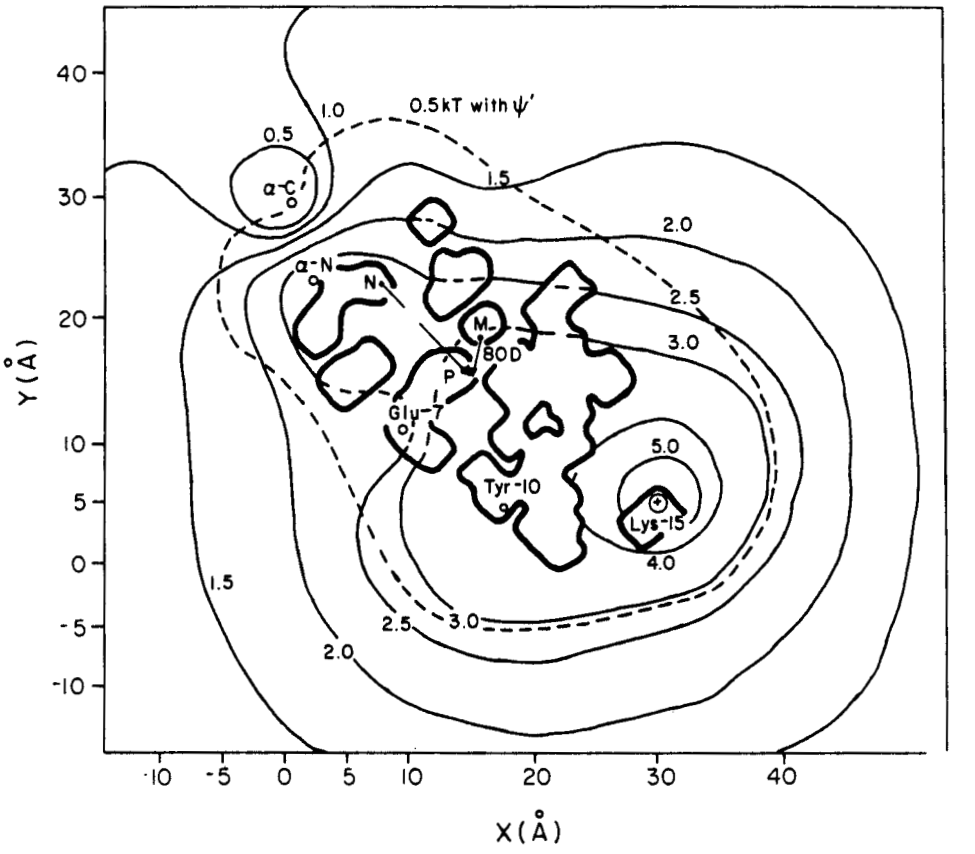

FIGURE 42. Longitudinal section of BPTI with protein atoms defined by bold outlines. Solid lines represent equipotentials in units of kT calculated without attenuation by SA. The dotted line represents the kT/2 equipotential calculated with SA attenuation. Also shown are projections of the center of mass (M) and the positive (P) and negative (N) centers of charge. (From March, K. L., Electrostatic Interactions and Ion Binding in Trypsin, Bovine Pancreatic Trypsin Inhibitor, and Other Proteins, Ph.D. thesis, Indiana University, Bloomington, 1983.)

3. *Folding of Myoglobin*

Electrostatic contributions to the stability of the native conformation of myoglobins as a function of pH for a particular ionic strength have been described in Figure 30[81] based on numerous individual (Table 7) and paired (Table 8) contributions. The early work followed the formalism of the product $(1 - \underline{SA}_j)(1 - SA_i)$ whereas that to be presented here[139] follows the more recent form $(1 - SA_{ij})$ which expresses less attenuation and hence larger absolute values $-\Delta G_{el}$.[29,71]

The pH-dependent contributions of helical and nonhelical structural elements were evaluated by the formal excision of these structural domains from the structure one at a time by hypothetical cleavages. The excised components are removed leaving no charged ends. The summed ΔG_{el} values computed separately for both the remaining protein core and the excised component allow an estimation of the stabilizing or destabilizing contributions of that segment's ionizable groups. Since the contributions of the turns which join the helixes are relatively small but uniformly consonant with those of the major structural parts, they were not included in the illustrations.

Figure 45 shows the pH dependence of the summed ΔG_{el} at 25°C and I = 0.01 *M* for the full sperm whale myoglobin structure (top), and then for the residual structures lacking

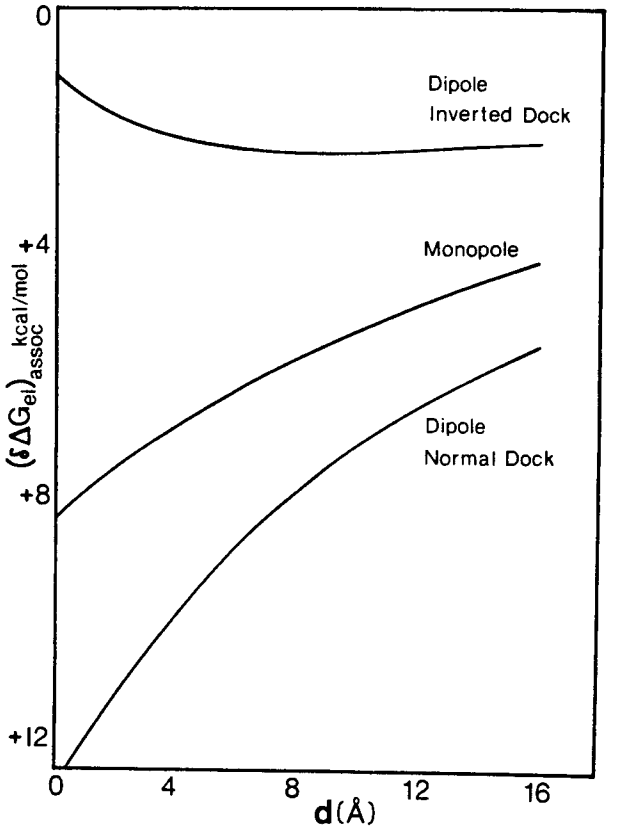

FIGURE 43. Several computations of the intermolecular electrostatic free energy of approach of T′ and I′, $(\Delta G_{el})_{inter}$, in kcal/mol at pH 7, I = 0.00, are shown as a function of the separation distance d (Å) of the component molecules, where d = 0 is defined as the final complex. Calculations were performed as indicated using monopolar and dipolar approximations as well as with a hypothetical inverted BPTI-dipole system (see text for further details.) (From March, K. L., Electrostatic Interactions and Ion Binding in Trypsin, Bovine Pancreatic Trypsin Inhibitor, and Other Proteins, Ph.D. thesis, Indiana University, Bloomington, 1983.)

each helix in turn, as marked. The three-dimensional structure of each residual protein is taken to be undisturbed except for the increased solvent access to the newly exposed surfaces which will change the attenuation of certain pairwise interactions. However, the distinctions shown in Figure 45 result almost entirely from the loss of the interactions between residual protein and individual helix. The importance of the longer helixes A, H, G, and E is apparent. Helixes A and H are particularly interesting from the architectural point of view because they knit up the two ends of the fabric. Groupings of helixes containing fewer components provide similar results, showing the importance of electrostatic interactions in promoting the native folding pattern.

Figure 46 illustrates the pH dependence under the same conditions of ΔG_{el} for the individual helixes considered in isolation from the rest of the myoglobin. Note first that the stabilizing interactions are relatively small and that their sum consistently falls well short of those summed for the protein in Figure 45. Helix H reflects substantial self-stabilization although much less than it contributes to the molecule as a whole (Figure 45). In contrast, helix A shows substantially no intrinsic electrostatic stabilization despite its leading role in the

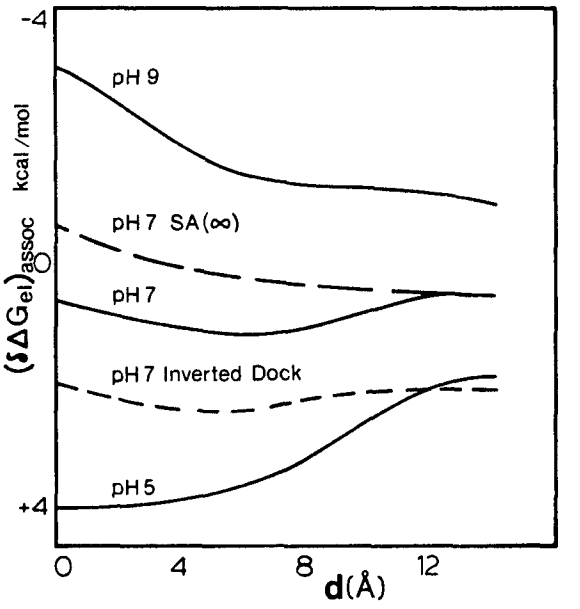

FIGURE 44. The solid lines show dependence on distance of separation, d, of the intermolecular electrostatic free energy of approach of T′ and I′ (kcal/mol) at pH values 5, 7, and 9, I = 0.00 as in Figure 43 except computed according to the SA-modified Tanford-Kirkwood discrete charge theory. The dashed lines represent calculations with all SA values equivalent to those in the isolated molecules (d = ∞), labeled SA (∞), and with a hypothetical inverted BPTI charge array (see text for further details.) (From March, K. L., Electrostatic Interactions and Ion Binding in Trypsin, Bovine Pancreatic Trypsin Inhibitor, and Other Proteins, Ph.D. thesis, Indiana University, Bloomington, 1983.)

molecule as a whole. The F helix is considered to contain only one charge site and hence to have no intrinsic electrostatic stabilization.[139]

The three assembly processes considered here represent very different examples of the operation of the specificity of electrostatic interactions. In the hemoglobin case, the formation of very stable αβ dimer is controlled nearly completely by nonelectrostatic rather than by the modest electrostatic interactions (Table 10). In the tetramer assembly processes both energetic categories are well represented and their roles are clearly illustrated by the effects of substitutions in mutants (Table 11).

In the case of the trypsin-BPTI complex the very great stabilization energy[154] is supplied almost totally by nonelectrostatic interactions. The role of the charge interactions is to guide the docking. Note that the components undergo some rearrangement to achieve favorable electrostatic configurations, somewhat like a tertiary rearrangement coupled to a quaternary one. An interesting quality illustrated by BPTI (Figure 42) is that the potentially strongly repulsive external field is efficiently collapsed by interaction with the solvent. This illustrates a difference in function between mobile solvent components and reacting macroions.

The example of the dissection of myoglobin to understand its three-dimensional assembly reveals a very strong role for electrostatic interactions. This molecule has a very symmetrical charge distribution so arranged that all helical and interhelical elements form stabilizing interactions with the rest of the molecule. Comparisons of related myoglobin species indicate the importance for stability of the various electrostatic and nonelectrostatic factors identified in the hemoglobin studies described above.[71]

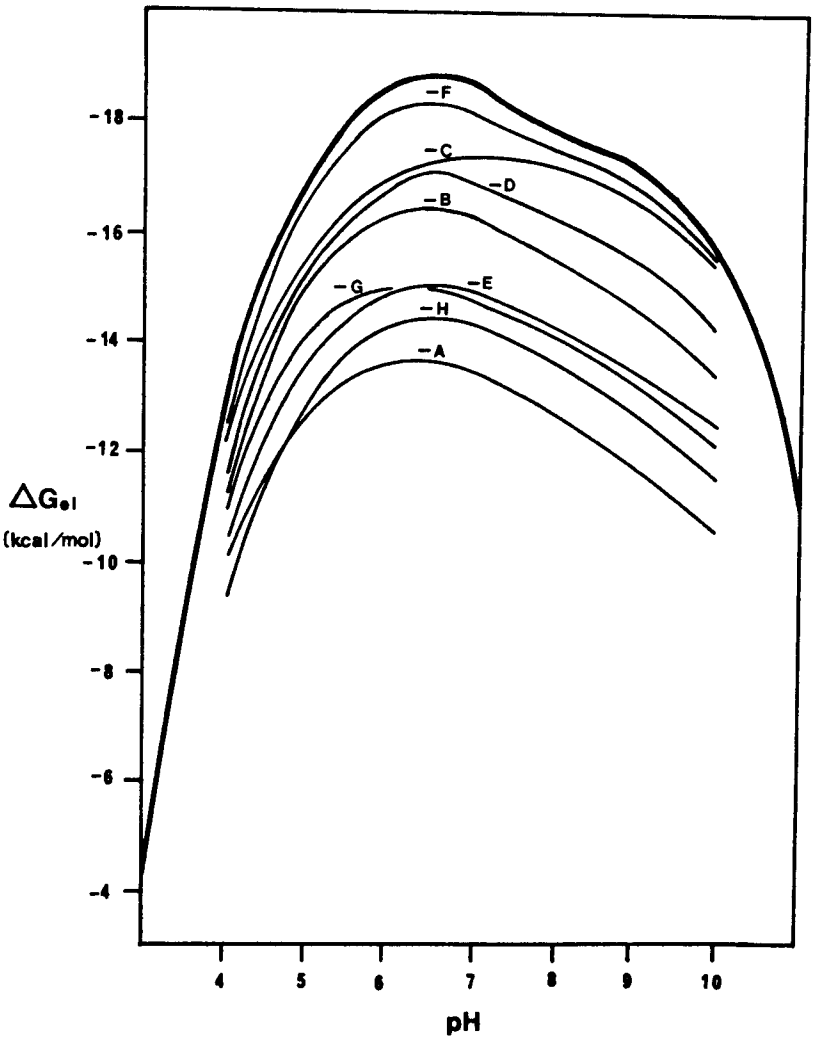

FIGURE 45. The top curve represents the electrostatic free energy of sperm whale myoglobin. The other curves indicate the effects that removal of single helixes, identified by letters A through H, have on the electrostatic free energy of the residual protein core. Free energies were calculated with I = 0.01 *M*, 25°C. (From Garcia-Moreno E., B., Chen, L. X., and Gurd, F. R. N., *Biophys. J.*, 45, 376a, 1984. With permission.)

V. SPECIFIC ION BINDING

In this section the concept of specific ion binding is considered. First, examples are examined of effects of ion binding at crystallographically determined sites on $pK_{1/2}$ values, total protein charge, Z, and electrostatic free energy of stabilization. Next, the use of the electrostatic calculations to uncover potential ion binding sites will be described.

A. Effect of Ion Binding on Computed Proton Binding Behavior and Electrostatic Stabilization

1. Hemoglobin Effectors

The anionic centers in allosteric effectors of hemoglobin function, CO_2 (carbamino adduct), 2,3-DPG, and chloride ions may be modeled as discrete point charges. The coordinates for

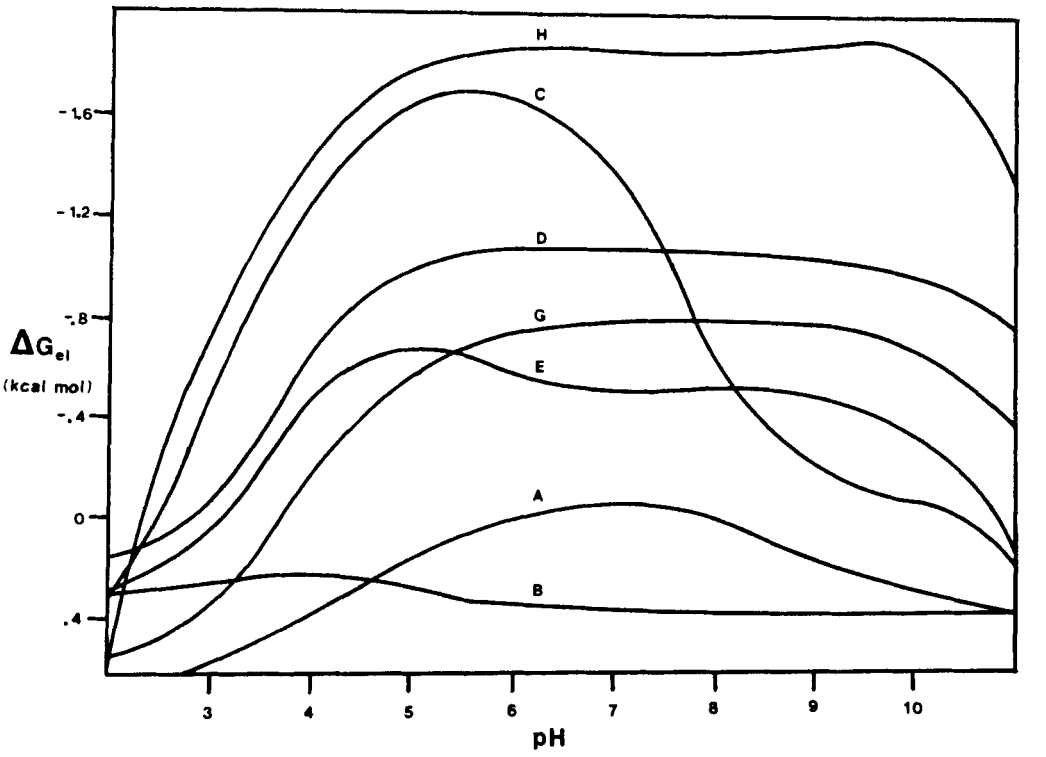

FIGURE 46. This figure shows the electrostatic free energy curves of the individual helixes in myoglobin after having been removed from the protein core. Free energies were calculated with I = 0.01 *M*, 25°C. (From Garcia-Moreno E., B., Chen, L. X., and Gurd, F. R. N., *Biophys. J.*, 45, 376a, 1984. With permission.)

the negatively charged carbamino adduct and 2,3-DPG were chosen to be consistent with crystallographic data and solution studies showing the preferential binding of CO_2 and 2,3-DPG in the vicinity of the amino-terminal of the β chains in deoxyhemoglobin (see Figure 47).[68,155] The chloride ion binding sites are those used for the proton binding studies of hemoglobin involving α-chain and β-cleft locations,[68] shown schematically in Figure 25 along with the 2,3-DPG binding site.[64] No chlorides were considered in the β cleft for ionic strengths below 0.10 *M*. At I = 0.10 *M*, each tetramer was assumed to bind four chloride ions. The crystallographically determined site near Val-1α was always assumed to be occupied[67] and one of the three other proposed anion sites was used per αβ dimer. The net charge on a chloride ion site was −1.0, to simulate total charge occupancy over the entire physiological range. The pK_{int} values were assigned for the five charged groups on 2,3-DPG on the basis of solution titration behavior.[68] The pK_{int} value used for the carbamino adduct was 5.0.[116]

Table 12 tabulates the computed electrostatic effects for the 13 hemoglobin tetramer sites that titrate within the physiological pH range when these various anions are included explicitly in the calculation of $pK_{1/2}$ values.[68] For I = 0.10 *M*, the effects of including one or two fully occupied chloride sites are shown. The computed $pK_{1/2}$ values in the three columns in Table 12 dealing with different sets of chloride binding sites primarily differ for those groups within or neighboring the β-cleft region. The results for carbamino and 2,3-DPG are striking in that computed perturbations induced by the negatively charged effectors are observed throughout the protein structure even at I = 0.10 *M*. The predicted increases in $pK_{1/2}$ values in the presence of carbamino formation are amplified for the binding of the pentavalent anion 2,3-DPG. The magnitudes of the calculated $pK_{1/2}$ changes are of the proper degree

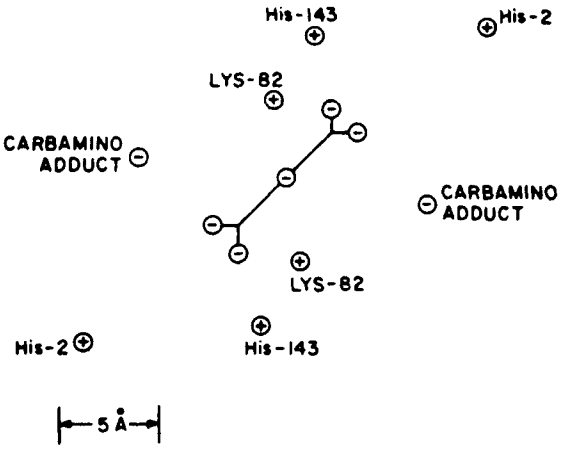

FIGURE 47. Diagram of the form of Figure 25 showing the positions assigned to the negative charge sites of the carbamino adducts borne by the β chains. (From Matthew, J. B., Friend, S. H., and Gurd, F. R. N., in *Hemoglobin and Oxygen Binding*, Ho, C., Ed., Elsevier/North Holland, Amsterdam, 1982, 231. With permission.)

Table 12
VALUES OF $pK_{1/2}$ FOR VARIOUS SITES IN DEOXYGENATED HEMOGLOBIN IN THE PRESENCE AND ABSENCE OF CARBAMINO FORMATION, CHLORIDE ION BINDING, OR DIPHOSPHOGLYCERATE BINDING IN THE β CLEFT

	Adduct, I = 0.10 *M*					Adduct, I = 0.01 *M*		
Residue	**Cl^{-a}**	**Cl^{-b}**	**Cl^{-c}**	**Carbamino[d]**	**P_2-Glycerate[d]**	**None**	**Carbamino**	**P_2-Glycerate**
Val-1α	8.02	8.02	8.02	8.02	8.02	8.10	8.11	8.12
His-20α	6.76	6.76	6.76	6.76	6.77	6.87	6.88	6.88
His-45α	6.85	6.85	6.85	6.85	6.85	7.12	7.16	7.16
His-50α	7.45	7.45	7.45	7.48	7.48	7.84	7.87	7.88
His-72α	6.32	6.32	6.32	6.34	6.34	6.52	6.53	6.53
His-89α	7.21	7.21	7.21	7.21	7.21	7.48	7.51	7.49
His-112α	7.74	7.69	7.69	7.74	7.74	8.18	8.20	8.12
Val-1β	7.00	7.44	7.15	—	7.62	7.14	—	8.15
His-2β	6.53	6.60	6.90	6.84	6.84	6.53	7.09	7.08
His-77β	6.58	6.62	6.60	6.70	6.63	6.58	6.86	6.76
His-117β	8.20	7.75	7.75	7.75	7.75	8.08	8.11	8.11
His-143β	6.07	6.33	6.65	6.80	7.27	6.03	6.80	7.75
His-146β	8.48	8.48	8.52	8.52	8.57	9.00	9.15	9.26

[a] Chloride at Val-1α and His-117β sites.
[b] Chloride at Val-1α and Lys-82β position one sites.
[c] Chloride at Val-1α and Lys-82β position two sites.
[d] Chloride at Val-1α site only.

Taken from Matthews, J. B., Friend, S. H., and Gurd, F. R. N., *Biochemistry*, 20, 571, 1981. With permission.

to account for an increased alkaline Bohr effect in the presence of 2,3-DPG[156] and are intermediate in magnitude to observed $pK_{1/2}$ changes in the presence of inositol hexaphosphate.

In the presence of the polyanion inositol hexaphosphate, the $pK_{1/2}$ value of His-β in

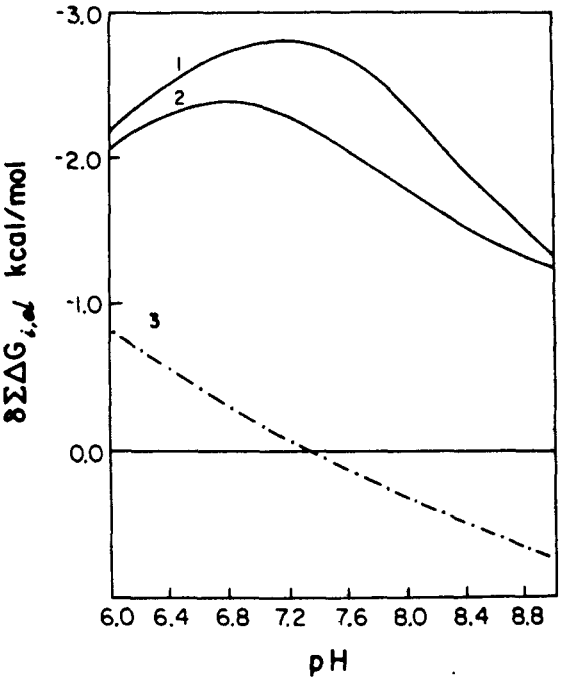

FIGURE 48. Additional electrostatic stabilization, $\delta\Sigma\Delta G_{i,el}$, in kilocalories per mole, produced by the binding of P_2-glycerate to deoxyhemoglobin A_o at 25°C. Curves 1 and 2 refer to I = 0.01 *M* and 0.10 *M*, respectively. Curve 3 shows the corresponding stabilization, passing to destabilization at higher pH, with P_2-glycerate binding in the presence of carbamino adducts to both Val-1α sites, I = 0.10 *M*. (From Matthew, J. B., Friend, S. H., and Gurd, F. R. N., in *Hemoglobin and Oxygen Binding*, Ho, C., Ed., Elsevier/North Holland, Amsterdam, 1982, 231. With permission.)

deoxyhemoglobin has been observed to increase by 0.80 pK unit while the His-146β residue was little affected.[157] Table 12 indicates the calculated $\Delta pK_{1/2}$ values for 2,3-DPG binding as 0.31 for His-2β and 0.05 to 0.09 for His-146β at 0.10 *M* ionic strength.

The dependence of the computed alkaline Bohr effect on specific ion binding at certain sites was demonstrated by Matthew et al.[67] The diagram in Figure 47 of the β-cleft region shows the 2,3-DPG site along with the location of the negative charges created by converting the Val-1β amino groups into the carbamino forms, $-NHCO_2^-$.[64] In Figure 48, the effect of including the 2,3-DPG anion in the charge array is illustrated as the difference between overall electrostatic stabilization in its presence and absence.[64,68] Curves 1 and 2 refer to I = 0.01 *M* and 0.10 *M*, respectively. The experimentally determined free energy for 2,3-DPG binding is 5.1 kcal/mol at pH 7.4 and 25°C.[158,159] It has been observed crystallographically that through side-chain rearrangements stabilizing charge pairs are formed upon binding of 2,3-DPG to the deoxyhemoglobin A_o structure.[155] These structural alterations were not taken into account in the computations.

Since 2,3-DPG and CO_2 both bind preferentially to the β-chain NH_2- terminal site in the deoxy tetramer, it is to be expected that they will experience competitive binding. Calculation of the electrostatic free energy of stabilization of deoxyhemoglobin A_o from 2,3-DPG binding in the presence of Val-1β carbamino adducts illustrates the implications of simultaneous binding as shown in Figure 48, curve 3 (see Figure 47).[64] The effect of forming the carbamino derivatives is to weaken the stabilizing effect of 2,3-DPG to the extent of producing destabilization above physiological pH.[64,68]

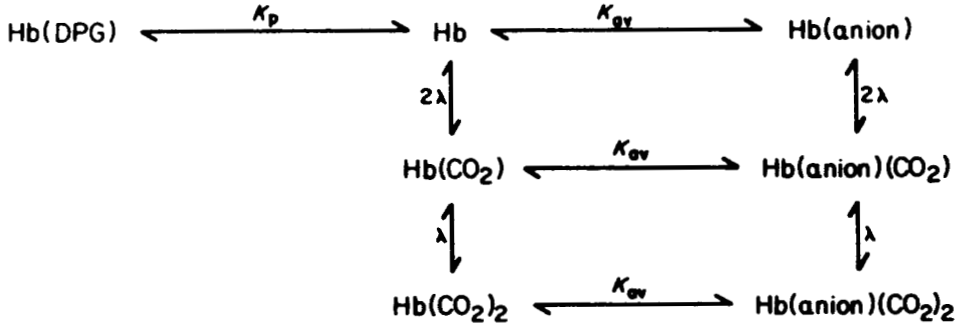

$$Z_\beta = \frac{\lambda[CO_2] + 2\lambda^2[CO_2]^2 + K_{av}\lambda[CO_2][anion] + 2K_{av}\lambda^2[anion][CO_2]^2}{1 + K_p[DPG] + K_{av}[anion] + 2\lambda[CO_2] + 2\lambda^2[CO_2]^2 + 2K_{av}\lambda[CO_2][anion] + 2K_{av}\lambda^2[anion][CO_2]^2}$$

$$[anion] = [Cl^-] + [HCO_3^-]\,;\lambda = [RNHCO_2^-]/[RNH_2][CO_2]\,;K_{av} = [Hb\text{-}anion]/[Hb][anion]$$

FIGURE 49. Scheme for mutually exclusive binding of 2,3-DPG and CO_2 to the β-cleft region of deoxyhemoglobin tetramer. The vertical arrows represent the formation and decomposition of carbamino derivatives written as $Hb(CO_2)$ and $Hb(CO_2)_2$ to denote occupancy of one and both Val-1β sites. The combined anion population, e.g., HCO_3^- and Cl^-, is assumed to compete with 2,3-DPG for the β-cleft site but much less with the carbamino formation. Indeed, the effect of anion binding on the pH-dependent carbamino formation constants λ is not distinguished because λ is determined in the presence of the anion. The anion binding is treated in terms of one anion site per 2,3-DPG binding site. (From Matthew, J. B., Friend, S. H., and Gurd, F. R. N., *Biochemistry*, 20, 571, 1981. With permission.)

At pH 7.4 the extent of carbamino formation at the β-chain terminus is significantly reduced in the presence of 2,3-DPG.[115,116,160] Experimental measurements of β-chain carbamino formation between pH 7 and 8 in the presence of varying concentrations of 2,3-DPG have been found to accord with a competitive scheme[68,161] (Figure 49) that takes into account the effects of this direct competition and also that between 2,3-DPG and Cl^- for the common site domain in the β cleft.

2. Linkage of Azide Binding in Myoglobin

The second example of specific ion binding to be considered is the electrostatic heme linkage of azide binding to sperm whale ferrimyoglobin.[150,162] The experimentally determined azide binding constants, k_L, were analyzed in terms of the modified discrete charge theory. Azide has a relatively high association constant, $\sim 100\ nM^{-1}$. It forms a low-spin coordination complex with the iron atom, and the resultant cancellation of charge is easily treated by the electrostatic theory. The X-ray crystallographic difference map for azide myoglobin indicates no major structural rearrangement upon azide binding,[22,163] and NMR studies[39,164-166] indicate that azide and other low-spin complexes of myoglobins differ in only a few respects from aquoferrimyoglobins in terms of histidine titration and general structural properties in solution. See Section III for some examples of special effects.[39]

The ligand binding reaction of azide ion with ferrimyoglobin may be represented by the overall chemical equilibrium

$$Fe^+ (H_2O) + N_3^- = Fe - N_3 + H_2O \quad (21)$$

in which coordinate bond formation neutralizes the positive charge on the iron as the azide ion displaces the bound water molecule.[163]

However, the iron-bound H_2O in sperm whale ferrimyoglobin is known to undergo acid dissociation into the low-spin state, Fe-OH, with ionization pK_{Fe} near 8.9.[9,14,138,167] Similarly, the acid HN_3 is in equilibrium with its conjugate base, the ligand N_3^-, with an acid dissociation pK_a near 4.6.[168] Therefore, the experimentally measurable equilibrium constant, k_{obsd}, is defined by

$$k_{obsd} = [Fe - N_3]/[([Fe^+ (H_2O)] + [Fe - OH])([N_3H] + [N_3^-])] \quad (22)$$

The association constant for the formation of the ligand state, K_L, is related to k_{obsd} as

$$k_L = k_{obsd}\,(1 + K_{Fe}/H)(1 + H/K_a) \quad (23)$$

where H is the H^+ thermodynamic activity obtained from the measured pH. Since in the work under discussion the measurements were confined to range pH 4 to 6, terms K_{Fe}/H will have negligible effect.

Although the equilibrium constant k_L takes the above two acid dissociation equilibria into account, it nevertheless remains pH dependent, particularly so at low ionic strength. This is referred to as the heme-linked effect, attributable to the ionization of amino acid side-chain groups on the protein molecule.[169] A group is said to be linked to the heme if its free energy of ionization, pK_i, is altered upon ligand binding to the iron atom, just as the free energy of ligand binding varies with the degree of ionization of the heme-linked group regardless of the mechanism of linkage.

The modified discrete charge model which takes into account the mutual intramolecular interactions of all charged sites may be applied to prediction of both $\Delta\bar{v}$ and ΔG_{el} accompanying the ligand binding.[162] The calculations yield pK_i values for each titratable group.

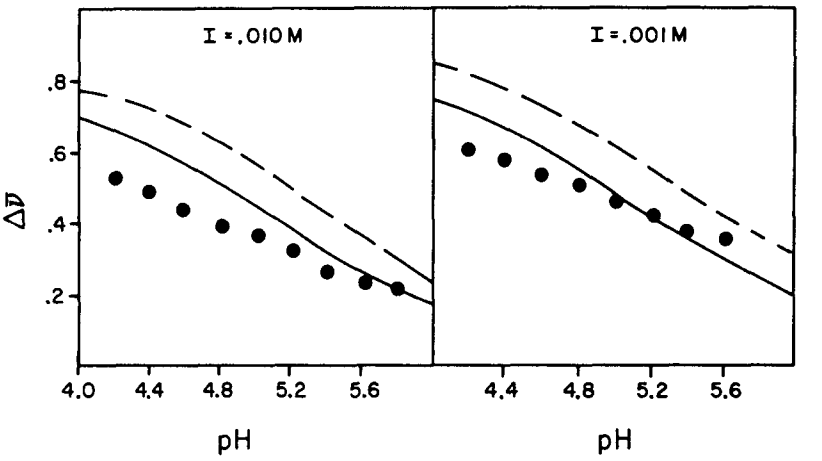

FIGURE 50. Plots of the net proton uptake upon azide binding $\Delta\bar{\nu}$, obtained from the slope of the experimental log K_L vs. pH data (●), compared with predictions of the discrete-charge solvent accessibility treatment applied with the $(1 - SA_i)^{162}$ (- - -) and $(1 - \overline{SA}_{ij})$ (—) formalism. (From March, K. L., Electrostatic Interactions and Ion Binding in Trypsin, Bovine Pancreatic Trypsin Inhibitor, and Other Proteins, Ph.D. thesis, Indiana University, Bloomington, 1983.)

In reactant ferrimyoglobin, these are $(pK_r)_i$ values. In ferrimyoglobin azide, where the charge at the iron site is taken to be zero, the pK_i values are $(pK_p)_i$ for the product. The corresponding effective charges on the groups, $(Z_r)_i$ and $(Z_p)_i$, are then calculated for each group. It follows that the total change in protons bound to the protein accompanying azide binding is given by

$$\Delta\bar{\nu} = \sum (Z_p - Z_r)_i \tag{24}$$

Here Z_p and Z_r represent the fractional group charge borne by the protein in the presence and absence of bound azide. Figure 50 shows theoretical curves for variation of $\Delta\bar{\nu}$ with pH over the range from pH 6 to 4 at two ionic strengths.[150,162] A net uptake of protons upon azide binding is predicted, varying from about 0.2 equiv at pH 6 to 0.8 equiv at pH 4.0, with a minimal ionic strength effect. This increase in bound protons, especially at low pH, would largely compensate for the loss of charge at the iron atom upon azide binding. Such a factor is not taken into account by any independent-site model.

The theoretical estimation of the heme-linked effect by this means may be compared with the experimental $\Delta\bar{\nu}$ values obtained from the data for $(d \log k_L/d\ pH)_T$, see Equation 23.[162] The experimental values are shown as solid circles at 0.2 pH intervals in Figure 50. Agreement between theory and experiment is encouraging because the data have not been normalized and the electrostatic calculations are completely independent of assumptions about mechanism of heme linkage. At lower pH values, the trend toward higher $\Delta\bar{\nu}$ is found for both theory and experiment.

The heme-linked effect can be considered as the difference between the free energy of azide binding in the presence of charged-site interactions with the iron and the corresponding free energy of reaction in the absence of these interactions.[8] By definition, electrostatic interactions with the iron site are zero in the absence of electrostatic heme linkage, and they are zero in ferrimyoglobin azide which has zero charge at the iron site. Consequently, $(\Delta G_{el})_L$

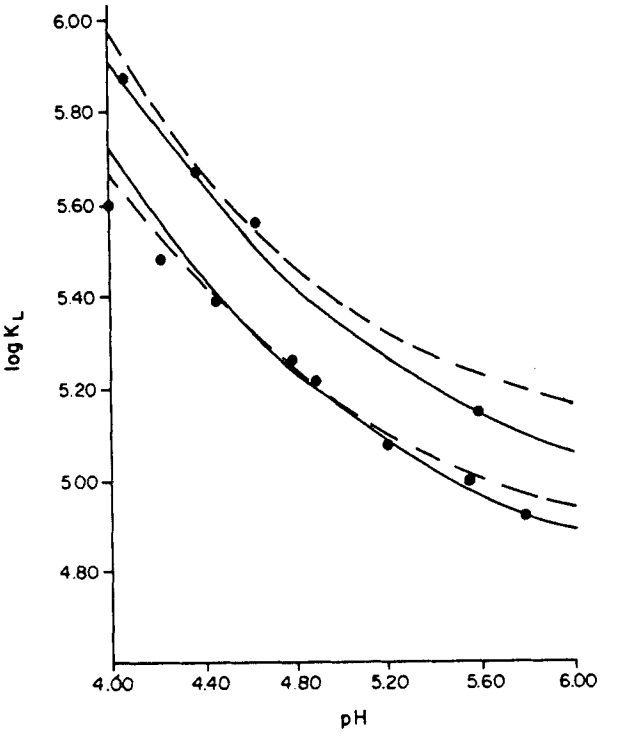

FIGURE 51. Comparisons of experimental log K_L values (●) for azide binding with the pH variation computed according to the ΔG_L model, Equation 24, using as formalisms the revised $(1 - \overline{SA}_{ij})$, solid curves, and the previous $(1 - SA_j)$, broken curves. The upper curves and points apply to I = 0.001 *M*, and the lower to I = 0.01 *M*. (From March, K. L., Electrostatic Interactions and Ion Binding in Trypsin, Bovine Pancreatic Trypsin Inhibitor, and Other Proteins, Ph.D. thesis, Indiana University, Bloomington, 1983.)

is computed directly from interactions of charged sites with the iron in ferrimyoglobin. The equilibrium constant k_L (Equation 23) is obtained from

$$\log k_L = \log k_L^0 - (\Delta G_{el})_L/2.303\ RT \tag{25}$$

The values for the logarithm of the pH-independent binding constant, log k_L^0, at each ionic strength can be taken from the experimental values of log k_L at the pH where $(\Delta G_{el})_L$ is equal to zero; that is, where the iron senses a summed null electrostatic environment.

Figure 51 shows the experimentally determined log k_L values as a function of pH for I = 0.010 and 0.001 *M*, along with the theoretical curves computed from log k_L^0 and $(\Delta G_{el})_L$ according to Equation 25. Throughout the range from pH 6 to 4 the theoretical curves are within 0.10 units of the experimentally determined log k_L values.[150,162] Such a good correlation suggests that the pH-dependent changes in azide binding affinity due to heme linkage can be almost entirely accounted for in electrostatic terms. The treatment serves as a sensitive probe of electrostatic interactions at a particular site in the myoglobin molecule.

Table 13 shows the computed electrostatic free energy contribution to heme linkage, $(\Delta G_{el})_L$, in calories per mole as a function of pH at two ionic strength values. The computations follow the $(1 - \overline{SA}_{ij})$ formalism[150] with substantially the same results as with the

Table 13
ELECTROSTATIC FREE ENERGY CONTRIBUTION TO HEME-LINKAGE, $(\Delta G_{el})_L$ (cal/mol)

pH	$(\Delta G_{el})_L$ (I = 0.01)	$(\Delta G_{el})_L$ (I = 0.00)
4.0	−740	−960
4.5	−290	−500
5.0	+ 50	−170
5.5	+260	+ 50
6.0	+390	+230
pH[$(\Delta G_{el})_L$ = 0]	4.92	5.39
log K_L^o	5.19	5.21

Taken from March, K. L., Electrostatic Interactions and Ion Binding in Trypsin, Bovine Pancreatic Trypsin Inhibitor, and Other Proteins, Ph.D. thesis, Indiana University, Bloomington, 1983.

Table 14
STRONGLY HEME-LINKED GROUPS IN THE AZIDE BINDING REACTION OF SPERM WHALE FERRIMYOGLOBIN AT pH 4.0, I = 0.01 *M*

Heme-linked groups	$(1 - SA_j)$	$R_{Fe,j}$ (Å)	Z_j	$(\Delta G_{j,el})_L$ (cal/mol)
His-36	0.85	15.6	+1.00	−150
Glu-38	0.90	15.1	−1.00	170
Lys-42	0.75	11.5	+1.00	−260
Asp-44	0.60	14.5	−0.97	150
Arg-45	0.75	10.4	+1.00	−310
Asp-60	0.60	13.4	−1.00	180
His-64	0.95	5.8	+0.44	−370
Glu-85	0.75	10.4	−0.80	250
Arg-139	0.95	16.4	+1.00	−150
Prop-155	0.70	6.3	−0.64	420
Prop-156	0.50	8.6	−0.53	190

Taken from March, K. L., Electrostatic Interactions and Ion Binding in Trypsin, Bovine Pancreatic Trypsin Inhibitor, and Other Proteins, Ph.D. thesis, Indiana University, Bloomington, 1983.

earlier formalism.[162] Note the considerable pH dependence. The pH value at which $(\Delta G_{el})_L = 0$ is dependent on ionic strength, yet leads via Equation 25 to a substantially I-independent log k_L^0. This result indicates that the heme-linked ionic interactions are effectively treated by the theory.

The number and variety of strongly heme-linked groups in the azide binding reaction of ferrimyoglobin are shown in Table 14 for pH 4.0, I = 0.01 *M*, 25°C. The 5 columns cover 11 such groups, the $(1 - SA_j)$ value for the particular group, the distance of separation from the iron atom $r_{Fe,j}$ in Å, the (partial) charge Z_j borne by the group and, lastly, the pairwise interaction term with the iron $(\Delta G_{j,el})_L$ in calories per mole. This latter term represents the stabilization contributed by group j in the absence of the azide ligand that obliterates the charge at the iron site. Note that the contributing groups have relatively large values of $(1 - SA_j)$. Many are distant from the iron by nearly the radius of the protein.

B. The Use of Electrostatic Criteria to Locate Sites of Ion Binding

The foregoing examples of the effects of specific ion binding on electrostatic interactions and hence on the proton-binding behavior of proteins point up the importance of defining the locations of bound ions and ultimately of determining their binding affinity at such sites. In view of the limited direct experimental data, a procedure was developed to identify specific ion binding sites at the protein surface based on electrostatic criteria. With the calculated charge array and the known surface topography of ribonuclease as a basis for analysis, the method was outlined in Section II to identify the active site of ribonuclease as a general anion binding site.[62] These considerations are now extended.

1. Effect of Charged Ligands on the Functional Properties of Ribonuclease

In a systematic application of the method used to generate the electrostatic potential maps shown in Figure 8 of the section on Formalism, two sites with exceptionally positive potential at pH 6.0 were identified.[62] The number of solvent-accessible, high-potential sites increases to at least five by pH 4.0. One of the positive centers identified at pH 6.0 is the active-site cluster, while a second site is approximately 8 Å away on the same protein face and aligned in such a way as to suggest a role in orienting or docking a substrate RNA fragment.[170]

In Figure 52 the relative positions in the active-site charge cluster on the protein surface are shown.[62] Lysine-41, histidine-12, and histidine-119 have all been implicated in ligand and inhibitor binding reactions and in enzymatic cleavage of substrate.[171] Two positions from the potential contours have been chosen to illustrate the sensitivity of these calculations to anion placement in this positive center. These positions correspond closely with crystallographic observations of anion binding. Position A1 is close to the phosphorus atom in the dinucleotide inhibitor UpcA.[172] Position A2 corresponds to the divalent sulfate ion intercalated between the active-site histidine residues in RNase-A.[173]

In the following we review the calculated response of the protein charge array to the binding of mono- and divalent phosphate ligands at the active site as a function of pH. To avoid confusion, the partial occupancies of the four other anion sites were not included as they were shown to exert a negligible effect on the active site potential.[62] Since the net charge of a phosphate ligand is influenced by and also influences the protonation of its binding domain, the net proton uptake or release was calculated by considering both components.[68] The experimentally determined apparent proton affinities for the active-site histidine residues of ribonuclease are tabulated in Table 15. In the presence of ions with higher anionic charge, the observed $pK_{1/2}$ values are seen to increase from ~6 to 8.

Table 15 gives the computed effective $pK_{1/2}$ values for histidine-12 and histidine-119 when full ligand occupancy is simulated at two alternative positions in the active site. The values computed for the case in which the sites are unoccupied are listed in column one for reference. The predicted effects of ligand binding should be viewed as underestimates as no side-chain rearrangements were allowed in the calculation to maximize coulombic interactions. At these interactive distances of less than 5 Å, a movement to more realistic chelate geometry involving a reduction in distance of 1 Å can easily increase the effects listed in Table 15 by 20%.

In Figure 53, the solid curve shows the calculated net proton uptake or release from RNase-S in response to inorganic phosphate association (Figure 52, position A1, I = 0.01). Curves 2 and 3 resolve this effect into protein uptake and phosphate release. The insert in Figure 53 shows the proton uptake or release observed when saturating quantities of 2′-CMP or 3′-CMP are added to RNase-A. These data support the calculated sensitivity to exact charge placement.

The additional electrostatic stabilizations of the overall protein charge array introduced by anion binding are cast as pH-dependent association constants, $\log K_{anion} = -\Delta G_{el}/(2.3\ RT)$. These pH-dependent association constants are plotted in Figure 54 for a monovalent

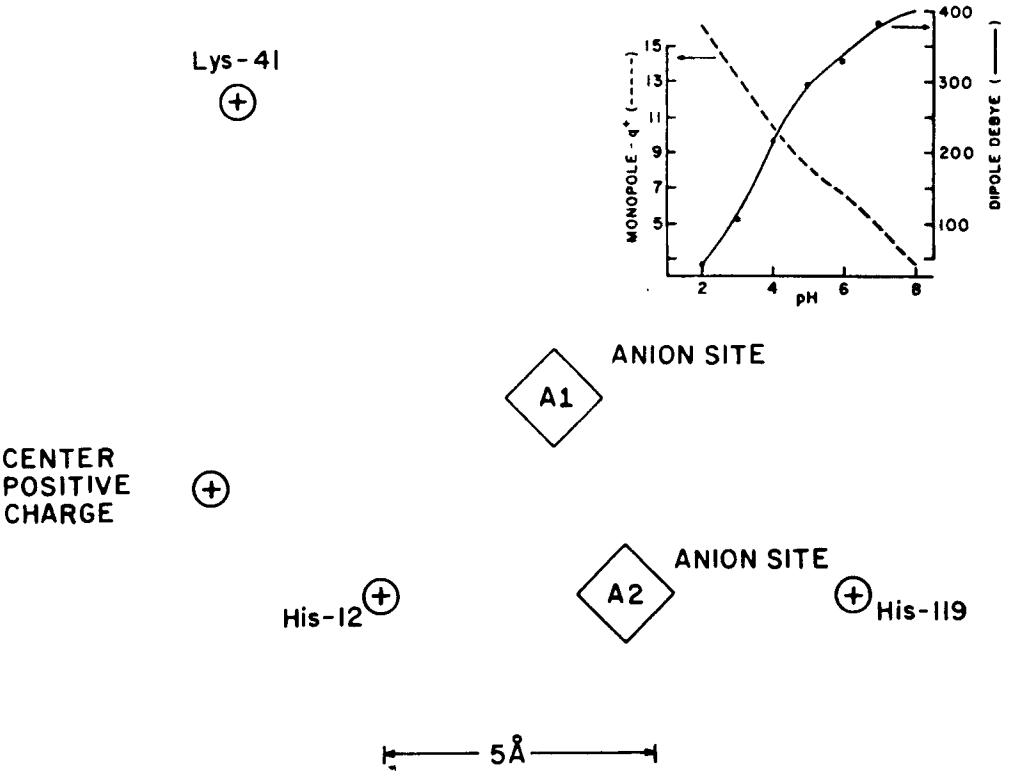

FIGURE 52. Diagram illustrating the relative locations of the charge sites constituting the active center for RNase S. This plane through the protein is determined by the charge sites of His-12, His-119, and Lys-41. Positions labeled A1 and A2 represent two alternative positionings for anions in the active site. Also shown is the coordinate of the center for positive charge of the protein representing the positive pole of the molecular dipole. These three sites, A1, A2, and the positive center of charges, all fall within 1 Å of the defined plane. The magnitude of the monopole in units of net charge and the molecular dipole in Debye units (1 debye = 1×10^{-18} ESU cm) are plotted vs. pH in the insert. (From Matthew, J. B. and Richards, F. M., *Biochemistry*, 21, 4989, 1982. With permission.)

ion such as chloride and for inorganic phosphate at ionic strengths of 0.01 and 0.10 *M*. Figure 54 also shows the experimental association constants for inorganic phosphate, 2′-CMP, 3′-CMP, and 3′-UMP.[177] The broken lines drawn through the nucleotide data correspond to the predicted pH dependence of inorganic phosphate, demonstrating that these anions follow the pH-dependent behavior observed and predicted for inorganic phosphate. By difference, the pH-dependent component of 3′-UMP and 3′-CMP must account for 2.5 kcal/mol while the specific interactions of 2′-CMP must account for 4.0 kcal/mol. A portion of the difference in the 2′- and 3′-pyrimidine nucleotide binding energy can be attributed to the different electrostatic field at the position of the 2′- and 3′-phosphate groups. The nature of such a shift is shown by curves 2 and 2′ in Figure 54.

2. Calcium Ion Binding Site in Trypsin

Potential field calculation for trypsin at pH 7, I = 0.00 reveals the calcium binding site to be the only negative region of the entire protein larger than a single functional group.[150] The overall field gradient may thus be viewed as a funnel directing positive ions to the crystallographically documented site. Figure 55 shows a representative cross section at the Ca^{++} binding site level in the yz-plane of the crystallographic structure.

Table 15
HISTIDINE RESIDUES IN THE ACTIVE SITE OF RIBONUCLEASE

Observed $pK_{1/2}$ Values in the Presence of Several Active-Site Ligands

	Monovalent		Mono- and divalent		Divalent		
	0.10 *M* NaCl	UpCa	0.1 *M* NaCl + 0.02 *M* PO_4^{2-}	0.1 *M* NaCl + 0.1 *M* PO_4^{2-}	3′-UMP	3′-CMP	2′-CMP
Histidine-12	6.0[a]	5.8[b]	6.75[a]	7.15[a]	6.4[b]	7.4[b]	8.0[b]
Histidine-119	6.3[a]	6.1[b]	7.03[a]	7.63[a]	7.8[b]	8.0[b]	8.0[b]

Calculated $pK_{1/2}$ Values in the Presence of Bound Mono- or Divalent Anion[c]

		Cl^-		PO_4^{2-}/HPO_4	
	Unoccupied[d]	Position A1	Position A2	Position A1	Position A2
Histidine-12	6.38	6.86	6.80	7.20	7.52
Histidine-119	6.34	6.64	7.02	6.82	7.24

[a] Cohen et al.[174]
[b] Griffin et al.[175]
[c] Positions A1 and A2 for bound anion placement correspond to those given in Figure 52.
[d] All the calculated $pK_{1/2}$ values were calculated assuming a Debye screening of 0.10; the explicit exclusion of a site-bound ion is given as a reference for comparison with the site-bound cases.

Taken from Matthew, J. B. and Richards, F. M., *Biochemistry*, 21, 4989, 1982. With permission.

To clarify the energetics of calcium binding to the primary sites, the system was defined as consisting of three components: the calcium ion; the surrounding anionic residues 70, 71, 77, and 80; and the remainder of the protein. The magnitude of nonchelating protein interaction with the Ca^{++} is calculated to be about half the magnitude of the interaction within the chelation site, bearing an absolute charge of -4. Consideration of ionic strength effects reveals the long-range interaction to be selectively reduced by ionic strength so that as I increases from 0 to 0.01, the energies are attenuated by a factor of about 0.60 for these interactions with the nonchelating protein, but only by about 0.20 for the intrasite and calcium to site interactions.

A variety of experimental methods have been employed to evaluate the $pK_{Ca^{++}}$ for calcium binding to the trypsin primary site under various conditions. Four studies were performed within the narrow pH range 7.7 to 8.1 yet yielded values of $pK_{Ca^{++}}$ ranging from 3.5 to 5.39.[178-181] A plot of these separate data relating the observed $pK_{Ca^{++}}$ to the $-\log$ (ionic strength) is shown in Figure 56 to form very nearly a straight line. As described by Record et al.,[182] this suggests some form of competition between the major ion(s) contributing to the ionic strength and calcium. The most likely competing ion in these experiments is Na^+, based on its like charge and similar radius.[183,184] In a simple competition governed by mass action, the slope of this line may be shown to represent the total number of Na^+ able to replace a CA^{++} ion. For the data plotted, this slope is 1.6, a physically unappealing number, suggestive of effects other than simple competition.

Computation of the $pK_{Ca^{++}}$ as a function of ionic strength from the difference in electrostatic free energy of trypsin in the presence and absence of the Ca^{++} at pH 8 yields the curve labeled 1 (Figure 56). Although the experimental trend is reasonably matched, the predicted binding constants exceed the observed by more than three orders of magnitude.

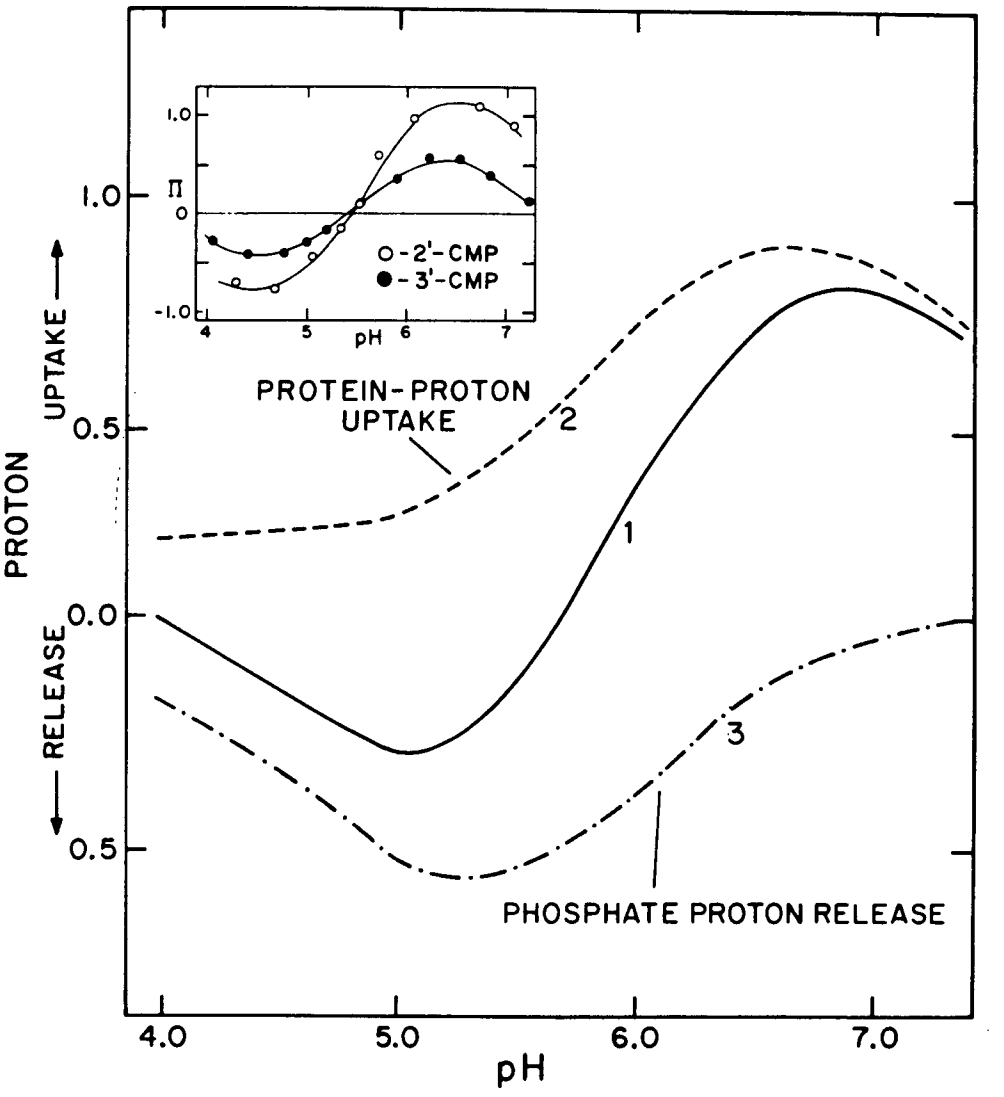

FIGURE 53. Calculated proton uptake or release induced by full occupancy of anion site A1 by phosphate at I = 0.01 as a function of pH (solid curve). This calculated uptake or release is resolved into the dashed curve: protein-proton uptake (curve 2) and phosphate ion proton release (curve 3). The insert shows the observed proton uptake or release for 2'-CMP (○) and 3' (●).[176] (From Matthew, J. B. and Richards, F. M., *Biochemistry*, 21, 4989, 1982. With permission.)

A simple model for ion competition is

$$PNa_n^+ \xleftarrow{K_{Na^+}} P \xrightarrow{K_{Ca^{++}}} PCa^{++}$$

$$K_{Na^+} = \frac{P.[Na^+]^n}{[P{:}Na_n^+]} \qquad K_{Ca^{++}} = \frac{P.[Ca^{++}]}{[P{:}Ca^{++}]}$$

$$\therefore K_{Ca^{++},obs} = K_{Ca^{++}} \left\{ 1 + \frac{[Na^+]^n}{K_{Na^+}} \right\}$$

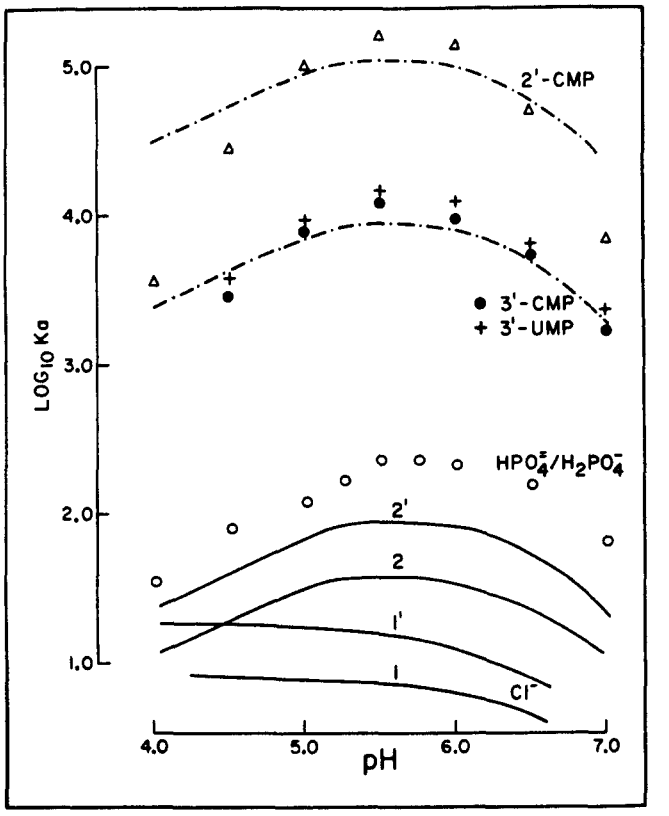

FIGURE 54. pH-dependent additional electrostatic stabilization produced by the binding of univalent and divalent anions in the RNase-S active site (position A1) expressed as pH-dependent association constants. Curves 1 and 1′ are for a univalent anion such as chloride at ionic strengths of 0.10 and 0.01, while curves 2 and 2′ are calculated for the titratable phosphate ion. Data are those of Anderson et al.[177] determined spectrophotometrically for the pH-dependent binding of inorganic phosphate (○), 3′-CMP (●), 3′-UMP (+), and 2′-CMP (△). The broken lines drawn through the nucleotide data are the calculated pH-dependent phosphate curves translated up to demonstrate the common pH dependence of these phosphate compounds. The protonation of the pyrimidine ring nitrogen in the acid region has not been taken into account in these calculations but would lead to a decrease in binding for CMP at pH values near 4.0. (From Matthew, J. B. and Richards, F. M., *Biochemistry*, 21, 4989, 1982. With permission.)

In this scheme, if we set n = 1, thus assuming a direct stoichiometric competition, we get the predicted curve 2 in Figure 56. This curve is very nearly linear, closely matching the slope of the data as well as their absolute magnitude. By including the ionic strength effect, the physically meaningful 1:1 ion-exchange ratio is found to explain the observed binding energies quite well, implying that the nonelectrostatic components of binding are minimal or cancelling.

C. Nucleic Acid Interactions

Matthew and Richards[185] have applied the discrete charge, solvent accessibility treatment to compute potential envelopes and counterion binding patterns of the A, B, and Z forms of DNA as represented by regularized segments of 20 base pairs in each geometry. An

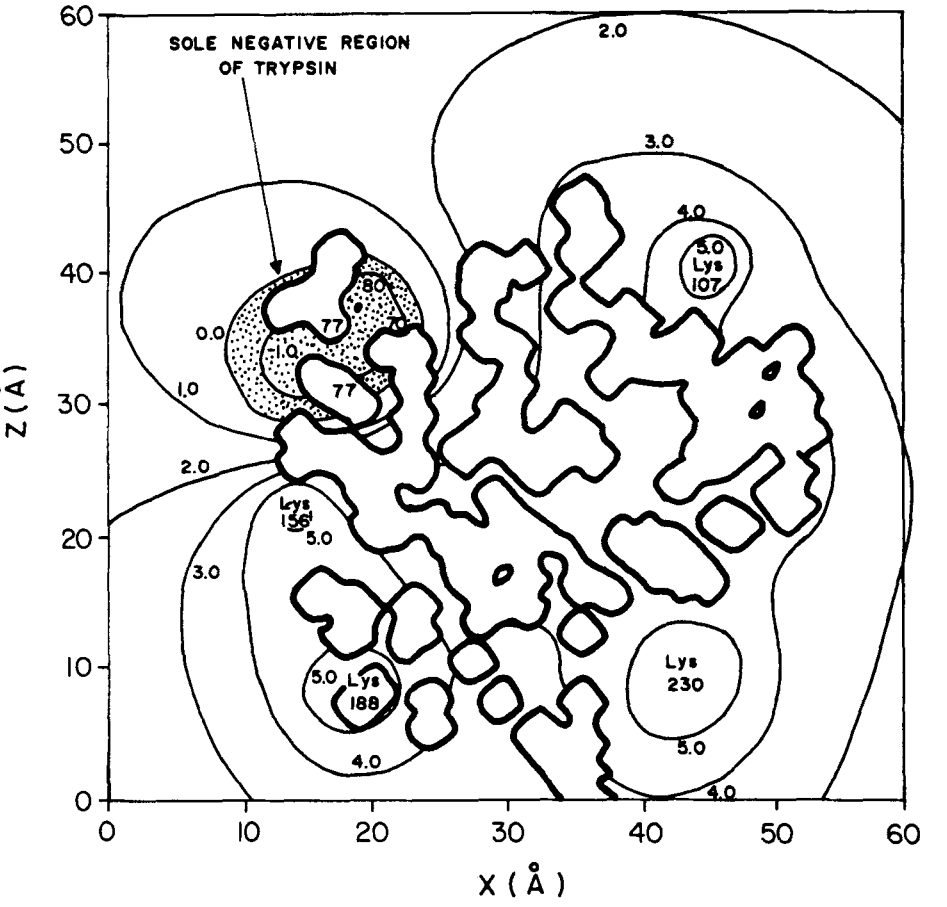

FIGURE 55. Representative cross section of trypsin with protein atoms defined by bold outlines. Solid lines represent equipotentials in units of kT calculated without attenuation by SA. The shaded region is the negative calcium binding site, with the projected calcium location marked by a dot. (From March, K. L., Electrostatic Interactions and Ion Binding in Trypsin, Bovine Pancreatic Trypsin Inhibitor, and Other Proteins, Ph.D. thesis, Indiana University, Bloomington, 1983.)

expression of the form of Equation 16 was used to compute the electrostatic work to place a diffusible ion, q, at the solvent interface summed over all phosphate in the 20 base pair fragment. In view of the insensitivity of the W_{ij} values to the radius chosen for the sphere relative to the ionic strength effects,[61,62] the 18 Å radius was chosen as the average radius for DNA charge interactions. For systems of similar geometry, Gueron and Weisbuch have calculated that counterion distributions are not strongly shape dependent.[186]

These considerations open the way for evaluating the specific binding or localization of counterions such as sodium in the minor phosphate-containing groove, describing partitioning between specific sites and a diffuse layer. The analysis is therefore responsive to the discrete three-dimensional charge array and the molecular topography, more directly so than the charged cylinder-diffuse layer of Zimm and Le Bret.[187] In order to treat the closely spaced ion sites in the DNA minor groove, the electrostatic model was extended to calculate ion site partial occupancies in the same fashion that fractional charges are calculated for titrating side chains. Between the different double-helical structures and the single-stranded forms, subtle differences are computed that follow the general patterns of observed behavior. In this treatment it is seen that a given set of neighboring counter-ion sites will tend to be filled

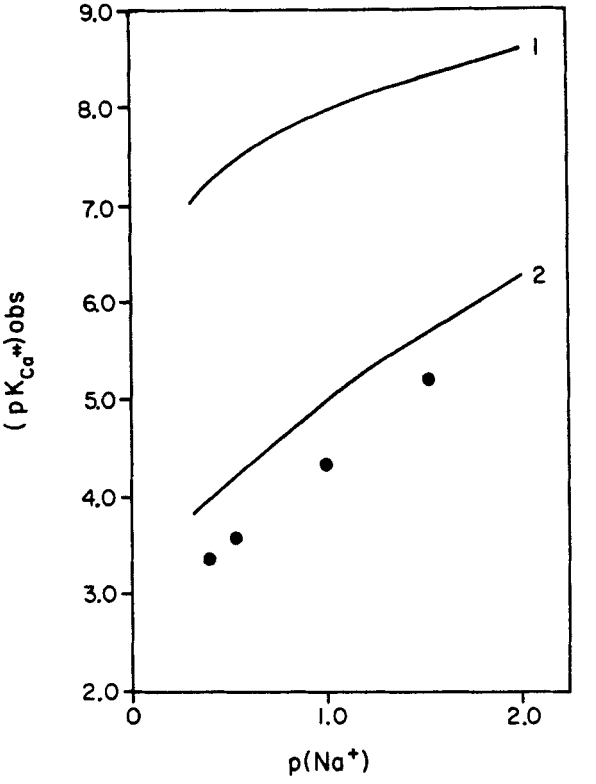

FIGURE 56. Dependence of experimental values for $pK_{Ca^{++}}$, shown as dots, upon p(Na) of determination. The predicted $pK_{CA^{++}}$ as obtained from Tanford-Kirkwood theory is given as curve 1, and from this theory with superimposed sodium-calcium 1:1 competition as curve 2. (From March, K. L., Electrostatic Interactions and Ion Binding in Trypsin, Bovine Pancreatic Trypsin Inhibitor, and Other Proteins, Ph.D. thesis, Indiana University, Bloomington, 1983.)

to a certain partial occupancy which depends on the occupancy of other ion sites as well as the DNA charge sites. This treatment successfully accounts for observable ionic strength-dependent properties of DNA. Computer simulations of catabolite gene activation protein (CAP) binding to DNA suggest that electrostatic interactions between CAP and DNA may constrain the protein diffusion on DNA to one or two dimensions.[188,189] The electrostatic treatments lay a basis for analysis of protein-nucleic acid docking modes in which counterion activity, occupancy, and mobility are explicitly considered.[148,185,188,190] A contrast between the roles of large and small ions in docking has already been drawn in the discussion of the trypsin-inhibitor interaction (see Section IV.B.2).[150,191]

D. Catalysis of Solvent Exchange Processes

The pH dependence of hydrogen exchange in BPTI and RNase-S was studied by Matthew and Richards.[63] First, the discrete charge, SA treatment was employed with Equation 9 to define the overall electrostatic stabilization as a function of pH. The exchange rates were correlated with the electrostatic stabilization profile which accounted for the offset of the rate minimum relative to an unstructured polypeptide on the notion that the electrostatic lattice stability constrains the small internal displacements required for the slow exchange

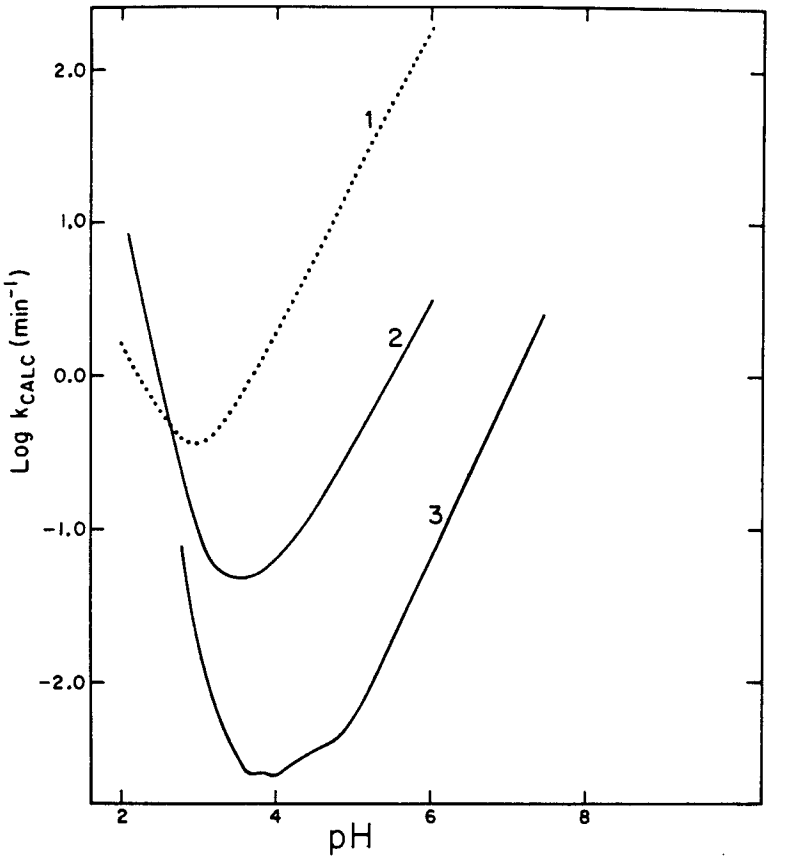

FIGURE 57. Predicted amide hydrogen exchange rates as a function of pH. Curve 1, rate profile for poly-DL-alanine calculated from Equation 1 with $K_{int}^{H^+} = 10\ min^{-1}$ and $K_{int}^{OH^-} = 10^{10}\ min^{-1}$. Curve 2, rates from curve 1 as modified by the inclusion of ΔG_{el} for BPTI as described by Equations 1 through 6, omitting the $\Delta G_q +/-$ terms. Curve 3, rates from curve 1 as modified by inclusion of ΔG_{el} for RNase-S. (From Matthew, J. B. and Richards, F. M., *J. Biol. Chem.*, 258, 3039, 1983. With permission.)

processes to occur.[42,71,86,103,192,193] Second, the treatment was applied to defining field effects at specific protons by applying a positive or negative charge at the amide N (Equations 12 to 16). As expressed in Equation 15, the required activation energy is the sum of the two terms. The electrostatic analysis for ribonuclease was based on Matthew and Richards[62] and the hydrogen exchange data on Rosa and Richards.[192] The calculations for BPTI stabilization are in substantial agreement with March et al.[29]

Figure 57 shows predicted amide hydrogen exchange rates as a function of pH.[63] Curve 1 is the rate profile for poly-D,L-alanine calculated from Equations 13 and 14. Curve 2 shows rates from curve 1 as modified by the inclusion of ΔG_{el} for BPTI without including local field effects for catalysis. Except in the lowest pH range where conformational changes are observed,[29,194] the slowing of the predicted exchange is marked. Curve 3 represents rates from curve 1 as modified by inclusion of ΔG_{el} for RNase-S.

Figures 58 and 59 illustrate computed exchange profiles for the two residues Tyr-35 and Glu-31 in BPTI. In Figure 58 the overall electrostatic stability, ΔG_{el}, and the individual site catalytic ion approach energies, ΔG_q^- and ΔG_q^+, are included in the calculated free energy of activation (Equations 12 to 18). The upper dotted curve is the reference curve for poly-

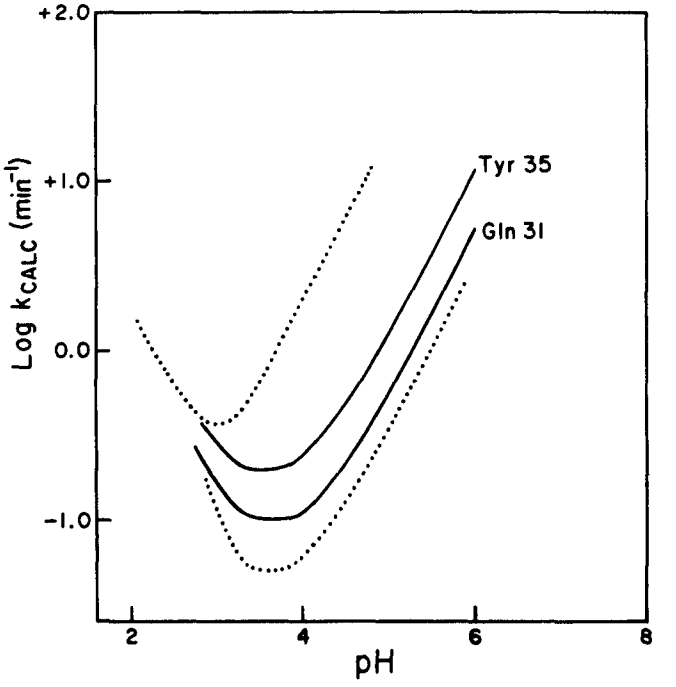

FIGURE 58. Calculated exchange profiles of Tyr-35 and Gln-31 in pancreatic trypsin inhibitor as a function of pH. The overall electrostatic stability, ΔG_{el}, and the individual site catalytic ion approach energies, ΔG_q^- and ΔG_q^+, are included in the calculated free energy of activation (Equations 1 through 7). The upper dotted line is the reference curve for poly-DL-alanine taken from Figure 57. The lower dotted line is the predicted profile, applicable to all residues, when only ΔG_{el} is included in the calculated $\Delta G^{\ddagger}$. (From Matthew, J. B. and Richards, F. M., *J. Biol. Chem.*, 258, 3039, 1983. With permission.)

D,L-alanine (Figure 57). The lower dotted curve is the predicted profile, applicable to all residues, when only ΔG_{el} is included in the calculated $\Delta G^{\ddagger}$. In Figure 59 the exchange data by proton NMR methods of Richarz et al.[195] at 22°C are shown for the same two residues. The solid curves are the calculated ones from Figure 58 translated vertically with a single displacement to get the best fit for the pair. The required translation corresponds to the non-pH-dependent component of the overall influence of the three-dimensional structure on the exchange rates.[63]

Although the calculations per se do not differentiate between a solvent penetration mechanism for buried proton exchange or a local unfolding reaction, they are based on the native coordinates from crystallographic analysis.[63] Either mechanism will require some deviation from the average, static structure,[42,196] and may require redistributions of stabilization energy between different categories. In considering either type of process, note that the overall electrostatic stabilization may remain unchanged as a function of some deviation from the average structure while the pairwise interactions between structural units do not.[63,71,74,130,150]

VI. CONCLUSION

The methods and approach outlined in this paper successfully analyze and predict a variety of pH-dependent processes in proteins. These range from titration and buffering properties through stability characteristics and quaternary assembly to specific ion binding and poten-

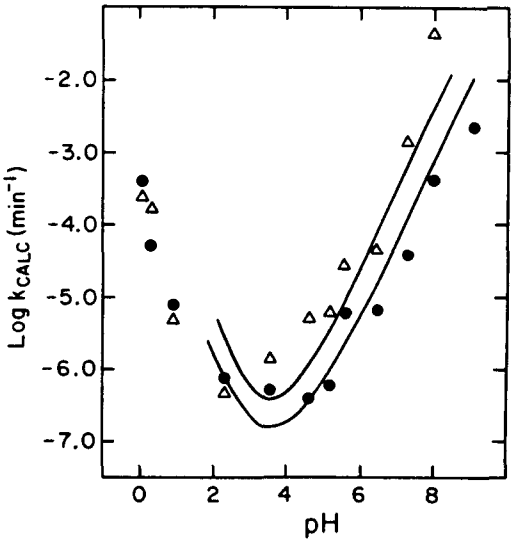

FIGURE 59. Exchange of the amide protons of Tyr-35 (△) and Gln-31 (●) in BPTI. The data are those of Richarz et al.[195] (obtained by proton NMR techniques at 22°C). The solid lines are the calculated curves taken from Figure 58 and translated vertically with a single displacement to get the best fit for the pair. The required translation corresponds to the non-pH-dependent component of the overall influence of the three-dimensional structure on the exchange rates. (From Matthew, J. B. and Richards, F. M., *J. Biol. Chem.*, 258, 3039, 1983. With permission.)

tiation of catalytic effects. To summarize the present state of development of the treatment and to point to its future potential the final sections deal with the characteristics of the interactions within the electrostatic lattice and with interconversions between the energy categories.

Although the Tanford-Kirkwood basis for computing the W_{ij} function does not offer overwhelming advantages over estimations based on coulombic screening parameters, Equations 3 and 4, nevertheless it offers a simple, systematic methodology that includes the cases of charged groups contained within media of low dielectric constant.[8,51] The treatment reflects the curvature of the dielectric interface and is not limited to the original portrayal of the protein in spherical geometry. The success of this treatment suggests that the protein structure enhances long-range electrostatic interactions predominately by restricting access of counterions to charge sites. The magnitude of the coulombic interaction between protein charge pairs apparently follows (1) the distance dependence of the Debye screening function and (2) an intensity reduction reflecting the average solvent accessibility of the pairs.

Only charge-pair interactions on the dielectric interface with separation distances less than 10 Å are significantly affected by the presence of the low dielectric region. At these short distances a 36-Å diameter spherical dielectric boundary approximates a planar surface of slight curvature. The implication that this treatment is not dependent on a spherical geometry is reinforced by its successful application to pear-shaped RNase and cylindrical BPTI and DNA. The transition between D_{int} and D_{ext} probably is artifically abrupt for a hydrated protein, but the ion-exclusion geometry, expressed in the SA term, provides an effective estimate of dielectric screening of individual sites. Whatever basis is adopted for W_{ij}, the most distinctive electrostatic characteristics will be reflected in the more sensitive SA term.

A. Characteristics of Electrostatic Lattice Interactions

We have used the term "lattice" to indicate the interactive communication between charged groups on a protein. The lattice is three-dimensional both geometrically and functionally. General communication is ordinarily sustained whether or not a given charge point is introduced or obliterated.[71,162] Correspondingly, the functional role of a given group is conditioned by potential field contributions from many or all other groups. With any addition or subtraction from the electrostatic lattice, spontaneous shifts of charge site occupancy will work to dampen the overall change in energy state.[162] One result is that the characteristics of the charge-site lattice will tend to be conserved over a functional range of pH or ionic conditions. Conversely, any given lattice brought into contact with a compatible one will have the capability of forming an extended lattice with it in assembly or docking.

The energy of a given interacting pair of charges in the lattice depends first on a function of the distance of separation, r_{ij}, and second on the static accessibility term $(1 - SA_{ij})$. Of these terms, the more important in many cases proves to be the latter one. This point has been illustrated repeatedly in previous sections, perhaps most broadly in the comparison of the charge lattices in hemoglobin[61,64,67,68,74] and myoglobin.[55,71,81,82,91-93]

An interesting situation in which r_{ij} and SA_{ij} often interact is one in which the location of either or both charge sites is not constrained.[22,27,29,42,67] Usually an unconstrained residue is highly exposed to the solvent so that the interaction energy is small no matter how r_{ij} may vary. In such cases, the geometrical uncertainty is not expressed to a strong degree at the level of the lattice energy. Conversely, a highly constrained, relatively inaccessible site will tend to enter into strong, predictable interactions.[150,162,191]

The impact of the degree of SA in computations of charge array stabilization takes at least three forms. One is the general decrease in interaction strength as noted for ferrimyoglobin.[81,82] Another is the more specific tolerance of a net positive or negative charge arising from a skewed distribution of SA values tending to shield one charge sign.[29,67,150,191] A third reflects highly specific influences at particular sites leading to $\Delta G_{i,el}$ or $\Delta G_{ij,el}$ of distinctive magnitude.[29,82,191] An example of this last is given by the α-NH_2 of trypsin with its very low SA of 0.05 engaging in a structurally important interaction with Asp-194, while most other positive charges are rather exposed ($SA_+ = 0.52$) and unable to compete specifically in influencing the anion. For the anionic sites as a whole $SA_- = 0.14$, all stabilized at pH 7.[150]

The roles of charged and polar groups in a protein are divided between promoting solvation and solubility and entering into the intramolecular interactions that have been emphasized here.[7] A similar dichotomy of function is found in the protein crystals themselves. The majority of interactions of this type are intramolecular but a certain proportion help stabilize the crystal lattice. Internal stability and the external lattice role compete for the placement of certain charged groups. Intermolecular contacts may exert unacknowledged control over some r_{ij} and SA values in a given protein molecule.[71,106] Since imidazole and α-NH_2 groups are less commonly involved in the intermolecular contacts, the pH-dependent component of ΔG_{el} for a given protein structure is potentially less sensitive to the intermolecular contact patterns than its less pH-sensitive counterpart involving strongly basic and acidic residues.

Another example of unacknowledged control by the intermolecular interactions would result from their effects on the asymmetric potential fields of the individual molecules. This is illustrated with the $T \rightarrow T'$ and $I \rightarrow I'$ transitions in the trypsin-BPTI system.[150] The intermolecular interactions in this way could control side-chain placement or the (potentially undetected) intercalation of small ions, so that the natural potential fields surrounding the individual molecule would be somewhat distorted in certain regions of the molecule. It is important to compute the external potential fields around any protein to evaluate possible ion binding sites and to test for their control by the crystal lattice.

B. Interconversion of Energy Categories

The stabilization of a particular protein conformation depends on contributions from the various polar and nonpolar categories of interaction.[71,74,76,146] We have chosen to stress the category of discrete charge interactions because substantial experimental evidence is available and the geometrical precision is the least demanding on account of the dependence on the reciprocal first power of r_{ij}. Furthermore, a wide range of functional roles are known and have yielded reasonably to analysis by the present methods in all cases that we have tested. However, the charge lattice and surrounding medium are not isolated from the rest of the protein. The influence of the potential gradient of the charge lattice on a given charged site will affect its short-range interactions with polar parts of the protein side chains and backbone and so will transfer energy from one category to another. The interchange between the discrete charge lattice and the polar, usually hydrogen bonding components depends more critically on separation distance and orientation and requires for analysis crystallographic or other evidence of very high accuracy. Effects on other packing forces are likewise difficult to evaluate.[196] In considering the interactions of charged groups with permanent dipoles, including water, it is important to bear in mind that the protonation state will control the nature and strength of interaction. Thus, changes in the discrete charge lattice will work to redistribute energy among different categories and produce local structural reorganization. For example, in the systems presented in Table 11, the computed ΔG_{el} values may be relieved to some degree by energy redistribution.[130]

The coupling of changes in the charge lattice with the alteration of protein structure has been illustrated for the case of pH-dependent transitions in BPTI, apparent from NMR and crystallographic analyses and analyzed in terms of electrostatic stabilization and changes in pK_i values.[29] Corresponding coupling is well known for the quaternary transition in hemoglobin involving pK_i values associated with the Bohr protons.[64,68,118,149] More drastic examples are provided by the acid denaturation of myoglobin.[9,14,71,81] Early examples of coupling with synthetic polypeptides were described in the Introduction.[18-21] If the coupling of a structural change with the change in protonation state is strong but goes unobserved, the electrostatic analysis may appear to be in conflict. In a like sense, almost any energy-requiring conformation transition in a protein system may carry with it some change in ΔG_{el}.

C. Multiple Roles of Charged, Polar, and Nonpolar Structural Elements

The multiple roles of the charged, polar, and nonpolar structural elements in proteins have long been recognized but are very difficult to define quantitatively. Recognition of the chemical nature of a given residue defines its potentialities which, however, will be expressed according to the influence of other structural elements. The electrostatic influences on charged groups are relatively predictable in the framework of the current treatment. Likewise, they will be open in the future to formulations of the properties of the solvent interface in more physically detailed, microscopic terms to extend the analyses of the internal structure and energetics of the protein molecules. In such treatments, the W'_{ij} input in Figure 9 will have a similar magnitude but a modified computational origin. Any such alternatives to the present treatment should be shown to deal equally inclusively with properties of diverse proteins as the present one does.

Characteristically, the role of a charged residue is expressed at several levels. If it is part of an ion pair, its importance for stability may be suggested by inspection of the crystal structure.[110] A higher level of interpretation will recognize the relations with other charged groups in overall stabilization to modulate the pK_i values,[61,64,67,68] to control residual external fields that influence ionic substrate binding,[62] or to control the linkage with a larger electrostatic lattice.[74,130] Equally important are functional alterations in charge type such as with changes in carbamino content[64] or phosphorylation state. All these examples are likely to require full lattice treatment for satisfactory analysis.

The next most prominent role of a charged residue will be the interaction with dipolar structures found in many side chains, in the backbone, and in numerous molecules that may bind functionally to the protein. The present treatment does not deal overtly with these interactions under most conditions but does bring out their importance in a number of ways.[27,71,74,130] The hydrogen bonding and other dipolar interactions are not directly dependent on pH except when a member group changes protonation state. In general such interactions are much more localized in their scope although their influence can be widespread depending on packing effects and the internal rigidity or fluidity of the particular regions in some given protein.[74,130,132,149,196]

Table 11 illustrates several examples of the consequences of substitution of a charge-bearing residue for hemoglobin tetramer assembly. Perhaps the paradigmatic example is that of hemoglobin Kempsey, β99 Asp → Asn. The formal charge lattice is somewhat stabilized by the replacement of the carboxyl group but the assembly concurrently is markedly destabilized by the loss of one or both strong dipolar interactions of the carboxyl group. If the formal electrostatic treatment of the interactions of β99 Asp were extended to include the close dipolar interactions, the net potential at its side chain would be corrected to show the discrete charge lattice interactions as more favorable than we have computed. Conversely, the charge borne by the Asp side chain makes possible particularly strong hydrogen bonding with its neighbor, which will have the effect of selectively lowering its effective pK_{int}. In practice, the free energy change computed for the Asn substitution may be partly transferred to other categories, for example, by driving a local conformational change.[130]

Because of the great influence of the potential fields of the charged group on the dipolar structures in a protein, it is essential that the electrostatic lattice analysis be made part of any overall plan to account completely for pairwise interactions in other polar categories. Either directly or through linkage with the discrete charge lattice, all polar or polarizable structures are, to some degree, under the influence of the solvent. This point applies as well to structures whose polarization can be induced as to those that have a primarily permanent polar nature, albeit with a difference in distance dependence.[25]

Returning to Table 11 and the results of the substitution in hemoglobin Yakima, the effect on the oxytetramer assembly is very slight by comparison with the deoxytetramer probably because the assembly interface is more distant. A partial parallel has been drawn with the same substitution in hemoglobin Barcelona β94 Asp → His in which the site of substitution is distant from both interfacial contacts and its consequences are minimal in both cases. These examples illustrate the variety of isoenergetic structures or substates that proteins can assume to channel or limit responses to substitutions.[42,196] Table 11 also gives examples of comparable changes in free energy in which the substitutions are concerned with uncharged residues only.

The fine shading in emphasis between one residue and another has also become apparent from the analysis of the properties of a series of myoglobins.[71] In the most stable myoglobins of the sperm whale group a strong hydrogen bonding network involving Arg-45 and several neighboring carboxylate groups contrasts with the less balanced network arrangement in the remaining species of myoglobins that contain Lys-45 instead. In compensation, however, the total ΔG_{el} for each of the latter myoglobin species is greater than that computed for the sperm whales.

Far more distinct contrasts in structural and functional emphasis are illustrated by molecules such as ribonuclease,[62] trypsin,[150] and BPTI[29] that show net electrostatic stabilization about an order of magnitude lower than for myoglobin or hemoglobin. The former groups possess several disulfide bonds whereas the latter have none. The disulfide-containing proteins seem able to rely on a limited number of charge sites whose effectiveness is controlled by special SA values, rather than on well-organized distribution of charge loci exemplified in the more neutral myoglobins.[150]

The titration of a given group can be defined either in terms of a general pK_{int} (Equation 8), or one that is adjusted further by a local dipolar field contribution, e.g., ± 0.5 unit, or one that is strongly offset by a major linkage with burial or complex formation. The large correction for the latter case is very difficult to predict and is treated as a separate question when encountered.[9,14,38,39,135] The consequences of coordination with a neighboring group are at best approximately treated with the ± 0.5 unit correction. Ion-dipole terms so far are neglected in the examples of the strongest ion-pair interactions that, indeed, often occur at hydrogen bonding distances (Table 5), but not necessarily with good vectorial alignment of the dipoles. An informative experimental and theoretical treatment of ion pair formation, pK displacement, and structural accommodation is reported by March et al.[29] Because of the sensitivity of side-chain functions to local structure, the choice of pK_{int} itself is not an infallible one. The set that has been used in the present work from 1975 on has proved predictive for a variety of proteins.[39-41,69,70] A good set of model peptides to represent pK_{int} for various amino acid residues in terminal positions is not available, however.[198]

The range of physiological functions connected with pH-dependent processes is very wide. Some are expressed in regular cycles as in hemoglobin function in the circulating erythrocyte, or in response to varying metabolic stress as in the glycolytic-oxidative cycle. Others form part of the unidirectional life cycle of a molecule reaching a stage of modification or degradation in an external organ such as the gut or in subcellular organelles, e.g., lysosomes, receptosomes, endosomes, mitochondria, and the like.[199,200] In these connections the importance of the pH-dependent stability profile of a given protein will extend from early processing of a precursor, through the action of a primary active or migrating form, to the role of substrate in a cleavage or degradative process. For these reasons it is useful to compute the stability profiles of proteins over a full range of pH since the decline at low pH may be as functionally adaptive as the maximum stability range at higher pH.

For a given average protonation state individual sites are occupied according to a distribution so that a given protein at any instant offers a range of configurations.[7,42,201] The specific binding of ionic species alters both the average protonation state and the configurations contributing significantly to it. Most substrates, products, and effectors of enzymic reactions are ionic and alter the charge lattice of the protein when bound. The same is true of many other types of regulatory molecules. Most cases of binding of regulators or substrates are inevitably accompanied by changes in SA values, so that the charge lattice will be influenced in that most important respect as well.

In considering the functional effects on a protein of changes in pH and ionic solutes it is useful to evaluate the other most common biological variable, temperature. Because of differences in enthalpy of dissociation of the different classes of proton-bearing sites, the charge-site lattice is directly sensitive to temperature changes.[7] As shown with respect to hemoglobin, the characteristics of the lattice produce a response to minimize the disturbance and increase the electrostatic stabilization as the temperature increases (Table 6).

Besides the local effects on charge placement and SA changes, coupled conformational changes may alter geometrical relationships and modify the discrete charge lattice over a distance. The driving force for the changes need not be primarily electrostatic in nature. Conversely, the alteration in the electrostatic lattice interactions need not produce a measurable structural change apart from changes in electrostatic fields controlling the binding or release of ions.[31] Hence, the idea that an allosteric effect necessarily involves an observable structural change in a monomeric protein or a rearrangement of subunits in an oligomeric one, though compatible with the work reviewed here, is not an inevitable consequence of it.

ACKNOWLEDGMENTS

Key contributions are gratefully acknowledged to the inception and development of this work by G. I. H. Hanania, G. K. Ackers, J. A. Berzofsky, L. H. Botelho, E. Breslow, R. D. England, R. J. Feldmann, S. H. Friend, C. Ho, J. S. Markley, J. S. Morrow, M. Crowl-Powers, F. M. Richards, T. M. Rothgeb, I. Russu, H. Scouloudi, and R. J. Wittebort. G. K. Ackers, J. M. Baldwin, M. Crowl-Powers, and J. A. Radding kindly provided information in advance of publication. J. T. Edsall, R. S. Gurd, D. C. Phillips, D. A. McQuarrie, A. Szabo, and C. Tanford provided advice and encouragement at numerous junctures. The skillful and tireless help of Sarah Burton in the preparation of the manuscript is warmly acknowledged.

REFERENCES

1. **Hardy, W. B.,** Colloidal solution. The globulins, *J. Physiol.*, 33, 251, 1905.
2. **Sörensen, S. P. L.,** Über die Messung und die Bedeutung der Wasserstoffionenkonzentration bei Enzymatischen Prozessen, *Biochem. Z.*, 21, 131, 1909.
3. **Ericksson-Quesnel, I.-B. and Svedberg, T.,** The molecular weights and pH stability regions in hemocyanins, *Biol. Bull.*, 71, 498, 1936.
4. **Cohn, E. J.,** Die Physikalische Chemie der Eiweisskörper, *Ergeb. Physiol.*, 33, 781, 1931.
5. **Bjerrum, N.,** Dissoziationskonstanten von Mehrbasischen Saüren und ihre Anwendung zur Berechnung Molekularer Dimensionen, *Z. Physik. Chem.*, 106, 219, 1923.
6. **Debye, P. and Hückel, E.,** Zur Theorie der Electrolyte, *Physik. Z.*, 24, 185, 1923.
7. **Cohn, E. J. and Edsall, J. T.,** *Proteins, Amino Acids and Peptides*, Reinhold, New York, 1943.
8. **Tanford, C.,** *Physical Chemistry of Macromolecules*, Wiley-Interscience, New York, 1961.
9. **Breslow, E. and Gurd, F. R. N.,** Reactivity of sperm whale metmyoglobin towards hydrogen ions and p-nitrophenyl acetate, *J. Biol. Chem.*, 237, 371, 1962.
10. **Anson, M. L.,** The sulfhydryl groups of egg albumen, *J. Gen. Physiol.*, 24, 399, 1940.
11. **Linderstrøm-Lang, K.,** On the ionisation of proteins, *C.R. Trav. Lab. Carlsberg*, 15 (7), 1, 1924.
12. **Katchalski, E. and Sela, M.,** The synthesis and spectrophotometric study of poly-L-tyrosine and poly-3,5-diiodotyrosine, *J. Am. Chem. Soc.*, 75, 5284, 1953.
13. **Scatchard, G., Hughes, W. L., Gurd, F. R. N., and Wilcox, P. E.,** The interaction of proteins with small molecules and ions, in *Chemical Specificity in Biological Interactions*, Gurd, F. R. N., Ed., Academic Press, New York, 1954, 193.
14. **Hartzell, C. R., Bradshaw, R. A., Hapner, K. D., and Gurd, F. R. N.,** Comparisons of myoglobins from harbor seal, porpoise, and sperm whale, *J. Biol. Chem.*, 243, 690, 1968.
15. **Mellanby, J.,** Globulin, *J. Physiol.*, 33, 338, 1905.
16. **Sørensen, S. P. L.,** De opløselige Proteinstoffers Konstitution, *C.R. Trav. Lab. Carlsberg*, 18(5), 1, 1930.
17. **Oncley, J. L., Ellenbogen, E., Gitlin, D., and Gurd, F. R. N.,** Protein-protein interactions, *J. Phys. Coll. Chem.*, 56, 85, 1952.
18. **Fasman, G. D., Lindblow, C., and Bodenheimer, E.,** Conformational studies on synthetic poly-α-amino acids: factors influencing the stability of the helical conformation of poly-L-glumatic acid and copolymers of L-glutamic acid and L-leucine, *Biochemistry*, 3, 155, 1964.
19. **Fasman, G. D.,** Factors responsible for conformational stability, in *Poly-α-Amino Acids*, Vol. 1 (Biological Macromolecules Series), Fasman, G. D., Ed., Marcel Dekker, New York, 1967, 499.
20. **Iizuka, I. and Yang, J. T.,** Effects of salts and dioxane on the coiled conformation of poly-L-glutamic acid in aqueous solution, *Biochemistry*, 4, 1249, 1965.
21. **Urnes, P. and Doty, P. M.,** Optical rotation and the conformation of polypeptides and proteins, *Adv. Protein Chem.*, 16, 401, 1961.
22. **Takano, T.,** Structure of myoglobin refined at 2·0 Å, *J. Mol. Biol.*, 110, 569, 1977.
23. **Wada, A.,** The α-helix as an electric macro-dipole, *Adv. Biophys.*, 9, 1, 1976.
24. **Rogers, N. K. and Sternberg, M. J. E.,** Electrostatic interactions in globular proteins. Different dielectric models applied to the packing of α-helices, *J. Mol. Biol.*, 174, 527, 1984.
25. **Moelwyn-Hughes, E. A.,** *States of Matter*, Oliver and Boyd, Edinburgh, 1961.

26. **Tanford, C. and Hauenstein, J. D.,** Hydrogen ion equilibria of ribonuclease, *J. Am. Chem. Soc.*, 78, 5287, 1956.
27. **Botelho, L. H. and Gurd, F. R. N.,** Proton nuclear magnetic resonance study of histidine ionizations in myoglobins of various species. Specific assignment of individual resonances, *Biochemistry*, 17, 5188, 1978.
28. **Russu, I. M., Ho, N., and Ho, C.,** Role of the β146 histidyl residue in the alkaline Bohr effect of hemoglobin, *Biochemistry*, 19, 1043, 1980.
29. **March, K. L., Maskalick, D. G., England, R. D., Friend, S. H., and Gurd, F. R. N.,** Analysis of electrostatic interactions and their relationship to conformation and stability of bovine pancreatic trypsin inhibitor, *Biochemistry*, 21, 5241, 1982.
30. **DiMarchi, R. D., Neireiter, G. W., Heath, W. F., and Gurd, F. R. N.,** Structural significance of the amino-terminal residues of sperm whale myoglobin, *Biochemistry*, 19, 2454, 1980.
31. **Jenkins, W. T.,** The specific anion effect on the chromophoric proton dissociation of heart aspartate amino transferase, *Arch. Biochem. Biophys.*, 205, 579, 1980.
32. **Hugli, T. E. and Gurd, F. R. N.,** Carboxymethylation of sperm whale myoglobin in the dissolved state, *J. Biol. Chem.*, 245, 1939, 1970.
33. **Doscher, M. and Richards, F. M.,** The activity of an enzyme in the crystalline state: ribonuclease S, *J. Biol. Chem.*, 238, 2399, 1963.
34. **Keniry, M. A., Rothgeb, T. M., Smith, R. L., Gutowsky, H. S., and Oldfield, E.,** Nuclear magnetic resonance studies of amino acids and proteins. Side-chain mobility of methionine in the crystalline amino acid and in crystalline sperm whale (*Physeter catodon*) myoglobin, *Biochemistry*, 22, 1917, 1983.
35. **Mavridis, A., Tulinsky, A., and Liebman, M. N.,** Asymmetrical changes in the tertiary structure of α-chymotrypsin with changes in pH, *Biochemistry*, 13, 3661, 1974.
36. **Shulman, R. G., Brown, T. R., Ugurbil, K., Ogawa, S., Cohen, S. M., and de Hollander, J. A.,** Cellular applications of ^{31}P and ^{13}C nuclear magnetic resonance, *Science*, 205, 160, 1979.
37. **Gurd, F. R. N. and Wilcox, P. E.,** Complex formation between metallic cations and proteins, peptides, and amino acids, *Adv. Protein Chem.*, 11, 311, 1956.
38. **Steinhardt, J. and Reynolds, J. A.,** *Multiple Equilibria in Proteins*, Academic Press, New York, 1969.
39. **Botelho, L. H.,** Histidine Ionizations in Myoglobins: A Study by Proton Nuclear Magnetic Resonance, Ph.D. thesis, Indiana University, Bloomington, 1975.
40. **Keim, P., Vigna, R. A., Morrow, J. S., Marshall, R. C., and Gurd, F. R. N.,** Carbon 13 nuclear magnetic resonance of pentapeptides of glycine containing central residues of serine, threonine, aspartic and glutamic acids, asparagine and glutamine, *J. Biol. Chem.*, 248, 7811, 1973.
41. **Keim, P., Vigna, R. A., Nigen, A. M., Morrow, J. S., and Gurd, F. R. N.,** Carbon 13 nuclear magnetic resonance of pentapeptides of glycine containing central residues of methionine, proline, arginine and lysine, *J. Biol. Chem.*, 249, 4149, 1974.
42. **Gurd, F. R. N. and Rothgeb, T. M.,** Motions in proteins, *Adv. Protein Chem.*, 33, 73, 1979.
43. **Warshel, A. and Levitt, M.,** Theoretical studies of enzymatic reactions: dielectric, electrostatic and steric stabilization of the carbonium ion in the reaction of lysozyme, *J. Mol. Biol.*, 103, 227, 1976.

43a. **Warshel, A., Russell, S. T., and Churg, A. K. C.,** Macroscopic models for studies of electrostatic interactions in proteins: limitations and applicability, *Proc. Natl. Acad. Sci. U.S.A.*, 81, 4785, 1984.

44. **Hol, W. G. J., van Duijnen, P. T., and Berendsen, H. J. C.,** The α-helix dipole and the properties of proteins, *Nature (London)*, 273, 443, 1978.
45. **Sheridan, R. P. and Allen, L. C.,** The electrostatic potential of the alpha helix, *Biophys. Chem.*, 11, 133, 1980.
46. **Sheridan, R. P., Levy, R. M., and Salemme, F. R.,** α-Helix dipole model and electrostatic stabilization of 4-α-helical proteins, *Proc. Natl. Acad. Sci. U.S.A.*, 79, 4545, 1982.
47. **Koppenol, W. H. and Margoliash, E.,** The asymmetric distribution of charges on the surface of horse cytochrome c, *J. Biol. Chem.*, 257, 4426, 1982.
48. **Karplus, M. and Mc Cammon, A.,** Protein structural fluctuations during a period of 100ps, *Nature (London)*, 277, 578, 1979.
49. **Buckingham, A. D.,** Basic theory of intermolecular forces: applications to small molecules, in *Intermolecular Interactions: From Diatomics to Biopolymers*, Pullman, B., Ed., John Wiley & Sons, Inc., Chichester, England, 1978, 1.
50. **Hill, T. L.,** Influence of electrolyte on effective dielectric constants on enzymes, proteins, and other molecules, *J. Phys. Chem.*, 60, 253, 1956.
51. **Tanford, C. and Kirkwood, J, G.,** Theory of protein titration curves, *J. Am. Chem. Soc.*, 79, 5333, 1957.
52. **Kirkwood, J. G.,** Theory of solutions of molecules containing widely separated charges with special application to zwitterions, *J. Chem. Phys.*, 2, 351, 1934.
53. **Davidson, N.,** *Statistical Mechanics*, McGraw-Hill, New York, 1962, 518.

54. **Nagasawa, M. and Holtzer, A.,** The use of the Debye-Hückel approximation in the analysis of protein potentiometric titration data, *J. Am. Chem. Soc.*, 86, 531, 1964.
55. **Lee, B. K. and Richards, F. M.,** The interpretation of protein structures: estimation of static accessibility, *J. Mol. Biol.*, 55, 379, 1971.
56. **Shire, S. J., Hanania, G. I. H., and Gurd, F. R. N.,** Electrostatic effects in myoglobins. Hydrogen ion equilibria in sperm whale ferrimyoglobin, *Biochemistry*, 13, 2967, 1974.
57. **Orttung, W. H.,** Interpretation of the titration curve of oxyhemoglobin. Detailed consideration of coulomb interactions at low ionic strength, *J. Am. Chem. Soc.*, 91, 162, 1969.
58. **Orttung, W. H.,** Proton binding and dipole moment of hemoglobin. Refined calculations, *Biochemistry*, 9, 2394, 1970.
59. **Tanford, C. and Roxby, R.,** Interpretation of protein titration curves. Application to lysozyme, *Biochemistry*, 11, 2192, 1972.
60. **Matthew, J. B., Hanania, G. I. H., and Gurd, F. R. N.,** Solvent accessibility calculations for sperm whale ferrimyoglobin based on refined crystallographic data, *Biochem. Biophys. Res. Commun.*, 81, 410, 1978.
61. **Matthew, J. B., Hanania, G. I. H., and Gurd, F. R. N.,** Electrostatic effects in hemoglobin: hydrogen ion equilibria in human deoxy- and oxyhemoglobin A, *Biochemistry*, 18, 1919, 1979.
62. **Matthew, J. B. and Richards, F. M.,** Anion binding and pH-dependent electrostatic effects in ribonuclease, *Biochemistry*, 21, 4989, 1982.
63. **Matthew, J. B. and Richards, F. M.,** The pH dependence of hydrogen exchange in proteins, *J. Biol. Chem.*, 258, 3039, 1983.
63a. **Rashin, A. A. and Honig, B.,** On the environment of ionizable groups in globular proteins, *J. Mol. Biol.*, 173, 515, 1984.
64. **Matthew, J. B., Friend, S. H., and Gurd, F. R. N.,** Electrostatic interactions associated with effector binding to hemoglobin, in *Hemoglobin and Oxygen Binding*, Ho, C., Ed., Elsevier/North Holland, Amsterdam, 1982, 231.
64a. **Hol, W. G. J., Halie, L. M., and Sander, C.,** Dipoles of the α-helix and β-sheet: their role in protein folding, *Nature (London)*, 294, 532, 1981.
64b. **Allen, L. C.,** The catalytic function of active site amino acid side chains in well-characterized enzymes, *Ann. N.Y. Acad. Sci.*, 367, 383, 1981.
64c. **Warwicker, J. and Watson, H. C.,** Calculation of the electric potential in the active site cleft due to α-helix dipoles, *J. Mol. Biol.*, 157, 671, 1982.
65. **Scatchard, G.,** The attractions of proteins for small molecules and ions, *Ann. N.Y. Acad. Sci.*, 51, 660, 1949.
66. **Gurd, F. R. N.,** Binding of protons and other ions, in *Physical Principles and Techniques of Protein Chemistry*, Vol. B, Leach, S. J., Ed., Academic Press, New York, 1970, 365.
67. **Matthew, J. B., Hanania, G. I. H., and Gurd, F. R. N.,** Electrostatic effects in hemoglobin: Bohr effect and ionic strength dependence of individual groups, *Biochemistry*, 18, 1928, 1979.
68. **Matthew, J. B., Friend, S. H., and Gurd, F. R. N.,** Electrostatic effects in hemoglobin: electrostatic energy associated with allosteric transition and effector binding, *Biochemistry*, 20, 571, 1981.
69. **Nozaki, Y. and Tanford, C.,** Intrinsic dissociation constants of aspartyl and glutamyl carboxyl groups, *J. Biol. Chem.*, 242, 4731, 1967.
70. **Gurd, F. R. N., Keim, P., Glushko, V., Lawson, P. J., Marshall, R. C., Nigen, A. M., and Vigna, R. A.,** Carbon-13 nuclear magnetic resonance of some pentapeptides, in *Chemistry and Biology of Peptides*, Meinhofer, J., Ed., Ann Arbor Science, Ann Arbor, Mich., 1972, 45.
71. **Flanagan, M. A., Garcia-Moreno E., B., Friend, S. H., Feldmann, R. J., Scouloudi, H., and Gurd, F. R. N.,** Contributions of individual amino acid residues to the structural stability of cetacean myoglobins, *Biochemistry*, 22, 6027, 1983.
72. **Bacarella, A. L., Grunwald, E., Marshall, H. P., and Purlee, E. L.,** The potentiometric measurement of acid dissociation constants and pH in the system methanol-water. pK_A values for carboxylic acids and anilinium ions, *J. Org. Chem.*, 20, 747, 1955.
73. **Grace, S. and Dunaway-Mariano, D.,** Examination of the solvent perturbation technique as a method to identify enzyme catalytic groups, *Biochemistry*, 22, 4238, 1983.
74. **Flanagan, M. A., Ackers, G. K., Matthew, J. B., Hanania, G. I. H., and Gurd, F. R. N.,** Electrostatic contributions to the energetics of dimer-tetramer assembly in human hemoglobin: pH dependence and effect of specifically bound chloride ions, *Biochemistry*, 20, 7439, 1981.
75. **Matthew, J. B. and Gurd, F. R. N.,** Enzyme structure: calculation of electrostatic interactions in proteins, *Methods Enzymol.*, in press.
76. **Levitt, M.,** A simplified representation for rapid simulation of protein folding, *J. Mol. Biol.*, 104, 59, 1976.

77. **Friedman, K. M. and Beychok, S.,** Probes of subunit assembly and reconstitution pathways in multisubunit proteins, *Annu. Rev. Biochem.*, 48, 217, 1979.
78. **Page, M. I. and Jencks, W. P.,** Entropic contributions to rate accelerations in enzymic and intramolecular reactions and the chelate effect, *Proc. Natl. Acad. Sci. U.S.A.*, 68, 1678, 1971.
79. **Chothia, C. H. and Janin, J.,** Principles of protein-protein recognition, *Nature (London)*, 256, 705, 1975.
80. **Chothia, C. H.,** Hydrophobic bonding and accessible surface area in proteins, *Nature (London)*, 248, 338, 1974.
81. **Friend, S. H. and Gurd, F. R. N.,** Electrostatic stabilization in myoglobin: pH dependence of summed electrostatic contributions, *Biochemistry*, 18, 4612, 1979.
82. **Friend, S. H. and Gurd, F. R. N.,** Electrostatic stabilization in myoglobin: interactive free energies between individual sites, *Biochemistry*, 18, 4620, 1979.
83. **Klotz, I. M. and Mueller, D. D.,** Local environment effects on hydrogen-deuterium exchange, *Biochemistry*, 8, 12, 1969.
84. **Sheinblatt, M.,** Determination of an acidity scale for peptide hydrogens from nuclear magnetic resonance-kinetic studies, *J. Am. Chem. Soc.*, 92, 2505, 1970.
85. **Molday, R. S., Englander, S. W., and Kallen, R. G.,** Primary structure effects on peptide group hydrogen exchange, *Biochemistry*, 11, 150, 1972.
86. **Englander, S. W. and Englander, J. J.,** Hydrogen-tritium exchange, *Methods Enzymol.*, 49, 24, 1978.
87. **Kim, P. S. and Baldwin, R. L.,** Influence of charge on the rate of amide proton exchange, *Biochemistry*, 21, 1, 1982.
88. **Vaughan, J. D., Mughrabi, Z., and Wu, E. C.,** The kinetics of deuteration of imidazole, *J. Org. Chem.*, 35, 1141, 1970.
89. **Bradbury, J. H., Chapman, B. E., and Pellegrino, F. A.,** Hydrogen-deuterium exchange kinetics of the C-2 protons of imidazole and histidine compounds, *J. Am. Chem. Soc.*, 95, 6139, 1973.
90. **Szabo, A. and Karplus, M.,** A mathematical model for structure-function relations in hemoglobin, *J. Mol. Biol.*, 72, 163, 1972.
91. **Botelho, L. H., Friend, S. H., Matthew, J. B., Lehman, L. D., Hanania, G. I. H., and Gurd, F. R. N.,** Proton nuclear magnetic resonance study of histidine ionizations in myoglobins of various species. Comparison of observed and computed pK values, *Biochemistry*, 17, 5197, 1978.
92. **Shire, S. J., Hanania, G. I. H., and Gurd, F. R. N.,** Electrostatic effects in myoglobin. pH and ionic strength variations of ionization equilibria for individual groups in sperm whale ferrimyoglobin, *Biochemistry*, 13, 2974, 1974.
93. **Shire, S. J., Hanania, G. I. H., and Gurd, F. R. N.,** Electrostatic effects in myoglobin. Application of the modified Tanford-Kirkwood theory to myoglobins from horse, California grey whale, harbor seal, and California sea lion, *Biochemistry*, 14, 1352, 1975.
94. **Watson, H. C.,** The stereochemistry of the protein myoglobin, *Prog. Stereochem.*, 4, 299, 1969.
95. **Edmundson, A. B.,** Amino-acid sequence of sperm whale myoglobin, *Nature (London)*, 205, 883, 1965.
96. **Romero-Herrera, A. E. and Lehmann, H.,** Residue 122 of sperm whale and horse myoglobin, *Biochim. Biophys. Acta*, 336, 318, 1974.
97. **Banaszak, L. J., Andrews, P. A., Burgner, J. W., Eylar, E. H., and Gurd, F. R. N.,** Carboxymethylation of sperm whale myoglobin, *J. Biol. Chem.*, 238, 3307, 1963.
98. **Nigen, A. M. and Gurd, F. R. N.,** Comparison of carboxymethylation patterns of harbor seal and sperm whale myoglobins, *J. Biol. Chem.*, 248, 3708, 1973.
99. **Bogardt, R. A., Jones, B. N., Dwulet, F. E., Garner, W. H., Lehman, L. D., and Gurd, F. R. N.,** Evolution of the amino acid substitution in the mammalian myoglobin gene, *J. Mol. Evol.*, 15, 197, 1980.
100. **Hugli, T. E. and Gurd, F. R. N.,** Carboxymethylation of sperm whale myoglobin in the crystalline state, *J. Biol. Chem.*, 245, 1930, 1970.
101. **Watson, H. C. and Chance, B.,** Crystallographic studies of ligand binding (CN^-, OH^-, F^-), in *Hemes and Hemoproteins*, Chance, B., Estabrook, R. W., and Yonetani, T., Eds., Academic Press, New York, 1966, 149.
102. **Nobbs, C. L., Watson, H. C., and Kendrew, J. C.,** Structure of deoxymyoglobin: a crystallographic study, *Nature (London)*, 209, 339, 1966.
103. **Gurd, F. R. N., Wittebort, R. J., Rothgeb, T. M., and Neireiter, G.,** Motions of aliphatic residues in proteins, in *Biochemical Structure Determination by NMR*, Bothner-By, A. A., Glickson, J. D., and Sykes, B. D., Eds., Marcel Dekker, New York, 1982, 1.
104. **Berzofsky, J. A., Buckenmeyer, G. K., Hicks, G., Gurd, F. R. N., Feldmann, R. J., and Minna, J.,** Topographic antigenic determinants recognized by monoclonal antibodies to sperm whale myoglobin, *J. Biol. Chem.*, 257, 3189, 1982.
105. **Berkower, I., Buckenmeyer, G. K., Gurd, F. R. N., and Berzofsky, J. A.,** A possible immunodominant epitope recognized by murine T lympocytes immune to different myoglobins, *Proc. Natl. Acad. Sci. U.S.A.*, 79, 4723, 1982.

106. **Flanagan, M. A.,** Role of Electrostatic Interactions in the Structure and Function of Myoglobin, Lysozyme and Hemoglobin, Ph.D. thesis, Indiana University, Bloomington, 1983.
107. **Matthew, J. B., Friend, S. H., Botelho, L. H., Lehman, L. D., Hanania, G. I. H., and Gurd, F. R. N.,** Discrete charge calculations of potentiometric titrations for globular proteins: sperm whale myoglobin, hemoglobin alpha chain, cytochrome c, *Biochem. Biophys. Res. Commun.*, 81, 416, 1978.
108. **Wilbur, D. J. and Allerhand, A.,** Titration behavior of individual tyrosine residues of myoglobins from sperm whale, horse, and red kangaroo, *J. Biol. Chem.*, 251, 5187, 1976.
109. **Gurd, F. R. N., Falk, K.-E., Malmström, B. G., and Vänngård, T.,** A magnetic resonance study of sperm whale ferrimyoglobin and its complex with 1 cupric ion, *J. Biol. Chem.*, 242, 5724, 1967.
110. **Fermi, G. and Perutz, M.,** in *Haemoglobin and Myoglobin: Atlas of Moleuclar Structures in Biology*, Vol. 2, Phillips D. C. and Richards, F. M., Eds., Oxford University Press, London, 1981.
111. **Dickerson, R. E. and Geis, I.,** *Hemoglobin: Structure, Function, Evolution, and Pathology*, Benjamin-Cummings Publ. Co., Menlo Park, Calif., 1983.
112. **Muirhead, H., Cox, J. M., Mazzarella, L., and Perutz, M. F.,** Structure and function of haemoglobin, III. A three-dimensional fourier synthesis of human deoxyhaemoglobin at 5.5 Å resolution, *J. Mol. Biol.*, 28, 117, 1967.
113. **Perutz, M. F. and Ten Eyck, L. F.,** Stereochemistry of cooperative effects in hemoglobin, *Cold Spring Harbor Symp. Quant. Biol.*, 36, 295, 1971.
114. **Ho, C. and Russu, I. M.,** Proton nuclear magnetic resonance studies of sickle cell hemoglobin, in *Clinical and Biochemical Aspects of Hemoglobin Abnormalities*, Caughey, W. S., Ed., Academic Press, New York, 1978, 179.
115. **Morrow, J. S., Matthew, J. B., Wittebort, R. J., and Gurd, F. R. N.,** Carbon 13 resonances of $^{13}CO_2$ carbamino adducts of α and β chains of human adult hemoglobin, *J. Biol. Chem.*, 251, 477, 1976.
116. **Matthew, J. B., Morrow, J. S., Wittebort, R. J., and Gurd, F. R. N.,** Quantitative determinations of carbamino adducts of α and β chains in human adult hemoglobin in presence and absence of carbon monoxide and 2,3-diphosphoglycerate, *J. Biol. Chem.*, 252, 2234, 1977.
117. **Garner, W. H., Bogardt, R. A., Jr., and Gurd, F. R. N.,** Determination of the pK values for the α-amino groups of human hemoglobin, *J. Biol. Chem.*, 250, 4398, 1975.
118. **Russu, I. M., Ho, N. T., and Ho, C.,** A proton nuclear magnetic resonance investigation of histidyl residues in normal adult hemoglobin, *Biochemistry*, 21, 5031, 1982.
119. **Shaanan, B.,** Structure of human oxyhaemoglobin at 2.1 Å resolution, *J. Mol. Biol.*, 171, 31, 1983.
120. **Baldwin, J. M.,** The structure of human carbonmonoxy haemoglobin at 2.7 Å resolution, *J. Mol. Biol.*, 136, 103, 1980.
121. **Kilmartin, J. V., Breen, J. J., Roberts, G. C. K., and Ho, C.,** Direct measurement of the pK values of an alkaline Bohr group in human hemoglobin, *Proc. Natl. Acad. Sci. U.S.A.*, 70, 1246, 1973.
122. **Rollema, H. S., de Bruin, S. H., Janssen, L. H. M., and van Os, G. A. J.,** The effect of potassium chloride on the Bohr effect of human hemoglobin, *J. Biol. Chem.*, 250, 1333, 1975.
123. **Perutz, M. F.,** Preparation of haemoglobin crystals, *J. Cryst. Growth*, 2, 54, 1968.
124. **Atha, D. H. and Riggs, A.,** Tetramer-dimer dissociation in hemoglobin and the Bohr effect, *J. Biol. Chem.*, 251, 5537, 1976.
125. **Chu, A. and Ackers, G. K.,** Mutual effect of protons, NaCl, and oxygen on the dimer-tetramer assembly of human hemoglobin, *J. Biol. Chem.*, 256, 1199, 1981.
126. **Kirschner, A. G. and Tanford, C.,** The dissociation of hemoglobin by inorganic salts, *Biochemistry*, 3, 291, 1964.
127. **Thomas, J. O. and Edelstein, S. J.,** Observation of the dissociation of unliganded hemoglobin, *J. Biol. Chem.*, 248, 2901, 1973.
128. **Farmer, M.,** The influence of Carbamino Carbon Dioxide on Vertebrate Hemoglobin Function, Ph.D. thesis, Duke University, Durham, N.C., 1979.
129. **Caughey, W. S., Shimada, H., Hazzard, J. H., Houtchens, R. A., Potter, W. T., and Einarsdottir, O.,** Dynamic protein structures at oxygen reaction sites in hemoglobins, myoglobins, and cytochrome c oxidase, *Fed. Proc. Fed. Am. Soc. Exp. Biol.*, 42, 2000, 1983.
130. **Crowl-Powers, M. L.,** Electrostatic Modelling of Assembly and Functional Interactions in Hemoglobins and Characteristics of Ancestral Myoglobin, Ph.D. thesis, Indiana University, Bloomington, 1985.
131. **Kilmartin, J. V.,** The interaction of inositol hexaphosphate with methaemoglobin, *Biochem. J.*, 133, 725, 1973.
132. **Chu, A. H., Turner, B. W., and Ackers, G. K.,** Effects of protons on the oxygenation-linked subunit assembly in human hemoglobin, *Biochemistry*, 22, 604, 1983.
133. **Mills, F. C., Ackers, G. K., Gaud, H. T., and Gill, S. J.,** Thermodynamic studies on ligand binding and subunit association of human hemoglobins, *J. Biol. Chem.*, 254, 2875, 1979.
134. **Antonini, E., Wyman, J., Brunori, M., Franticella, C., Bucci, E., and Rossi-Fanelli, A.,** Studies on the relations between molecular and functional properties of hemoglobin, *J. Biol. Chem.*, 240, 1096, 1965.

135. **Acampora, G. and Hermans, J.,** Reversible denaturation of sperm whale myoglobin. I. Dependence on temperature, pH, and composition, *J. Am. Chem. Soc.*, 89, 1543, 1967.
136. **Gurd, F. R. N., Friend, S. H., Rothgeb, T. M., Gurd, R. S., and Scouloudi, H.,** Electrostatic stabilization in sperm whale and harbor seal myoglobins, *Biophys. J.*, 32, 65, 1980.
137. **Radding, J. A.,** The Chemical Modification of Tryptophans in Sperm Whale Myoglobin, Ph.D. thesis, Indiana University, Bloomington, 1983.
138. **Nakhleh, E. T.,** Thermodynamics of Some Ferrimyoglobin Reactions, Ph.D. thesis, American University of Beirut, Lebanon, 1971.
139. **Garcia-Moreno E., B., Chen, L. X., and Gurd, F. R. N.,** The nature of electrostatic interactions in myoglobin, *Biophys. J.*, 45, 376a, 1984.
140. **Deisenhofer, J. and Steigemann, W.,** Crystallographic refinement of the structure of bovine pancreatic trypsin inhibitor at 1.5 Å resolution, *Acta Crystallogr. Sect. B*, B31, 238, 1975.
141. **Brown, L. R., De Marco, A., Wagner, G., and Wüthrich, K.,** A study of lysyl residues in the basic pancreatic trypsin inhibitor using ^{1}H nuclear magnetic resonance at 360 MHz, *Eur. J. Biochem.*, 62, 103, 1976.
142. **Vincent, J., Chicheportiche, R., and Lazdunski, M.,** The conformational properties of the basic pancreatic trypsin-inhibitor, *Eur. J. Biochem.*, 23, 401, 1971.
143. **Masson, A. and Wüthrich, K.,** Proton magnetic resonance investigation of the conformational properties of the basic pancreatic trypsin inhibitor, *FEBS Lett.*, 31, 114, 1973.
144. **Harina, B. M., Dyckes, D. F., Willcott, M. R., and Jones, W. C.,** Denaturation studies by ^{13}C nuclear magnetic resonance on modified basic pancreatic trypsin inhibitor using the novel S-[^{13}C] methyl methionyl probe, *J. Am. Chem. Soc.*, 102, 1120, 1980.
145. **Wagner, G. and Wüthrich, K.,** Dynamic model of globular protein conformations based on NMR studies in solutions, *Nature (London)*, 275, 247, 1978.
146. **Friend, S. H., Matthew, J. B., and Gurd, F. R. N.,** Protein-protein interactions: nature of the electrostatic stabilization of deoxyhemoglobin tetramer formation, *Biochemistry*, 20, 580, 1981.
147. **Salemme, F. R.,** An hypothetical structure for an intermolecular electron transfer complex of cytochromes c and b_5, *J. Mol. Biol.*, 102, 563, 1976.
148. **Matthew, J. B., Weber, P. C., Salemme, F. R., and Richards, R. M.,** Electrostatic orientation during electron transfer between flavodoxin and cytochrome c, *Nature (London)*, 301, 169, 1983.
149. **Pettigrew, D. W., Romeo, P. H., Tsapis, A., Thillet, J., Smith, M. L., Turner, B. W., and Ackers, G. K.,** Probing the energetics of proteins through structural perturbation: sites of regulatory energy in human hemoglobin, *Proc. Natl. Acad. Sci. U.S.A.*, 79, 1849, 1982.
150. **March, K. L.,** Electrostatic Interactions and Ion Binding in Trypsin. Bovine Pancreatic Trypsin Inhibitor, and Other Proteins, Ph.D. thesis, Indiana University, Bloomington, 1983.
151. **Huber, R., Kukla, D., Bode, W., Schwager, P., Bartels, K., Deisenhofer, J., and Steigemann, W.,** Structure of the complex formed by bovine trypsin and bovine pancreatic trypsin inhibitor, *J. Mol. Biol.*, 89, 73, 1974.
152. **Antonini, E., Ascenzi, P., Bolognesi, M., Gatti, G., Guarneri, M., and Menegatti, E.,** Interactions between serine (pro)enzymes, and Kazal and Kunitz inhibitors, *J. Mol. Biol.*, 165, 543, 1983.
153. **Antonini, E., Ascenzi, P., Menegatti, E., and Guarneri, M.,** Multiple intermediates in the reaction of bovine β-trypsin with bovine pancreatic trypsin inhibitor (Kunitz), *Biopolymers*, 22, 363, 1983.
154. **Vincent, J. P. and Lazdunski, M.,** Trypsin-pancreatic trypsin inhibitor association. Dynamics of the interaction and role of disulfide, *Biochemistry*, 11, 2967, 1972.
155. **Arnone, A.,** X-ray diffraction study of binding of 2,3-diphosphoglycerate to human deoxyhemoglobin, *Nature (London)*, 237, 146, 1972.
156. **de Bruin, S. H., Janssen, L. H. M., and van Os, G. A. J.,** Effect of 2,3-diphosphoglycerate on the Bohr effect of human adult hemoglobin, *Biochem. Biophys. Res. Commun.*, 45, 544, 1971.
157. **Ohe, M. and Kajita, A.,** Studies on the heterotropic interaction of hemoglobin, *J. Biochem.*, 82, 839, 1977.
158. **Hedlund, B. and Lovrien, R. E.,** Thermodynamics of 2,3-diphosphoglycerate association with human oxy- and deoxyhemoglobin, *Biochem. Biophys. Res. Commun.*, 61, 859, 1975.
159. **Tyuma, I., Imai, K., and Shimizu, K.,** Analysis of oxygen equilibrium of hemoglobin and control mechanism of organic phosphates, *Biochemistry*, 12, 1491, 1973.
160. **Perella, M., Kilmartin, J. V., Fogg, J., and Rossi-Bernardi, L.,** Identification of the high and low affinity CO_2-binding sites of human hemoglobin, *Nature (London)*, 256, 759, 1975.
161. **Matthew, J. B.,** Hemoglobin Interactions with Hydrogen Ion, Carbon Dixoide and 2,3-Diphosphoglycerate: A Study by ^{13}C Nuclear Magnetic Resonance and Electrostatic Theory, Ph.D. thesis, Indiana University, Bloomington, 1978.
162. **Friend, S. H., March, K. L., Hanania, G. I. H., and Gurd, F. R. N.,** Charge-site communication in proteins: electrostatic heme linkage of azide binding by sperm whale myoglobin, *Biochemistry*, 19, 3039, 1980.

163. **Stryer, L., Kendrew, J. C., and Watson, H. C.,** The mode of attachment of the azide ion to sperm whale metmyoglobin, *J. Mol. Biol.*, 8, 96, 1964.
164. **Wittebort, R. J.,** Atomic Rotations and Nuclear Magnetic Relaxation in Proteins and Polypeptides and Related Topics, Ph.D. thesis, Indiana University, Bloomington, 1978.
165. **Wittebort, R. J., Rothgeb, T. M., Szabo, A., and Gurd, F. R. N.,** Aliphatic groups of sperm whale myoglobin: ^{13}C NMR study, *Proc. Natl. Acad. Sci. U.S.A.*, 76, 1059, 1979.
166. **Neireiter, G. W.,** Carbon-13 Nuclear Magnetic Resonance Investigations Sperm Whale Myoglobins: An Examination of the pH-Dependent Motions of the NH_2-Terminus in Comparison with a Model System, Ph.D. thesis, Indiana University, Bloomington, 1979.
167. **Hanania, G. I. H. and Irvine, D. H.,** Ionization of the metal-bound water in sperm whale ferrimyoglobin, *J. Chem. Soc.*, A, 2389, 1970.
168. **Boughton, J. H. and Keller, R. N.,** Dissociation constants of hydropseudohalic acids, *J. Inorg. Nucl. Chem.*, 28, 2851, 1966.
169. **Coryell, C. D. and Pauling, L.,** A structural interpretation of the acidity of groups associated with the hemes of hemoglobin and hemoglobin derivatives, *J. Biol. Chem.*, 132, 769, 1940.
170. **Richards, F. M.,** Comments on the present and future problems in protein structure, in *Neutrons in Biology*, Vol. 27, Schoenborn, B. P., Ed., Plenum Press, New York, 1984, 1.
171. **Blackburn, P. and Moore, S.,** Pancreatic ribonuclease, in *The Enzymes*, 3rd. ed., Boyer, P. D., Ed., Academic Press, New York, 1982, 317.
172. **Wyckoff, H. W., Tsernoglou, D., Hanson, A. W., Knox, J. R., Lee, B., and Richards, F. M.,** The three dimensional structure of ribonuclease-S. Interpretation of an electron density map of a nominal resolution at 2 Å resolution, *Biochemistry*, 22, 2720, 1983.
173. **Wlowdower, A. and Sjölin, L.,** Structure of ribonuclease A: results of joint neutron and x-ray refinement at 2.0 Å resolution, *Biochemistry*, 22, 2720, 1983.
174. **Cohen, J. S., Griffin, J. H., and Schechter, A. N.,** Nuclear magnetic resonance titration curves of histidine ring protons. IV. The effects of phosphate and sulfate on ribonuclease, *J. Biol. Chem.*, 248, 4305, 1973.
175. **Griffin, J. H., Schechter, A. N., and Cohen, J. S.,** Nuclear magnetic resonance studies of a ribonuclease-dinucleoside phosphonate complex and their implications for the mechanism of the enzyme, *Ann. N.Y. Acad. Sci.*, 222, 693, 1973.
176. **Hummel, J. P. and Witzel, H.,** The binding of nucleotides by pancreatic ribonuclease. I. Proton uptake and release associated with anion binding, *J. Biol. Chem.*, 241, 1023, 1966.
177. **Anderson, D. G., Hammes, G. G., and Walz, F. G., Jr.,** Binding of phosphate ligands to ribonuclease A, *Biochemistry*, 7, 1637, 1968.
178. **Green, N. M. and Neurath, H.,** The effects of divalent cations on trypsin, *J. Biol. Chem.*, 204, 379, 1953.
179. **Gabel, D. and Kasche, V.,** Autolysis of β-trypsin. Influence of calcium ions and heat, *Acta Chem. Scand.*, 27, 1971, 1973.
180. **Abbott, F., Gomez, J. E., Birnbaum, E. R., and Darnall, D. W.,** The location of the calcium ion binding site in bovine α-trypsin and β-trypsin using lanthanide ion probes, *Biochemistry*, 14, 4935, 1975.
181. **Delaage, M. and Lazdunski, M.,** The binding of Ca^{2+} to trypsinogen and its relation to the mechanism of activation, *Biochem. Biophys. Res. Commun.*, 28, 390, 1967.
182. **Record, M. T., Lohman, T. M., and de Haseth, P.,** Ion effects on ligand-nucleic acid interactions, *J. Mol. Biol.*, 107, 145, 1976.
183. **Diamond, J. M. and Wright, E. M.,** Biological membranes: the physical basis of ion and non-electrolyte selectivity, *Annu. Rev. Physiol.*, 31, 582, 1969.
184. **Williams, R. J. P.,** The biochemistry of sodium, potassium, magnesium, and calcium, *Q. Rev. Chem. Soc.*, 24, 331, 1970.
185. **Matthew, J. B. and Richards, F. M.,** Differential electrostatic stabilization of A, B and Z forms of DNA, *Biopolymers*, 23, 2743, 1984.
186. **Gueron, M. and Weisbuch, G.,** Polyelectrolyte theory. I. Counterion accumulation, site binding, and their insensitivity to polyelectrolyte shape in solution containing finite salt concentrations, *Biopolymers*, 19, 353, 1980.
187. **Zimm, B. H. and Le Bret, M.,** Counter-ion condensation and system dimensionality, *J. Biomol. Struct. Dyn.*, 1, 461, 1983.
188. **Steitz, T. A., Weber, I. T., and Matthew, J. B.,** Catabolic gene activator protein: structure, homology with other proteins, and cyclic AMP and DNA binding, *Cold Spring Harbor Symp. Quant. Biol.*, 47, 419, 1982.
189. **Ohlendorf, D. H., Takeda, Y., Anderson, W. F., and Matthews, B. W.,** High resolution structural studies of cro repressor protein and implications for DNA recognition, *J. Biomol. Struct. Dyn.*, 1, 553, 1983.

190. **Kopka, M. L., Frantini, A. V., Drew, H. R., and Dickerson, R. E.,** Ordered water structure around a B-DNA dodecamer, *J. Mol. Biol.*, 163, 129, 1983.
191. **Gurd, F. R. N., March, K. L., and Garcia-Moreno E., B.,** Electrostatic analysis of trypsin: bovine pancreatic trypsin inhibitor association, *Fed. Proc. Fed. Am. Soc. Exp. Biol.*, 43, 1961, 1984.
192. **Rosa, J. J. and Richards, F. M.,** Hydrogen exchange from identified regions of the S-protein component of ribonuclease as a function of temperature, pH, and binding of the S-peptide, *J. Mol. Biol.*, 145, 835, 1981.
193. **Eden, D., Matthew, J. B., Rosa, J. J., and Richards, F. M.,** Increase in apparent compressibility of cytochrome c upon oxidation, *Proc. Natl. Acad. Sci. U.S.A.*, 79, 815, 1982.
194. **Hilton, B. D., Trudeau, K., and Woodward, C. K.,** Hydrogen exchange rates in pancreatic trypsin inhibitor are not correlated to thermal stability in urea, *Biochemistry*, 20, 4697, 1981.
195. **Richarz, R., Sehr, P., Wagner, G., and Wüthrich, K.,** Kinetics of the exchange of individual amide protons in the basic pancreatic trypsin inhibitor, *J. Mol. Biol.*, 130, 19, 1979.
196. **Richards, F. M.,** Packing defects, cavities, volume fluctuations, and access to the interior of proteins, including some general comments on surface area and protein structure, *Carlsberg Res. Commun.*, 44, 47, 1979.
197. **Kilmartin, J. V., Fogg, J. H., and Perutz, M. F.,** Role of C-terminal histidine in the alkaline Bohr effect of human hemoglobin, *Biochemistry*, 19, 3189, 1980.
198. **Busch, M. R., Maskalick, D. G., Neireiter, G. W., Harris, D. E., and Gurd, F. R. N.,** Electrostatic effects in an aliphatic series of semisynthetic amino terminal variants of sperm whale myoglobin, *Biophys. J.*, 45, 248a, 1984.
199. **Yamashiro, D. J., Fluss, S. R., and Maxfield, F. R.,** Acidification of endocytic vesicles by an ATP-dependent proton pump, *J. Cell Biol.*, 97, 929, 1983.
200. **Brown, M. S., Anderson, R. G. W., and Goldstein, J. L.,** Recycling of receptors: the round-trip itinerary of migrant membrane proteins, *Cell*, 32, 663, 1983.
201. **Cooper, A.,** Thermodynamic fluctuations in protein molecules, *Proc. Natl. Acad. Sci. U.S.A.*, 73, 2740, 1976.